Science

AAAS

Supplementary Materials for

A functional group–guided approach to aptamers for small molecules

Kyungae Yang *et al*.

Corresponding authors: Kyungae Yang, ky2231@cumc.columbia.edu; Milan N. Stojanovic, mns18@cumc.columbia.edu

The PDF file includes:

Materials and Methods
Figs. S1 to S62
Tables S1 to S5
References

Other Supplementary Material for this manuscript includes the following:

MDAR Reproducibility Checklist

TABLE OF CONTENTS

Methods and Materials

1.1. General. Chemicals were purchased from Sigma-Aldrich Co. (St. Louis, MO) unless otherwise noted. Oligonucleotides were ordered from Integrated DNA Technologies (Coralville, IA or Morrisville, NC) and used as received.

1.2. Selection procedures. Our general selection procedures have been reported previously (*41*). All selections were performed either directly or closely supervised by a single person (KY) to maximize the comparability of aptamers through consistent decision-making regarding the choices of target concentration ranges, numbers of pre-washes, and inclusion of counter-targets and their concentrations (if any). An example of a selection flow chart illustrating decision-making at each step is shown in Fig. S1 (*5*).

Standard desalted oligonucleotides were used for the library and primers as described in **Table S1**. Purification by HPLC was used for fluorophore-conjugated oligonucleotides. All oligonucleotides were dissolved in nuclease-free water and stored at -20 $^\circ$C. Each PCR was run with an initial cycle at 95 $^\circ$C for 2 min, followed by N cycles of [95 $^\circ$C for 15 s $\rightarrow$ 60 $^\circ$C for 20 s $\rightarrow$ 72 $^\circ$C for 30 s], ending with a single cycle at 72 $^\circ$C for 2 min. The PCR runs were 11 $\pm$ 2 cycles. Phosphate-buffered saline (PBS), pH 7.4 (Corning, Corning, NY) with 2 mM $MgCl_2$ and sometimes 5 mM KCl were used for selections as indicate in **Table S2**.

A general protocol where target concentrations are reduced in successive selection steps is as follows. Semiquantitative PCR was used to guide decision-making at each step (*i.e.*, band densities in a gel were compared). When differences between the prewash in the previous selection step and the first wash in the next step did not change and bands remain visible, the target concentration was reduced by half and the selection was continued. If after three additional selection-amplification cycles, there were no increases in the band densities between the last prewash and the first wash for a target, the last cycle where differences were observed was sequenced. The assumption was that the step contained fractions responsive to the lowest target concentration. Selections (precise conditions) varied across targets but typically, selections were stopped at <20 cycles.

1.3. Sequencing and sequence analysis. Due to the long-term nature of this project, selections for aptamers early in the study were carried out in combination with Sanger sequencing of the resulting selection pools. Aptamer pools selected later in the study were sequenced using next-generation sequencing (NGS). At the time of the transition, we ran both sequencing methods in parallel for one model target (tyrosine) and observed no differences in the top three aptamers identified. The sequencing methods for each target are noted in **Table S2**.

In the case of Sanger sequencing, the procedure was essentially the same as described in (*41*) where all sequences were screened for target binding using ThT displacement. For NGS sequencing, we used overlap extension PCR to increase sequence lengths to >140 bp for NGS (amplicon NGS service, Genewiz, South Plainfield, NJ). As shown below, we constructed the longer overhang NGS primers to include the 5'-ends of the partial sequences of each forward/reverse primer (F/R) (**Table S1).** The same PCR conditions were applied for longer

primers. The extended NGS PCR products were purified using a PCR purification column (ThermoFisher Scientific, Waltham, MA). Sample concentrations were normalized following guidelines from the sequencing service. We ranked sequences by read numbers provided by Genewiz and analyzed convergent motifs. Analyses were carried out in Excel in combination with applicable online programs (*e.g.*, AptaSUITE, https://drivenbyentropy.github.io/).
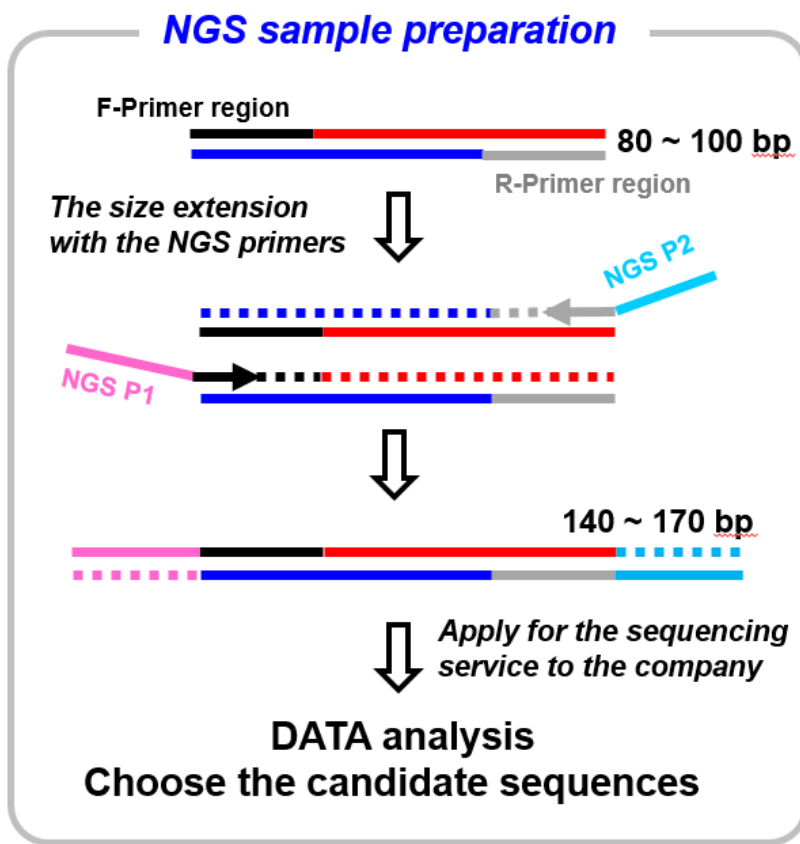
1.4. Thioflavin T dye displacement to screen for aptamer-target interactions.

Based on the rankings by read number (high to low), typically, we would select at least five sequences from each selection pool and fold them computationally into 2D structures using mFold (http://www.unafold.org/mfold/applications/dna-folding-form.php) (*42*). From the predicted 2D structures, the candidate sequences would be truncated to reduce the terminal stems to 5-6 base pairs. Truncated sequences were used in the Thioflavin T (ThT) dye displacement assay. Oligonucleotide sequence lengths were typically 44 ± 2 nucleotides for this step. Sequences underwent standard desalting purification. We used published ThT assay procedures (*43*) with buffer conditions as used in the selections.

Oligonucleotides were first placed in boiling water for 5 min, removed, and allowed to cool to room temperature. The ThT dye solution was mixed with an equal volume of aptamer solution and incubated at room temperature for ~40 min protected from light. During incubations, target

solutions (2× aptamer concentrations) were prepared and then mixed with the ThT/oligo solutions and incubated for another >40 min. Aptamer final concentrations were 400 nM, while the ThT dye was 4 μM. Fluorescence measurements were carried out in triplicate in 96- or 384-well black plates using FlexStation II or SpectraMax5 microplate readers (Molecular Devices, San Jose, CA) to record ThT fluorescence spectra at excitation and emission wavelengths of 425 nm and 490 nm, respectively. The 50% signal maximum was used to compare relative aptamer-target affinities. Among the candidates, we advanced sequences with the highest relative target binding (lowest half-point). If there were sequences that had high count in sequencing, yet little dye displacement, or enhancement of binding of ThT, we would order such candidates in the FAM/Dab format.

The procedure of Thioflavin T assay (96 wells)

4X concentrated oligo (1.6 μM), 35 μl Heat & Cool — 4X concentrated dye (16 μM), 35 μl → Mix and quick spin — 2X concentrated target solution, 70 μl → oligo/dye mixture incubation for 40 min → Mix and quick spin → oligo/dye/ target mixture incubation for 40 min → Measurement (135 μl)

The procedure of Thioflavin T assay (384 wells)

4X concentrated oligo (1.6 μM), 20 μl Heat & Cool — 4X concentrated dye (16 μM), 20 μl → Mix and quick spin — 2X concentrated target solution, 40 μl → oligo/dye mixture incubation for 40 min → Mix and quick spin → oligo/dye/ target mixture incubation for 40 min → Measurement (75 μl)

1.5. Displacement assay. The aptamer candidates selected *via* ThT screening were further characterized using a displacement assay with fluorescence readout. Fluorescein (FAM)-conjugated aptamers in their pre-truncated forms were used. Capture oligonucleotides were labeled with the fluorescence quencher dabcyl (Dab). Aptamers and capture strands for each target are listed in **Figure S4-37.** The FAM/Dab assay was carried out per the flowchart below in two steps.

A dissociation constant for the interaction between an aptamer and its capture strand was determined in the first step. This step was also used to determine the ratio of the dabcyl-labeled capture oligonucleotide to the FAM-labeled aptamer to be used in the next step. Each capture oligonucleotide was tested in serial dilutions starting from 500 nM with its corresponding aptamer at 50 nM.

The ratio of aptamer to quenching oligonucleotide that produced ~80-90% quenching was selected for the competition assay with each target. Target ratios were 3×, 5×, or 10× the aptamer concentration with the aptamer at 50 nM (See **S4-37** for ratios for specific targets). Prior to determining fluorescence, each FAM-labeled aptamer and the corresponding dabcyl-labeled capture strand were mixed at the pre-determined ratio, placed in boiling water for 5 min, and

7

allowed to cool to room temperature. Dilutions of the target solution were mixed with an equal volume of the oligonucleotide solution to obtain target-response curves. Solutions were incubated at room temperature for ~40 min in the dark. Samples were analyzed in triplicate in 384-well black plates using a Victor II microplate reader (PerkinElmer, Waltham, MA) with FAM excitation/emission at 480 nm/525 nm. Controls were run with fluorescently-labeled aptamers in the presences of their targets but without quencher-labeled capture strands to determine the effects of targets on quenching.
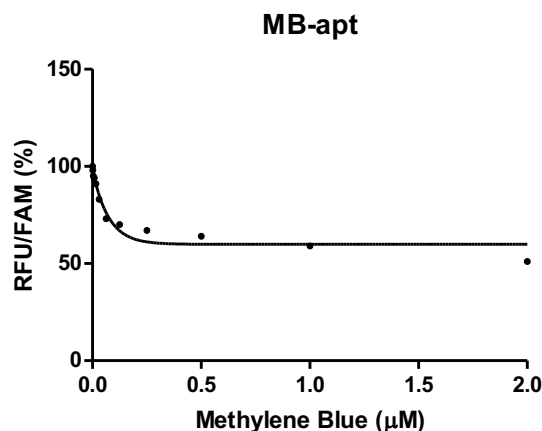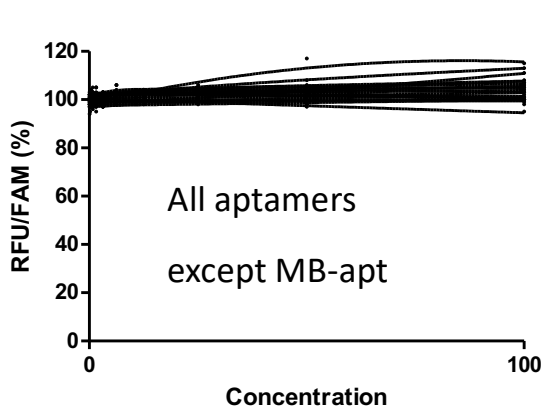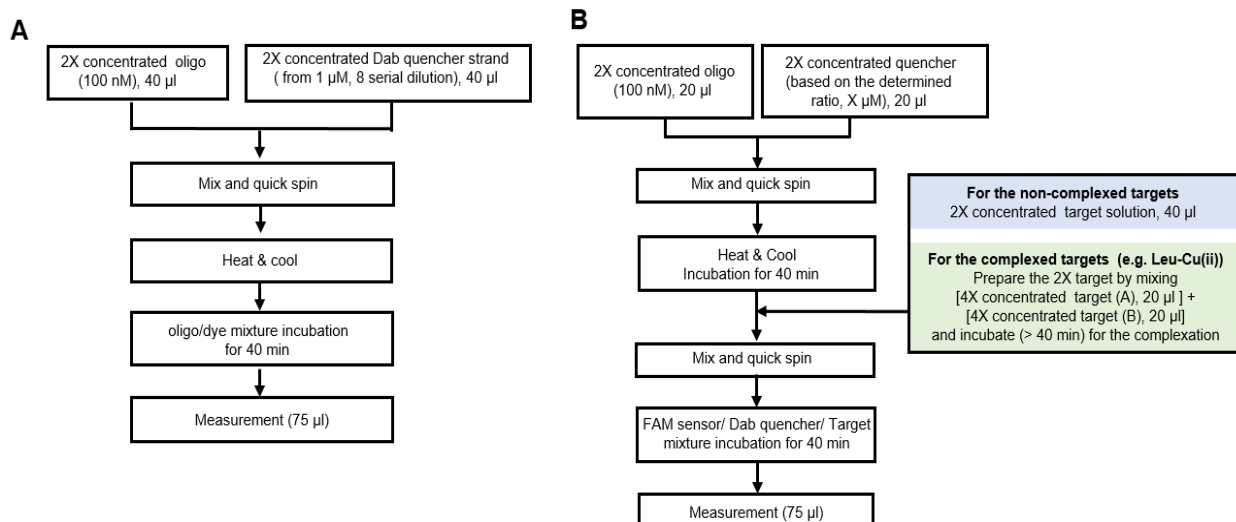
Aptamer with fluorescein (A) and no quencher. (Left) Receptor/sensor (R) with target (X) but no complementary oligonucleotide (A). These data show that targets have minimal impact on aptamer fluorescence by themselves and can be largely neglected. The results are for all targets, 0-100, relative concentration on x-axis. (Right) The exception is Methylene blue. Here, we see substantial quenching that needs to be accounted for.

1.6. Synthesis of the voriconazole analog 2a.

Materials and instrumentation

All solvents and reagents for chemical synthesis were purchased from commercial sources and used without further purification. Deuterated solvents were purchased from MilliporeSigma (St. Louis, MO). All reactions were carried out under nitrogen. Thin-layer chromatography was carried out on silica gel plates (pre-coated on glass, 0.25 mm thickness with fluorescent indicator UV_{254}). The ^1H and ^{13}C-NMR spectra were recorded on a 400 MHz NMR spectrometer (Agilent Technologies, Santa Clara, CA) using CD_3Cl as the solvent. Chemical shifts are reported in parts per million (ppm) and referenced to residue solvent peaks (7.26 ppm for $CDCl_3$ for ^1H-NMR and 77.2 ppm for $CDCl_3$ for ^{13}C-NMR). Abbreviations used in the NMR spectra are s = singlet, d = doublet, t = triplet, and m = multiplet. A single quadrupole liquid chromatograph mass spectrometer (LCMS-2020, Shimadzu Corp., Kyoto, Japan) equipped with a diode array detector and a C_{18} column (SunFire, 50 mm × 2.1 mm, 5 µm, Waters Corp., Milford, MA) was used to obtain low-resolution electrospray mass spectra and chromatograms.

*Synthesis of 2-(2,4-difluorophenyl)-1-(1H-1,2,4-triazol-1-yl)propan-2-ol)(**analog (2a)**)*
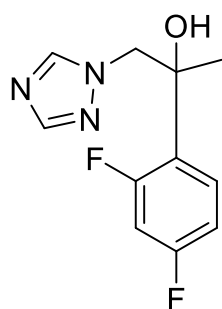
**(racemic)
analog (V1)**

Magnesium bromide ethyl etherate (2.80 g, 10.84 mmol, 2.4 eq) was added to a stirred solution of 1-(2,4-difluorophenyl)-2-(1H-1,2,4-triazol-1-yl) ethan-1-one (1.00 g, 4.48 mmol) in dichloromethane (anhydrous, 20 ml). The reaction mixture was stirred at room temperature for 1.5 h. The mixture was then cooled in an ice/water bath and a methylmagnesium bromide solution (3 M in ether, 4.1 ml, 12.3 mmol, 2.7 eq) was added dropwise. The resulting mixture was slowly warmed to room temperature and stirred for 3 d. The reaction was quenched with saturated ammonium chloride in water (20 ml). The product was extracted with dichloromethane (20 ml × 3). The combined organic phases were concentrated. The residue was purified with column chromatography (silica gel, CH_2C_2/MeOH: 100:1 to 100:2). The desired product was obtained as a white solid, 480 mg (yield = 44.8%). ^1H-NMR (400 MHz, $CDCl_3$): 7.92 (1H, s), 7.84 (1H, s), 7.54-7.47 (1s, m), 6.81-6.72 (2H, m), 4.73 (1H, d, J=14.0 Hz), 4.63 (1H, br. S), 4.45 (1H, d, J=14.4 Hz), 1.58 (3H, s). ^{13}C-NMR (100 MHz, $CDCl_3$): 163.61, 163.48, 161.13, 161.01, 160.03, 159.91, 157.57, 157.45, 150.92, 143.97, 128.97, 128.91, 128.88, 128.82, 126.98, 126.94, 126.85, 126.81, 111.26, 111.23, 111.05, 111.02, 104.29, 104.04, 104.03, 103.77, 72.75, 72.71, 57.95, 57.90, 25.85, 25.82. LC-MS: c*alc.* for $C_{11}H_{12}F_2N_3O$ [M+H]$^+$: m/z= 204.09; found: 240.0. HPLC: C_{18} column (SunFire, 2.1 x 50 mm, 5 µm); flow rate = 0.2 mL/min; mobile phase: H_2O (with 0.1% formic acid/B (B = MeCN with 0.1% formic acid, B-gradient (started with 8%, increased to 100% in 15 min, keep 100% for 3 min, decreased to 5% in 2 min)); 20 min; RT=8.14 min; 91.1% @254 nm.

Synthesis of voriconazole analog. *NMR analysis of analog (**2a**))*
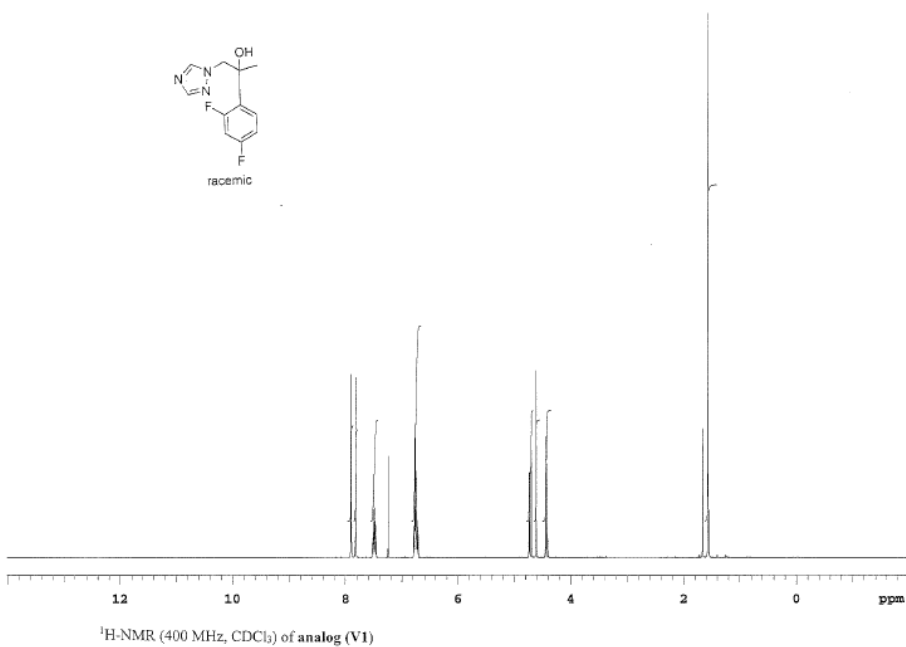
^{1}H-NMR (400 MHz, CDCl$_3$) of analog (V1)

Synthesis of voriconazole analog. *NMR analysis of analog (**2a**)*

^{13}C-NMR (100 MHz, CDCl$_3$) of analog (V1)
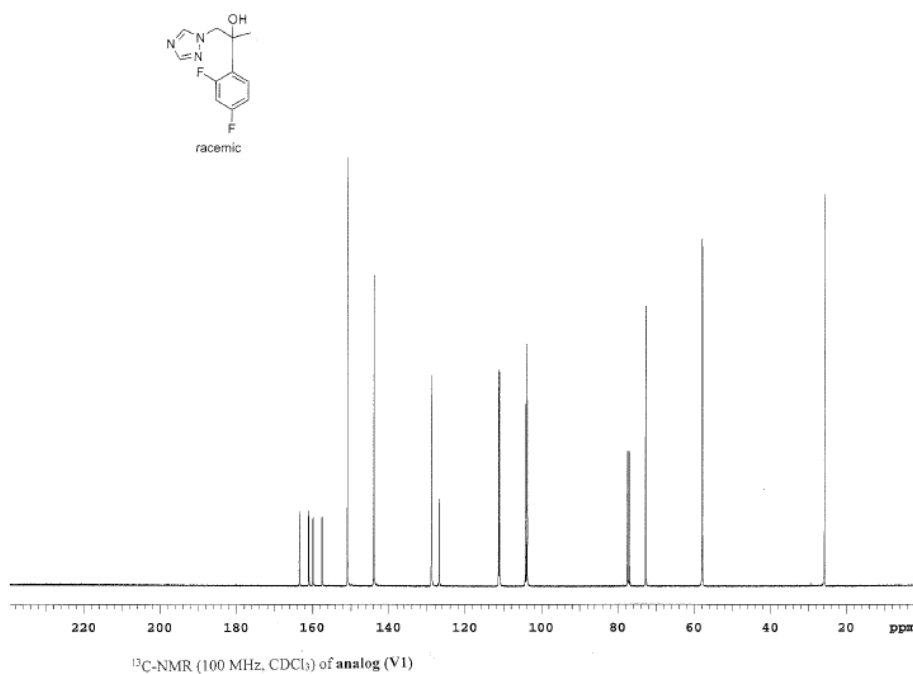
Synthesis of voriconazole analog. *HPLC chromatogram (*2a*)*

PDA Chromatogram - Ch2

mAU

PDA Multi 2 254nm,4nm

96.440

5.560
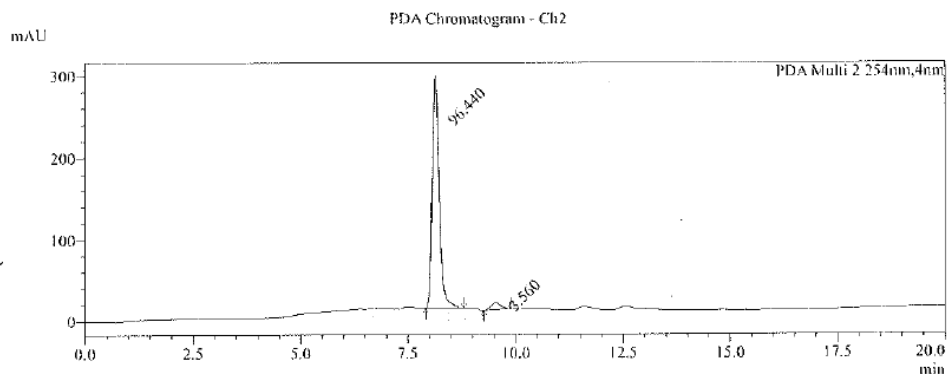
PDA Peak Table
PDA Ch2 254nm

Peak#	Ret. Time	Area	Area%
1	8.137	3258451	96.440
2	9.537	120288	3.560
Total		3378738	100.000

Synthesis of voriconazole analog. *Mass Spectrum (*2a*)*

MS Spectrum

R.Time:8.430(Scan#:2373)
MassPeaks:169
Segment 1 - Event 1

R.Time:8.433(Scan#:2374)
MassPeaks:541
Segment 1 - Event 2
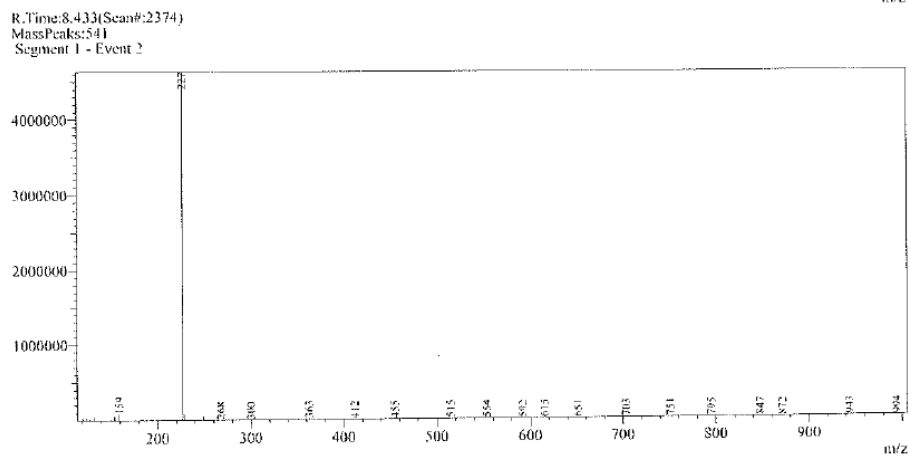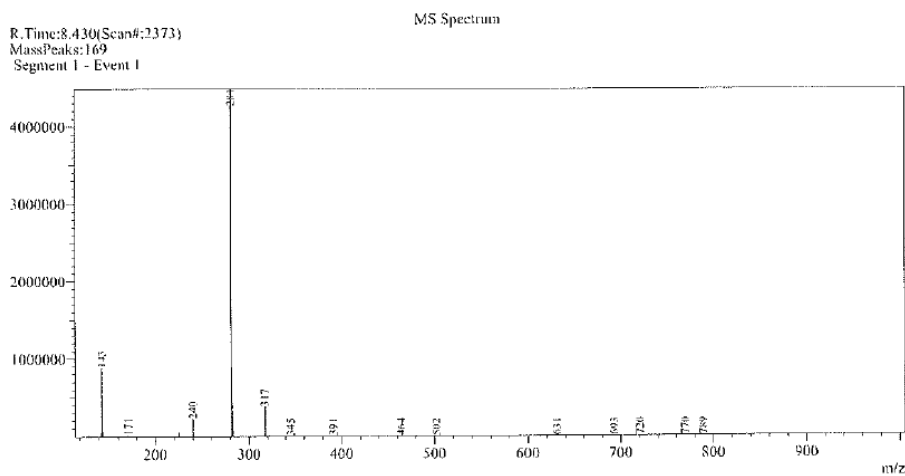
1.7. Isothermal titration calorimetry. Aptamer absorbance ratios were determined (260 nm/280 nm<1.8) to confirm DNA purity prior to ITC experiments, which were performed using a MicroCal iTC200 isothermal titration calorimeter (Malvern, Worcestershire, UK). Aptamers were first heated to 95 ⁰C for 5 min and slowly cooled to room temperature to reduce intermolecular interactions and facilitate the formation of native secondary structures. The reference cell contained 1× PBS with 2 mM MgCl$_2$ (300 µL). The sample cell contained the aptamer (300 µL, 5 µM) also in 1× PBS with 2 mM MgCl$_2$. The target (50 µM) in the same buffer was titrated into the sample cell using successive 1.5 µL injections until saturating changes in heat were observed.

Areas under the curve were integrated to calculate enthalpy changes for each target injection (kcal/mol). The molar ratio *vs.* the enthalpy of each injection was plotted to give ITC binding curves. Origin software was used to fit the titration curves to a one-site binding model. The slope of the isotherm gives the association constant. Its inverse is the dissociation constant, which was used to calculate ΔG:

$$\Delta G = RTln(K_D)$$

Table S1. Oligonucleotide sequences used in selections.

The oligonucleotide set for the N30, N36 or N45 random libraries (5' --> 3'), Ver.01	
Library	GGA GGC TCT CGG GAC GAC(N30,N36 or N45)GTC GTC CCG CCT TTA GGA TTT ACA G
Capture strand	GTC GTC CCG AGA GCC ATA /3BioTEG/
primer (Forward)	GGA GGC TCT CGG GAC GAC
primer (Reverse)	/5Biosg/ CTG TAA ATC CTA AAG GCG GGA CGA C (if apply cloning for sequencing, non-biotin sequence is needed)
NGS primer, Forward	GAA CAA CCG AAA AAA GGG GAA CCC AAG ACC CAA AGG AGG CTC TCG GGA CGA C
NGS primer, Reverse	GGA AAA ACC CAA GGA CCA AAC TGT AAA CCT GTA AAT CCT AAA GGC GGG ACG AC

The oligonucleotide set for the N36 random library, Ver.02	
Library	CAA TAT GAC CTC ACT CTC GGG ACG AC(N36)G TCG TCC CTA CTC AGG TCA CGC AGC
Capture strand	GTC GTC CCG AGA GTG TAA /3BioTEG/
primer (Forward)	CAA TAT GAC CTC ACT CTC GGG ACG AC
primer (Reverse)	/5Biosg/GCT GCG TGA CCT GAG TAG GGA CGA C
NGS primer, Forward	GAA CAA CCG AAA AAA GGG GAA CCC AAG ACC CAA ACA ATA TGA CCT CAC TCT CGG
NGS primer, Reverse	GGA AAA ACC CAA GGA CCA AAC TGT AAA CCT GTA AAT CCT GCT GCG TGA CCT GAG TAG

Cp*Rh (iii) insertion library set	
Library	CTC TCG GGA CGA CGG GTG AGC CTT AAT C(N22)A CGT GTT CAT CTG CTG TCG TCC C
Capture strand	GTC GTC CCG AGA GCC ATA /3BioTEG/
primer (Forward)	CTC TCG GGA CGA CGG GTG AGC CTT AAT C
primer (Reverse)	/5Biosg/GGG ACG ACA GCA GAT GAA CAC GT
NGS primer, Forward	GAA CAA CCG AAA AAA GGG GAA CCC AAG ACC CAA AGG AGG CTC TCG GGA CGA CGG GTG
NGS primer, Reverse	AGG ACC AAA CTG TAA ACC TGT AAA TCC TAA AGT AAA GGC GGG ACG ACA GCA GAT GAA

Leucine insertion library set	
Library	GGA GGC TCT CGG GAC GAC(N22)GT GGG TGG TGT CGG GGA TAA GAG TCG TCC C
Capture strand	GTC GTC CCG AGA GCC ATA/3BioTEG/
primer (Forward)	GGA GGC TCT CGG GAC GAC
primer (Reverse)	/5Biosg/GGG ACG ACT CTT ATC CCC GAC ACC ACC CAC
NGS primer, Forward	GAA CAA CCG AAA AAA GGG GAA CCC AAG ACC CAA AGG AGG CTC TCG GGA CGA C
NGS primer, Reverse	GGA AAA ACC CAA GGA CCA AAC TGT AAA CCT GTA AAT CCT AAA GGC GGG ACG ACT CTT ATC CCC

Isoleucine insertion library set	
Library	GGA GGC TCT CGG GAC GAC(N22)TG GGG ATG CAG GTG GGT CGA TTG TCG TCC C
Capture strand	GTC GTC CCG AGA GCC ATA/3BioTEG/
primer (Forward)	GGA GGC TCT CGG GAC GAC
primer (Reverse)	/5Biosg/GGG ACG ACA ATC GAC CCA CCT GCA TCC CCA
NGS primer, Forward	GAA CAA CCG AAA AAA GGG GAA CCC AAG ACC CAA AGG AGG CTC TCG GGA CGA C
NGS primer, Reverse	GGA AAA ACC CAA GGA CCA AAC TGT AAA CCT GTA AAT CCT AAA GGC GGG ACG ACA ATC GAC CCA

Table S2. The oligonucleotide library and sequencing method used for each aptamer isolation. The buffer for most targets was PBS (+ 2 mM MgCl₂) except where indicated (**PBS + 2 mM MgCl₂ + 5 mM KCl).

#	Aptamer ID	Target Name	Library	Sequencing
1	Leu 2.1-apt	Leucine	Leu insertion library	NGS
2	Vor-apt	Voriconazole	N36. ver.02	NGS
3	MEA-apt	Methylamine	N36. ver.01	NGS
4	PHEA-apt	Phenylethylamine	N36. ver.01	NGS
5	GLY-apt	Glycine	N36. ver.01	Sanger
6	PHE-apt(1)		Ref. (7)	
6	PHE-apt(2)		Ref. (7)	
6	PHE-apt(3)	Phenylalanine	Ref. (7)	
6	PHE-apt(4)		N36. ver.01	NGS
7	MBA-apt	Methylbutylamine	N36. ver.01	NGS
8	TRPA-apt	Tryptamine	N36. ver.01	NGS
9	MB-apt	Methylene Blue	N36. ver.01	Sanger
10	HIS-apt	Histamine	N36. ver.01	Sanger
11	SRTN-apt	Serotonin	Ref.(5)	
12	TRP-apt	Tryptophan	N36. ver.01	NGS
13	MLTN-apt	Melatonin	N36. ver.01	Sanger
14	DOPA-apt	L-DOPA	N36. ver.01	NGS
15	NE-apt	Norepinephrine	N36. ver.01	Sanger
16	EPI-apt	Epinephrine	N36. ver.01	Sanger
17	GABA-apt	GABA	N45 (N36 failed)	NGS
18	GABM-apt	GABAmid	N36. ver.01	NGS
19	GLN-apt	Glutamine	N36. ver.01	Sanger
20	PHMD-apt	Phenylalaninamide	N36. ver.01	NGS
21	TYRA-apt	Tyrosinamide	N36. ver.01	NGS
22	GAM-apt	Glycinamide	N36. ver.01	NGS
23	TYR-apt	Tyrosine	N36. ver.01	Sanger /NGS
24	TYRA-apt	Tyramine	N36. ver.01	NGS
25	AMT-apt	Agmatine	N36. ver.01	NGS
26	ARG-apt	Arginine	N36. ver.01	NGS
27	DA-apt	Dopamine	Ref.(5)	
28	Ammo-apt	Ammonia	N36. ver.01	NGS
	Cp*Rh-apt	Cp*Rh(III)**	N30	Sanger
	CpRhLeu-apt	Leu-Cp*Rh(III)**	Cp*Rh apt insertion library	NGS
	CuLeu-apt	Leu-Cu(II) **	Leu anchor insertion library	NGS
	CpRhIle-apt	Ile- Cp*Rh(III)**	Cp*Rh apt insertion library	NGS
	CuIle-apt	Ile-Cu(II)**	Ile anchor insertion library	NGS

Displacement Assay Rationale, K_D calculations, and ITC data

Introduction. Our approach is to view aptamer selection as a black box with the stem-loop library, here N_{36}, as a constant, and thus, an integral part of the black box. A target and its "winning" aptamer(s) are input and output(s), respectively. We ask, "Is there a connection between target structure and output, and if so, can this connection be used to search for aptamers, when a selection fails to produce outputs or if outputs are unsatisfactory?"

Black box approach:
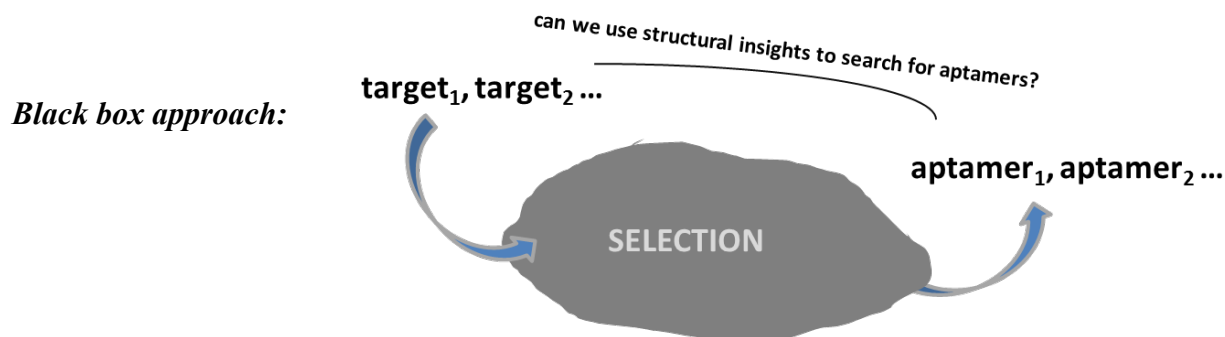
For the purpose of this work, we limit ourselves to the relationship between target structures and outcomes from the perspective of organic chemistry. Other approaches using the same set of aptamers are possible, such as focusing on informational content, mutagenesis, the prestructuring of space of N_{36} libraries, the impact of capture sequences, selectivity, or other characteristics of targets (*e.g.*, numbers of specific bonds or Connolly accessible surfaces). These approaches, while interesting, are beyond the current scope.

We need a parameter through which we can quantify the impact of controlled changes in target structures on outputs. This parameter should be able to be consistently applied to a large set of aptamers with K_D values for their targets spanning about three orders of magnitude ($\sim 10^{-8}\text{-}10^{-5}$ M) and should reflect anything that impacts selections, known and unknown, while ignoring all interactions irrelevant for selections. The parameter should be as parsimonious as possible and should be calculated under the same assumptions for all aptamers (to avoid cherry-picking and various biases). The results obtained using that parameter should pass tests as explained in the main text and be fully consistent with chemical intuition.

The fluorescence displacement assay, as studied in similar form and in depth by Li's group (*14*), with a capture oligonucleotide and an aptamer as it comes out of selection, is suitable for obtaining that parameter, because this type of displacement assay directly reflects equilibria and selection pressures within the column affinity domain in a way that is not replicated by other methods (*e.g.*, isothermal titration calorimetry (ITC), see below). For the purpose of simplicity, we neglect various degrees of allosteric antagonism between target and capture oligonucleotides (stronger the antagonism, more likely is the release of aptamer).

There are three primary components in the fluorescence displacement assay. They are a fluorescently labeled aptameric receptor (R), a partially complementary capture oligonucleotide labeled with a quencher (A), and a target (ligand) for the aptamer (X). These components are used in the same forms as those used in selections except that R and A are labeled with a fluorescent reporter and a quencher, respectively, and with the assay parameter [A] adjusted to achieve similar levels of quenching across different aptamers. We investigated all aptamers as "data points" rather

than as biosensor components that need to be optimized (which is beyond the scope of the current work). For biosensor applications, both aptamers and quenchers can be further optimized (see, *e.g.*, main text **Fig. 4D** for the voriconazole aptamer) to achieve maximum quenching and displacement.

In its simplest form, the fluorescence displacement assay considers aptameric receptor/capture strand hybridization in the absence of target and subsequent target concentration-dependent capture strand displacement. The equilibria governing hybridization and displacement are oligonucleotide specific. Hybridization positions the capture-strand quencher (dabcyl) next to the aptamer fluorophore (fluorescein, FAM) with all secondary interactions represented in the primary equilibria.

$$(i) \quad [X] + [R\mathbf{A}] \underset{}{\overset{K_A}{\rightleftharpoons}} [X] + [\mathbf{R}] + [\mathbf{A}] \underset{}{\overset{K_X}{\rightleftharpoons}} [\mathbf{XR}] + [\mathbf{A}] \Longleftarrow \text{competitor oligo (with quencher)}$$

aptamer*competitor (quenched)   aptamer (fluorescent)   aptamer*target (fluorescent)
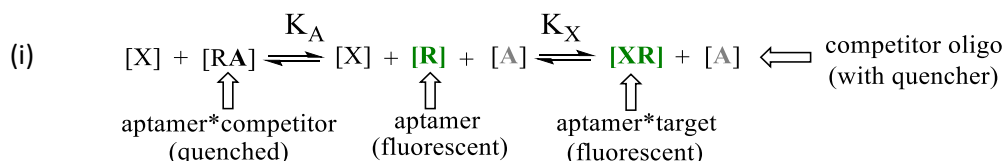
The fluorescence displacement assay consists of two experimental steps. First, we obtain K_A, which governs the equilibrium between R and A (the "quenching curve"). Second, we obtain the apparent equilibrium constant, K'_X, which governs the interactions of R with X in the presence of a constant concentration of A. This is a "displacement assay", where the target concentration is titrated while the concomitant increase in fluorescence is measured.

With quenching conditions kept relatively similar (*i.e.*, between 80-90% of the fluorescence of R on its own, without A; we correct differences, see **Table S4** and **Fig. S1**), the value of K'_X (the half-point in the equilibrium, $X_{50\%}$) and the change in free energy associated with target addition are characteristic of targets in the context of selections. By comparing pairwise aptamer-target-oligonucleotide-displacement free energies, we can extract the contributions of individual target functional groups.

To calculate actual K_X values, which are affinities normalized across interactions with capture oligonucleotides, we have a choice of several models of increasing complexity.

2.1. Obtaining the dissociation constant (K_A) for an aptamer-quencher interaction.

In our assay, K_A is derived from a traditional quenching assay, as in our previously reported studies (*5, 6*). Here, we typically perform a four-parameter logistic (4PL) curve fitting (*e.g.*, at Quest Graph™ Four Parameter Logistic (4PL) Curve Calculator. AAT Bioquest, Inc., 4 Jan. 2023) to obtain B$_{max}$ ("no quenching"). In PRISM (which gives same results, but more detailed confidence range report), this is "log(inhibitor) vs. response -- Variable slope". At this point, it is important to do a reality check,

Quenching curve: Leucine Aptamer

$$Y = 2844.1384 + \frac{72700.9326 - 2844.1384}{1 + \left(\frac{X}{88.2158}\right)^{1.1}}$$

● Real ✕ FIT

16
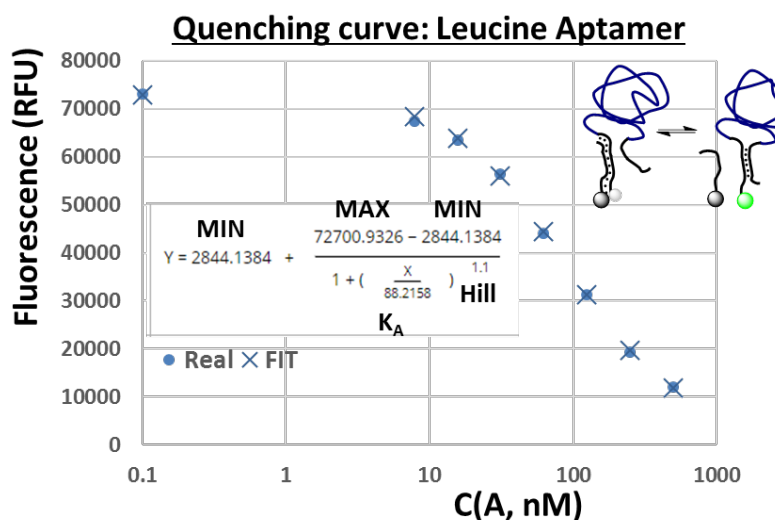
for example, such that the B_{max} value is not allowed to be more than about 2% higher than the fluorescence of the aptamer alone or of the aptamer in the presence of maximal target concentration.

The half-maximal value of quenching, K_A, is at one half of the value in the presence of an infinite amount of capture oligonucleotide with quencher. Again, a reality check is necessary, such that the total quenching should not be below of about 2% of the fluorescence of the aptameric receptor alone.

In this whole work, we use all aptamers as they come from selections with no attempts to optimize stems or displacement for analytical purposes. Thus, this is different from standard analytical work. Because library capture, while the column is washed without target, is one of the applied evolutionary pressures, we expect that those aptamers that bind to more than one capture strand oligonucleotide, and still can be released upon exposure to the target, will be evolutionarily favored. Indeed, we observe that many of our targets will have interactions with more than one capture oligonucleotide in solution, with Hill coefficients varying between 0.85-2.66. Importantly, for example, numbers such as 1.8 do not mean that we have 1.8 capture oligonucleotides, but that, for example, possibly two oligonucleotides mildly interfere with each other. This is not a proof, not even an indication, that these are happening on the column as well, because of the steric constraints on the capture oligonucleotides. Additional complication that makes HC difficult to interpret is that all our values are composite of microscopic constants in which aptamer and quencher are at various stages of hybridization, which have different affinities. Thus, we do not attempt to interpret these values.

We always perform an additional reality check to look for a large discrepancy in fit for the region of the quenching curve between 20-80%. If necessary, we adjust parameters manually to obtain a more realistic curve fit. The value, K_A for each aptamer together with the sequences of R and A appear in **S4-37**.

2.2. Obtaining the apparent dissociation constant (K'_X) for an aptamer-target interaction.

In our assay, K'_X ($^{app}K_D$) is derived from a competition assay in which the target (X) is titrated while the displacement of a complementary capture oligonucleotide labeled with dabcyl (A) from the aptamer labeled with fluorescein (R) is observed. We again perform four-parameter logistic (4PL) curve fitting to obtain B_{max} (the "maximum release"), the half-maximal value of release, K'_X or $X_{50\%}$, a minimal value (*i.e.*, a starting point or value in the presence of an infinite amount of capture-Dab/aptamer-FAM), and a Hill coefficient. The latter

parameter for all aptamers in our main set is always between 0.85-1.25 and is treated as a 1:1

binding between X and R. Apparently, even if two target molecules bind to one aptamer molecule, one target molecule is predominant in quenching (or aptamer release from the column). Of note, in PRISM, this is "log(agonist) vs. response -- Variable slope".

After we determine all K'x and Kx values, we calculate average contribution of oligonucleotide to free energy of displacement and correct all individual values to it as if assay conditions are absolutely identical. While this protocol is not necessary for most situations, this helped identify and eliminate any discussion points in which we were initially overinterpreting data. Thus, we left only those discussion points that would hold regardless of these corrections.

2.3. Allostery to model capture strand-aptamer-target interactions.

The fluorescence assay at a single capture strand conformation might not be optimal for high precision affinity characterization, but is practical for the purpose of this work.

We can calculate all constants using either competitive (which we used in the past) or allosteric model (which we clarify here). Which model we use will not have much practical impact on further use of aptamers, but we provide it as a helpful starting point for future work of others. We adapt this analysis from Ehlert, 1987 (*18*) where the basic equations and terminology are as follows:

In this scheme:

The K_A is the dissociation constant for the interaction between a fluorescent aptamer and a complementary oligonucleotide labeled with a quencher.

The K_X is the dissociation constant for the interaction between a fluorescent aptamer and its target (small molecule ligand).

The value α denotes a factor by which the presence of A or X increases or decreases K_x or K_A, respectively (the impact is reciprocal, and by definition, cooperative). At high concentrations, the target becomes fully competitive (*i.e.*, the target fully displaces the quencher-labeled capture strand). In this case, the equation below is reduced to a simpler form.

Ehlert derives the following equation to describe the binding of X in the presence of A:

$$ \text{(iii)} \qquad Y = \frac{[X]*[R_T]}{[X] + K_X'} \; ; \text{where: } K_X' = K_X * \left(\frac{K_A + [A]}{K_A + \frac{[A]}{\alpha}} \right) $$

In this equation:

The value Y is aptamer (reporter) bound to ligand X ($[Y] = [XR] + [XRA]$).

The K_X' value is the apparent dissociation constant of X (*i.e.*, estimated by the target concentration at half-maximal displacement).

The R_T denotes the total receptor concentration. In our case, R_T is the aptamer concentration added to the solution.

We apply conditions described by Ehlert (p. 189), "It is often more economical to estimate the binding parameters of a nonlabelled drug by measuring the binding of a fixed concentration of a radioligand in the presence of various concentrations of the nonlabelled drug"(*18*).

All K_A values are in nM and all $[A]_T$ (total concentration of competitor) are between 150-500 nM with similar quenching levels. These were fixed at such levels independently of this project, i.e., during initial characterization of our set.

We choose initial concentration of $[A]_T$ amongst three values, 150, 250, or 500 nM, or 1:3, 1:5, and 1:10 vs. aptamer, in order to achieve typically between 80-90% quenching. Spending too much time to precisely adjust these values to the exactly same level was deemed impractical, and we prefer to do subsequent correction to average.

2.4. Obtaining the α factor from K_A at saturating target concentrations

The factor **α** is, per Ehlert, estimated at saturating concentrations of X, using the following formula (p. 189):

(iv)
$$\alpha = (K_A^{\square} + [A]*(1-Y'))/(K_A^{\square} * Y')$$

Where [A] is calculated using Hill's coefficient, if appropriate. The Y' and (1-Y') are fractions best visualized *via* the following graph.
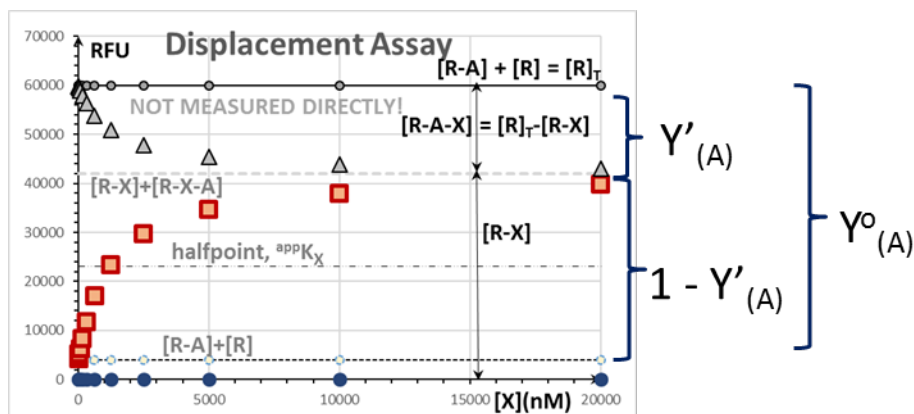
Here, Y^0 is the occupancy (R-A) at a maximum concentration of X and no A, while Y' and (1-Y') are fractions of the occupied and unoccupied receptor by A, respectively, in the presence of a saturating concentration of X. The grey points are the changes in concentrations in all fractions that we do not measure (dark), while the red points are an increase in the fractions that we can observe as an increase in fluorescence (*i.e.*, those that have activated fluorescein). The total Y fractions can be measured directly by measuring fluorescence at saturation (or any other) point.

2.5. Obtaining K_X from K'_X ($^{app}K_D$) and α

Traditional competitive antagonism occurs at a high value of α such that:

(v)
$$K_X^{\square} = K'_X/(1+[A]/K_A^{\square})$$

At lower α, we observe allosteric antagonism:

(vi)
$$K'_X = K'_X/(K_A^{\square}+[A])/(K_A^{\square}+[A]/\alpha)$$

Our values of α range from 3 to >100, and differences between competitive and allosteric model are usually minimal for us. Lower values of α typically result, in our case, in a 2-3-fold change in calculated affinity, which is negligible in the context of our limited conclusions but might be of interest to those pursuing high-precision affinity characterizations.

If of interest, modeling the next level of complexity would require using microscopic binding constants, one or two capture strands, and one or two target molecules, and their individual impacts on fluorescence and quenching, as appropriate, for each aptamer. That level of complexity could be, for example, with some aptamers, pursued by combining the approaches used to generalize a Monod-Wyman-Changeux framework (*44*). The rigorous mathematical treatment of up to three interacting molecules, as well as a window into the complexities that could be encountered while studying binding equilibria of more than two bodies are provided by Siegel and colleagues (*45*), while extending this approach to ITC experiments is possible (see below, and also (*46*)). However, these additional levels of complexity were deemed unlikely to be beneficial to our pursuit of the black box approach, requiring individual special considerations and assumptions for each aptamer.

2.6. Calculating ΔG_D values from $^{app}K_D$

ΔG_B is defined in medicinal chemistry as energy that is invested in a system to dissociate ligand from its complex. ΔG_D energy that a system releases when ligand is added, and it has a negative value. In Fig. 1B, we accordingly show $\Delta G_D = -RTln(1/^{app}K_D)$ in formula, which is same as $\Delta G_D = RTln(^{app}K_D)$.

This may cause some confusion, since we also defined free energy contribution of functional groups to displacement using letter B, not D, despite this difference in sigh. This also complicates some language (favorable contribution becomes negative), but it all works out in absolutely the same manner regardless of this choice, as long as it is used consistently.

We use $^{app}K_D$ values to assess the impact of individual target functional groups on selections (main text **Fig. 2**), via calculating, and then subtracting, pairwise ΔG_D values. Because levels of quenching are relatively the same (i.e., contribution of the presence of oligonucleotide is approximately constant 3.5+/-0.7 kJ/mol if we calculate K_X using allosteric model, and then average them across all targets, see Table **S4, Fig. S1**), we can use $^{app}K_D$ values "as they are" to calculate functional group contributions. However, in some cases, when $\Delta\Delta G_{GBE}$ values are close to 0, of displacement energies are close, we want to avoid overinterpreting small differences. Thus, we introduce corrections, by adjusting ΔG_D value so each oligonucleotide contribution is exactly at 3.5 kJ/mol, dismissing any conclusions that would depend on this change either way. That is,

if contribution due to level of quenching is calculated to be exactly 3.0 kJ/mol, we add to value 0.5 kJ/mol to adjust it to 3.5 kJ/mol. This "brings" all competitor oligonucleotides aspects of assays at exactly the same level, and substitutes adjusting endlessly all assay conditions.

2.7. Representative ITC experiments and some notes of caution.

Isothermal titration calorimetry (ITC), when possible, is widely accepted as the gold standard for characterizing the affinity of ligands for their receptors. We carried out ITC on representative aptamer-target pairs as an additional method of determining K_D and hence, ΔG. However, several issues complicated ITC for use with small aptameric receptors binding to small targets.

Our main goal is to define the impact of a target and its functional groups on our ability to select aptamers, which is not the same as defining aptamer-target binding by itself. A major difference lies in the additional equilibrium established with an aptamer in the presence of a capture oligonucleotide, which induces new conformations in the aptamer itself and the aptamer in the presence of the target. These additional equilibria, in principle, could be investigated by ITC by studying the binding of a capture oligonucleotide and an aptamer, and then trying to reproduce the selection pressure that arises from having all three species—aptamer, capture strand, and target—present at the same time, although this would be cumbersome.

The displacement assay, by design, reproduces in a much more straightforward manner the capture oligonucleotide-aptamer equilibrium and the subsequent impact of a target on this equilibrium replicating the dominant thermodynamic driving forces to release aptamer candidates from the column in the aptamer selection process. Further, the displacement assay focuses observable interactions strictly on those that cause an increase in fluorescence, which is a result of a chemical process identical to that which causes aptamer release from the column.

To obtain measurable changes in heat in ITC for small receptors and small ligands, even with microcalorimetry, we needed to use higher aptamer concentrations (5 μM for ITC *vs.* 50 nM for the displacement assay) and thus, higher target concentrations. Some of our targets have limited solubility and/or aggregate in selection buffers. Moreover, while we heated and cooled aptamer solutions prior to ITC, aptamer-aptamer interactions may still occur at the aptamer concentrations required for high signal-to-noise in isothermal calorimetry titrations. Moreover, some targets (or target classes) show evidence of multi-site binding.

On the next page, we show ITC examples for three aptamer-target pairs representing different target classes (*i.e.*, amines, amino acids, and α-amino amides) where targets were soluble, and the results were reproducible. In the case of the amide, we observe a complication of multiple binding sites, which obviously does not impact release from the column, thus, pointing to another advantage of fluorescence displacement assay for the purposes of this study. Some other aptamer-target pairs had complications that prevented us from obtaining clear-cut dissociation constants and therefore, from using ITC across the entire set to describe the impact of target functional groups on selection. Thus, while ITC is not suitable for our purposes, it can certainly be used in the future to "shine light" on the box, together with more detailed structural studies of individual aptamers.

Phenylalanine 6 (PHE-apt(1))
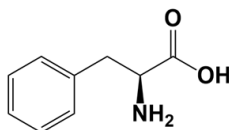
K_D via fluorescence assay=18 μM
K_D via ITC=19.5 ± 1.6 μM
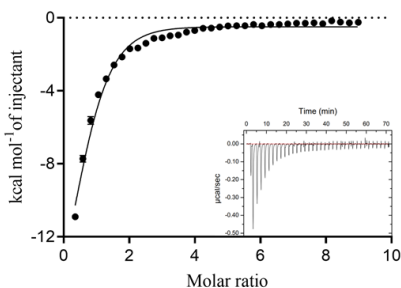
Histamine 10 (HIS-apt)
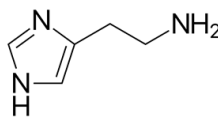
K_D via fluorescence assay=4.8 μM
K_D via ITC=3.7 ± 0.4 μM
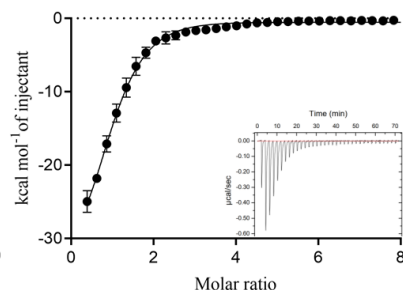
Tyrosinamide 21(TYRA-apt)
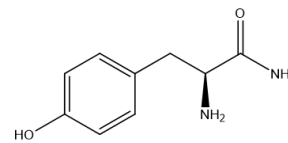
K_D via fluorescence assay= 0.22 μM
K_D via ITC=109.2 ± 26.0 μM
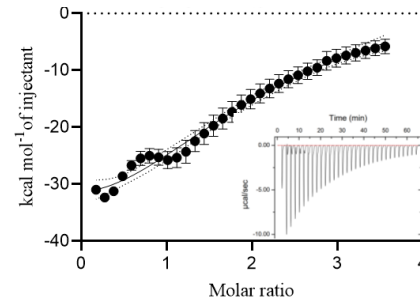
Mean ITC binding curves (fit to single site to obtain K_D values) and representative heat curves (insets) for targets from three different target classes (amino acids (PHE), amines (HIS), and α-amino amides (TYRA)). The binding curves for tyrosinamide showed reproducible evidence of low- and high-affinity aptamer binding sites. The dissociation constants (KD) determined by ITC *vs.* displacement assay (competitive model used) were similar for phenylalanine and histamine but differed greatly for tyrosinamide possibly due to the poor fit when using a one-site binding model. Data used to fit curves are means ± standard errors of the means for *N*=3 experiments run on different days.

Table S3. Target chemical list used for aptamer selection; chemical catalog numbers are from Sigma-Aldrich (MilliporeSigma), unless otherwise noted. Total 27 aptamers from this list were used in "Analysis of Free Energies of Oligonucleotide Displacement across Related Targets" sections, except Vor-apt.

#	Aptamer ID	Target Name	Cat. No.
1	Leu 2.1 apt	Leucine	L8000
2	Vor-apt	Voriconazole	PZ0005
3	MEA-apt	Methylamine (methylammonium chloride)	8.06020
4	PHEA-apt	Phenylethylamine	P6513
5	GLY-apt	Glycine	BP381-1 (Fisher Scientific)
6	PHE-apt(1)	Phenylalanine	P5482
6	PHE-apt(2)		
6	PHE-apt(3)		
6	PHE-apt(4)		
7	MBA-apt	Methylbutylamine (1-amino-3-methylbutane)	17773
8	TRPA-apt	Tryptamine	246557
9	MB-apt	Methylene blue	M9140
10	HIS-apt	Histamine	H7250
11	SRTN-apt	Serotonin	H9523
12	TRP-apt	Tryptophan	93659
13	MLTN-apt	Melatonin	461326 / M5250
14	DOPA-apt	DOPA	D9628
15	NE-apt	Norepinephrine	A7257
16	EPI-apt	Epinephrine	E4250
17	GABA-apt	GABA (γ-aminobutyric acid)	A2129
18	GABM-apt	GABA-amid (4-Aminobutyramide)	FA17704 (Biosynth)
19	GLN-apt	Glutamine	49419
20	PAM-apt	Phenylalaninamide	P1883
21	TYRA-apt	Tyrosinamide	T3879
22	GAM-apt	Glycinamide	G6104
23	TYR-apt	Tyrosine	T3754
24	TYM-apt	Tyramine	T90344
25	AMT-apt	Agmatine	A7127
26	ARG-apt	Arginine	A8094
27	DA-apt	Dopamine	H8502
28	Ammo-apt	Ammonia (ammonium chloride)	254134

Table S4. Relationship between ΔG_D (calculated from $^{app}K_D$, half point), ΔG_B competitive and allosteric, correction factor (deviation from average) to bring all oligonucleotide impacts on the same level, leading to corrected ΔG_D, which was used in presentation.

(all ΔG values are in kJ/mol)

Name	appKD (M)	Competitive model	Allosteric model	$\Delta^{app}G_D$ appDGD	ΔG^c_B DGB(competitive)	ΔG^a_B DGB(allosteric)	ΔG^c_{D-B} Competitive Difference	ΔG^a_{D-B} Allosteric Difference	Factor	$\Delta^{app}G^a_D$ all. corDGD
histamine	0.0000186	0.0000048	0.000005	-26.5	-29.8	-29.7	3.3	3.2	0.3	-26.2
phenylethylamine	0.0000072	0.00000119	0.000002	-28.8	-33.2	-32.0	4.4	3.1	0.4	-28.4
tyramine	0.000039	0.0000075	0.000008	-24.7	-28.7	-28.6	4.0	3.9	-0.3	-25.0
dopamine	0.00001	0.0000016	0.00000256	-28.0	-32.5	-31.4	4.5	3.3	0.2	-27.8
tryptamine	0.000000675	0.000000131	0.00000019	-34.6	-38.6	-37.7	4.0	3.1	0.5	-34.2
serotonin	0.000000138	0.000000034	0.00000005	-38.5	-41.9	-41.0	3.4	2.5	1.1	-37.4
norepinehrine 2	0.000011	0.0000019	0.0000019	-27.8	-32.1	-32.1	4.3	4.3	-0.7	-28.5
epinephrine 1	0.000039	0.0000067	0.0000067	-24.7	-29.0	-29.0	4.3	4.3	-0.7	-25.5
melatonin	0.00002	0.00000285	0.0000032	-26.4	-31.1	-30.8	4.7	4.5	-0.9	-27.3
MB	0.000000085	0.000000018	0.000000026	-39.7	-43.4	-42.5	3.8	2.9	0.7	-39.0
phenylalanine	0.000096	0.000018	0.00002	-22.5	-26.6	-26.4	4.1	3.8	-0.3	-22.8
tyrosine	0.0000094	0.0000014	0.0000018	-28.2	-32.8	-32.2	4.6	4.0	-0.5	-28.7
L-DOPA	0.000016	0.0000036	0.0000043	-26.9	-30.5	-30.1	3.6	3.2	0.3	-26.6
tryptophan	0.0000012	0.00000023	0.00000035	-33.2	-37.2	-36.2	4.0	3.0	0.5	-32.7
phenylalanine-amid	0.000002	0.000000383	0.00000039	-32.0	-36.0	-35.9	4.0	4.0	-0.4	-32.4
tyrosine-amid	0.000000756	0.000000216	0.000000242	-34.3	-37.4	-37.1	3.1	2.8	0.8	-33.6
Phe-1	0.000073	0.000019	0.000021	-23.2	-26.5	-26.2	3.3	3.0	0.5	-22.7
Phe-2	0.000054	0.000012	0.000013	-23.9	-27.6	-27.4	3.7	3.5	0.1	-23.9
Phe-3	0.00014	0.000033	0.000036	-21.6	-25.1	-24.9	3.5	3.3	0.2	-21.4
methylamine	0.0123	0.00169	0.0021	-10.7	-15.5	-15.0	4.8	4.3	-0.8	-11.5
methylbutylamine	0.00033	0.000091	0.000108	-19.5	-22.7	-22.2	3.1	2.7	0.8	-18.7
glycine	0.00305	0.00077	0.00077	-14.1	-17.5	-17.5	3.4	3.4	0.2	-13.9
glycine-amide	0.000312	0.00006	0.00007	-19.7	-23.7	-23.3	4.0	3.6	-0.1	-19.8
GABA	0.036	0.011	0.013	-8.1	-11.0	-10.6	2.9	2.5	1.1	-7.0
GABA-amid	0.000705	0.000152	0.00017	-17.7	-21.4	-21.1	3.7	3.5	0.1	-17.6
glutamine	0.00077	0.000154	0.00016	-17.5	-21.4	-21.3	3.9	3.8	-0.3	-17.7
leucine	0.063	0.0094	0.0097	-6.7	-11.4	-11.3	4.6	4.6	-1.0	-7.7
agmatine	0.00000245	0.000000214	0.000000476	-31.5	-37.4	-35.5	5.9	4.0	-0.4	-31.9
arginine	0.000089	0.0000105	0.0000115	-22.7	-27.9	-27.7	5.2	5.0	-1.4	-24.2
ammonia	0.00132	0.000418	0.0005	-16.2	-19.0	-18.5	2.8	2.4	1.2	-15.0
			AVG:				4.0	3.5	0	
			sd				0.71	0.67		

ΔG_D is calculated from $X_{50\%}$.

ΔG_B is calculated from K_D or $^{\alpha}K_D$, which are calculated from K_A and $X_{50\%}$, assuming either competitive or allosteric antagonism and the same binding site on R for both X and A. .

Fig. S1. Explanation of correction factors and corrected ΔG_D.

$^{app}\Delta G_D$ is calculated from $X_{50\%}$, a half-point of displacement assay. We could directly subtract two values to obtain functional group contribution to binding energy, however, that would assume that for each case in the pair contributions of oligonucleotides are identical (i.e., that aptamers with fluorescein are quenched to the same level). We can assess this assumption by taking an average $(\Delta G_D - \Delta G_B)$ values for, say, ΔG_B calculated through either allosteric or competitive model (see S.2). We obtain, e.g., for allosteric model, that average contribution of oligonucleotide is 3.5+/-0.7 kJ/mol, with extreme range from 2.8 to 5.9 kJ/mol (ammonia and arginine). This cautions us not to over-interpret close data points, particularly when subtracting pairs that are at extremes of this distribution.

To minimize impact of uneven contributions of the oligonucleotide with dabcyl to assay (due to using only three standard concentrations), we can adjust each data point (add or subtract) by the value that would bring it to the same level, of 3.5 kJ/mol. As a caution, we avoid making any statements about data points that would change significantly relative to other data points. Effectively, we used this process to eliminate those data points at which this uncertainty would impact our conclusion. For example, impact on these data points are minimal:
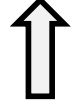
Allosteric model K_d(M)	appDGD	DGB(allosteric)	Allosteric Difference	Factor	all. corDGD
histamine	-26.5	-29.7	3.2	0.3	-26.2
phenylethylamine	-28.8	-32.0	3.1	0.4	-28.4
tyramine	-24.7	-28.6	3.9	-0.3	-25.0

calculated from $X_{50\%}$,

calculated from $X_{50\%}$, and K_A (oligonucleotide) using allosteric model

difference (average is 3.5)

Difference from average

Presented

Fig. S2. Data for individual aptamers

Data for all aptamers are reported in this format:

Aptamer 2D structures	Aptamer sequence information, terminology Aptamer ID, target, sequences from selection/fluorescent receptor, quencher/capture strand, truncated aptamer (e.g., for ThT dye displacement)
	all fitting parameters, and calculated constants (comp – competitive antagonist, allosteric antagonism) (α- cooperativity factor, HC – Hill's coefficient)

	quenching and displacement results, semi-log presentation — □ △ *experimental* ✕ ✳ *fit*	ThT dye displacement, used in initial screening
Target structure		

1

Fig. S3.

The fitting parameters are reported as:

K_A is from quenching curve

K_A

Displacement Assay

RFU

$[R\text{-}A] + [R] = [R]_T$

NOT MEASURED DIRECTLY!

$[R\text{-}A\text{-}X] = [R]_T\text{-}[R\text{-}X]$

$Y'_{(A)}$

$Y^0_{(A)}$

$[R\text{-}X]+[R\text{-}X\text{-}A]$

$[R\text{-}X]$

halfpoint, $^{app}K_X$

$1 - Y'_{(A)}$

$[R\text{-}A]+[R]$

$[X](nM)$
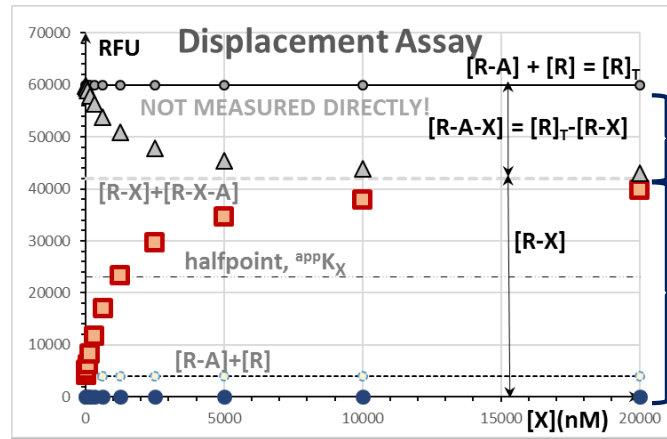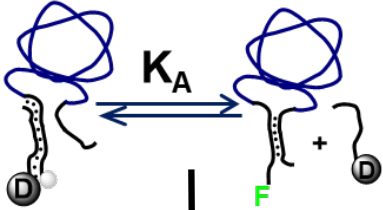
cooperativity factor: $\alpha = (K_A + [A]*(1-Y')/(K_A * Y')$

K_D^{app}
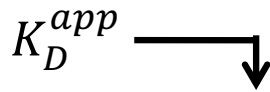
K_A (nM)	HC	K'_X		HC	α	K_X(comp)	K_X(allost)
225.00	0.82	1.32	mM	1	17.70942	0.418822	0.469709

K_A

$^{app}K_D$

K_X
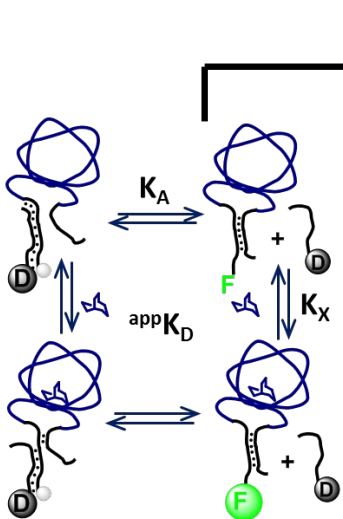
competitive antagonist: $K_X = K'_X/(1+[A]/K_A)$

allosteric antagonist: $K'_X = K'_X/(K_A + [A])/(K_A +[A]/\alpha)$

K'_X is from displacement curve

Fig. S4.

NH_4^+

Apt ID	Apt28 / Ammo-apt
Target, X	Ammonia, **28**
FAM Sensor, R	/56-FAM/CTC TCG GGA CGA CGG GAG TGT CTC CTA AGG CCT TAG TAA GAA GGG TCC TGT CGT CCC
Quencher Strand, A	GTC GTC CCG AGA G/3Dab/(10 times)
Truncated sequence	CGG GAG TGT CTC CTA AGG CCT TAG TAA GAA GGG TCC TG

Fitting parameters:

K_A (nM)	HC	K'_X		HC	α	K_X(comp)	K_X(allost)
225.00	0.82	1.3 mM		1	17.7	0.4	0.5

Ammo-apt_ThT

Figure. (Left) displacement and quenching curves plotted on the same graph; (Right) ThT displacement curve. For methods, see S.1.

Fig. S5.

Apt ID	**Apt22 / GAM-apt**
Target , X	Glycinamide, **22**
FAM Sensor, A	/56-FAM/CTC TCG GGA CGA CTG GAC CGG AGG GCT TTA TCA CTG CAC GAG AAC CGG AGT CGT CCC
Quencher Strand, R	GTC GTC CCG AGA G/3Dab/(5 times)
Truncated sequence	ACG ACT GGA CCG GAG GGC TTT ATC ACT GCA CGA GAA CCG GAG TCG T

Fitting parameters:

K_A (nM)	HC	K'_X		HC	α	K_X(comp)	K_X(allost)
57.00	1.4	0.31 **mM**		1	25.4	0.061	0.071

Figure. (Left) displacement and quenching curves plotted on the same graph; (Right) ThT displacement curve. For methods, see S.1 .

Fig. S6.

CH₃NH₃⁺

Apt ID	Apt03 / MEA-apt
Target , X	Methylamine, **3**
FAM Sensor, R	/56-FAM/CTC TCG GGA CGA CCG AGG AGG ATA TAC GTT TCC AGC GTG GTG GCA CTG GGT CGT CCC
Quencher Strand, A	GGT CGT CCC GAG AG/3Dab/ (5 times)
Truncated sequence	CGA CCG AGG AGG ATA TAC GTT TCC AGC GTG GTG GCA CTG GGT CG

Fitting parameters:

K$_A$ (nM)	HC	K'$_X$		HC	α	K$_X$(comp)	K$_X$(allost)
35.00	1.23	12.3	**mM**	0.898	22.6	1.7	2.1

Figure. (Left) displacement and quenching curves plotted on the same graph; (Right) ThT displacement curve. For methods, see S.1.

Fig. S7.

Apt ID	Apt04 / PHEA-apt
Target , X	Phenylethylamine, **4**
FAM Sensor, R	/56-FAM/CTC TCG GGA CGA CCA GTA GGG GAT CTG CAG CGT GGG GTT TGT ATG GGT GGT CGT CCC
Quencher Strand, A	GGT CGT CCC GAG AG/3Dab/ (5 times)
Truncated sequence	GAC CAG TAG GGG ATC TGC AGC GTG GGG TTT GTA TGG GTG GTC

Fitting parameters:

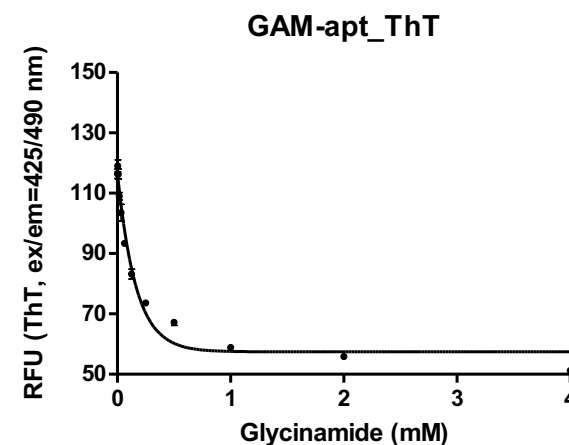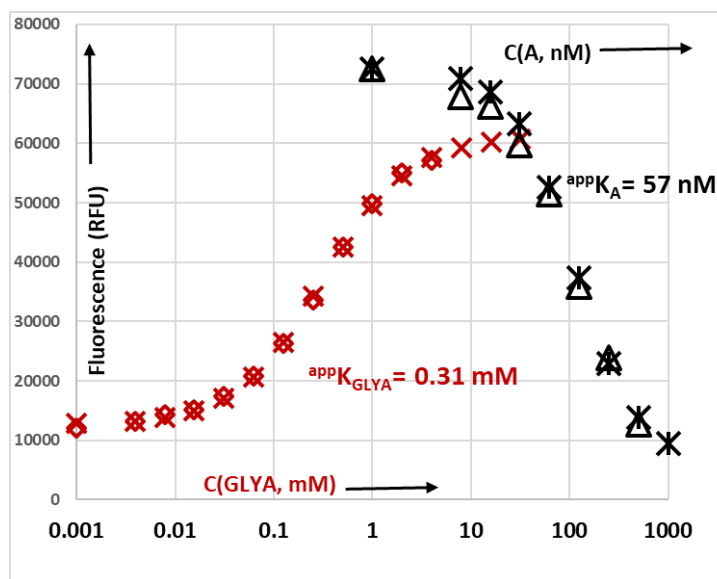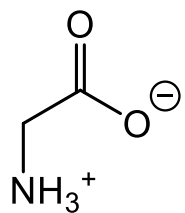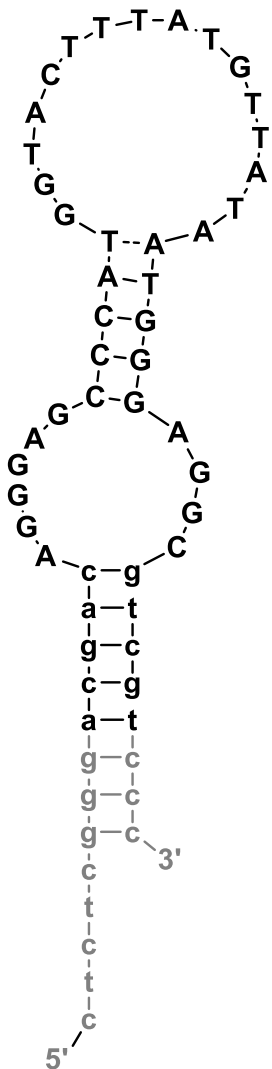| K_A (nM)	HC	K'_X		HC	α	K_X(comp)	K_X(allost)
45.00	1.29	7.2 μM		0.87	8.0	1.2	2.0

Figure. (Left) displacement and quenching curves plotted on the same graph; (Right) ThT displacement curve. For methods, see S.1.

This aptamer was one of the exceptions. It showed no displacement of the ThT dye but was selected for development because it was the most abundant.

Fig. S8.

Apt ID	Apt05 / GLY-apt
Target , X	Glycine, **5**
FAM Sensor, R	/56-FAM/CTC TCG GGA CGA CAG GGA GCC CAT GGT ACT TTA TGT TAT AAT GGG AGG CGT CGT CCC
Quencher Strand, A	GTC GTC CCG AGA G/3Dab/ (10 times)
Truncated sequence	ACG ACA GGG AGC CCA TGG TAC TTT ATG TTA TAA TGG GAG GCG TCG T

Fitting parameters:

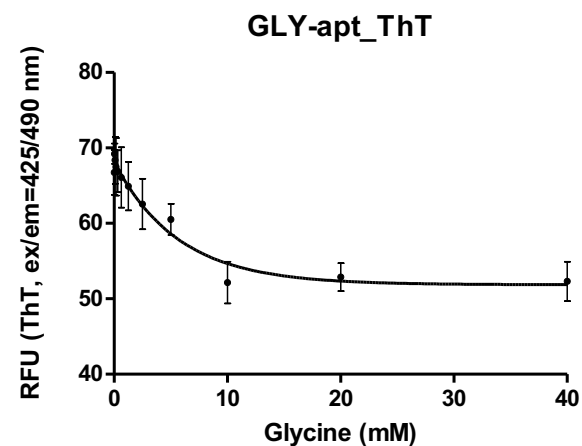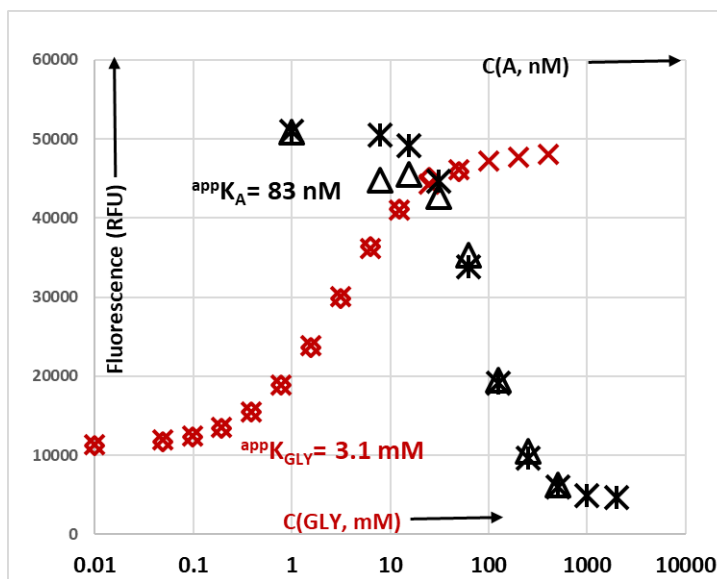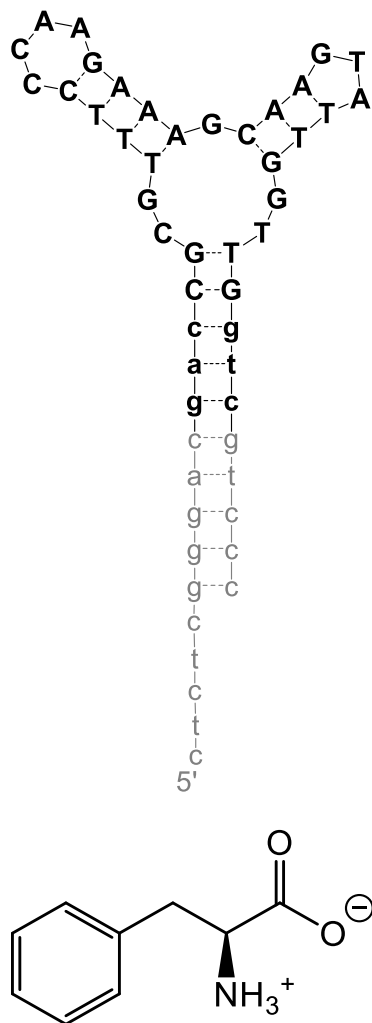| K_A (nM)	HC	K'_X		HC	α	K_X(comp)	K_X(allost)
83	1.9	3.1	**mM**	1	65	0.8	0.8

Figure. (Left) displacement and quenching curves plotted on the same graph; (Right) ThT displacement curve. For methods, see S.1.

Fig. S9.

Apt ID	Apt06/ PHE-apt(1)
Target, X	Phenylalanine, **6**
FAM Sensor, R	/56-FAM/CTC TCG GGA CGA CCG CGT TTC CCA AGA AAG CAA GTA TTG GTT GGT CGT CCC
Quencher Strand, A	GGT CGT CCC GAG AG/3Dab/ (3 times)
Truncated sequence	GAC CGC GTT TCC CAA GAA AGC AAG TAT TGG TTG GTC

Fitting parameters:

K_A (nM)	HC	K'_X		HC	α	K_X(comp)	K_X(allost)
50	2.2	73 μM		0.86	35	19	21

Figure. (Left) displacement and quenching curves plotted on the same graph; (Right) ThT displacement curve. For methods, see S.1.

NOTE: This aptamer was isolated as the highest affinity, non-cofactor (Cp*Rh(III))responsive byproduct from the selection performed in HEPES/1 M NaCl, other conditions standard. The assay is in standard, PBS-based buffer.

Fig. S10.

Apt ID	Apt06/ PHE-apt(2)
Target , X	Phenylalanine, **6**
FAM Sensor, R	/56-FAM/CTC TCG GGA CGA CCG GTG GGG GTT CTT TTT CAG GGG AGG TAC GGT CGT CCC
Quencher Strand, A	GTC GTC CCG AGA G/3Dab/ (3 times)
Truncated sequence	GAC CGG TGG GGG TTC TTT TTC AGG GGA GGT ACG GTC

Fitting parameters:

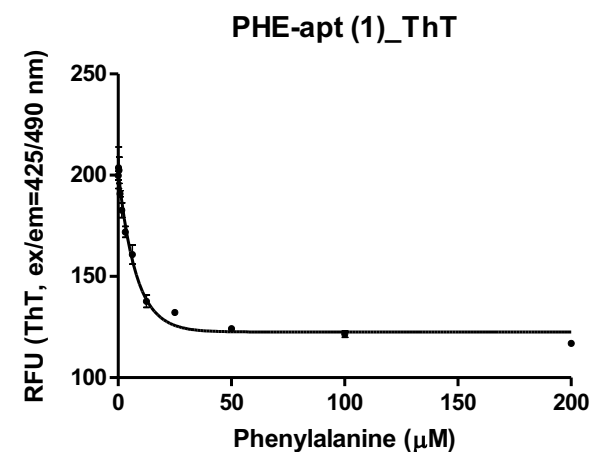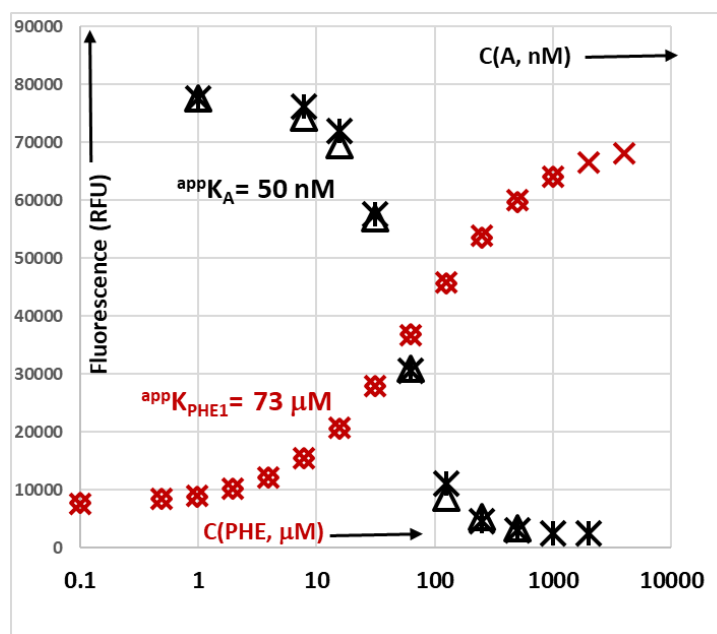| K_A (nM)	HC	K'_X		HC	α	K_X(comp)	K_X(allost)
45.00	2.3	54 μM		0.9	1000	12	13

Figure. (Left) displacement and quenching curves plotted on the same graph; (Right) ThT displacement curve. For methods, see S.1.

NOTE: This aptamer was isolated as the highest affinity, non-cofactor (Cp*Rh(III)-NHCOMe) responsive byproduct from the selection performed in HEPES/1 M NaCl, other conditions standard. The assay is in standard, PBS-based buffer.

Fig. S11.

Apt ID	Apt06/ PHE-apt(3)
Target, X	Phenylalanine, **6**
FAM Sensor, R	/56-FAM/CTC TCG GGA CGA CGA GGC TGG ATG CAT TCG CCG GAT GTT CGA TGT CGT CCC
Quencher Strand, A	GTC GTC CGG AGA G/3Dab/ (3 times)
Truncated sequence	CGA CGA GGC TGG ATG CAT TCG CCG GAT GTT CGA TGT CG

Fitting parameters:

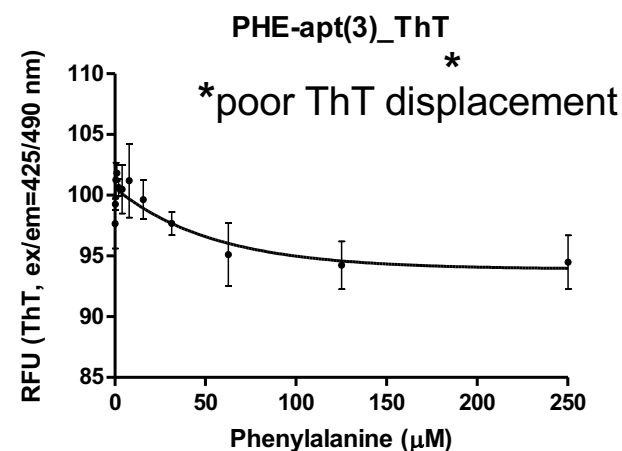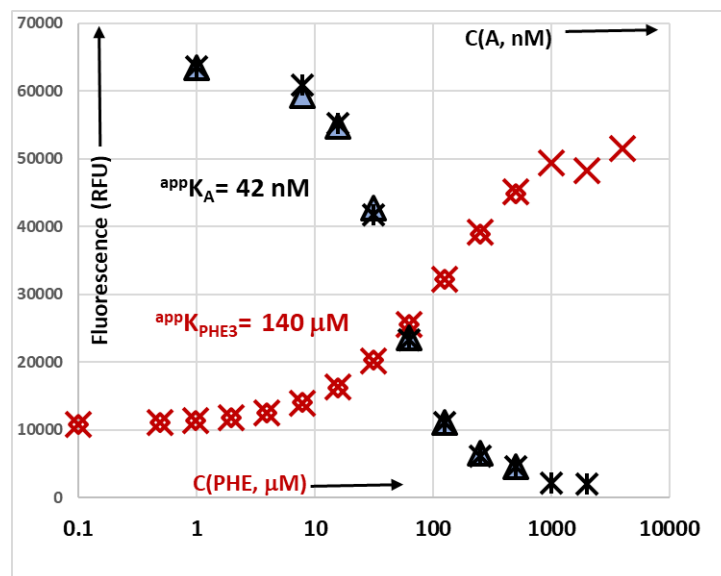| K_A (nM)	HC	K'_X		HC	α	K_X(comp)	K_X(allost)
42	1.84	140 µM		0.9	31	33	36

Figure. (Left) displacement and quenching curves plotted on the same graph; (Right) ThT displacement curve. For methods, see S.1.

NOTE: This aptamer was isolated as the highest affinity, non-cofactor (Cu(II)) responsive byproduct from the selection performed in HEPES/1 M NaCl, other conditions standard. The assay is in standard, PBS-based buffer.

Fig. S12.
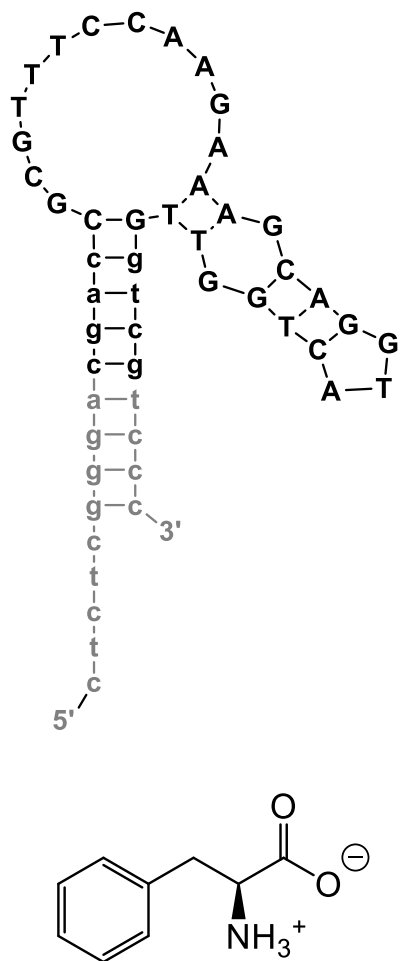
Apt ID	Apt06/ PHE-apt(4)
Target, X	Phenylalanine, **6**
FAM Sensor, R	/56-FAM/CTC TCG GGA CGA CCG CGT TTC CAA GAA AGC AGG TAC TGG TTG GTC GTC CC
Quencher Strand, A	GGT CGT CCC GAG AG/3Dab/ (3 times)
Truncated sequence	CGA CCG CGT TTC CAA GAA AGC AGG TAC TGG TTG GTC G

Fitting parameters:

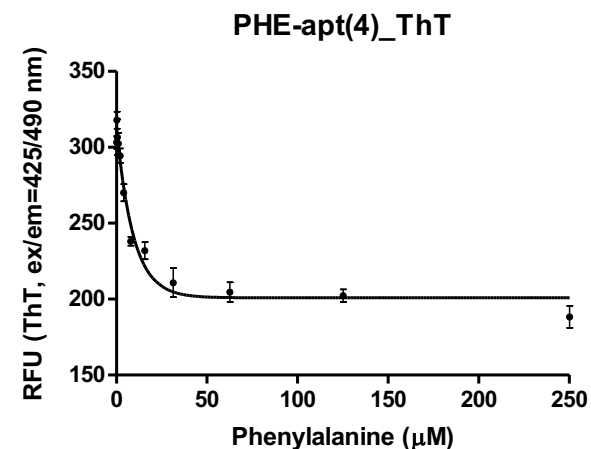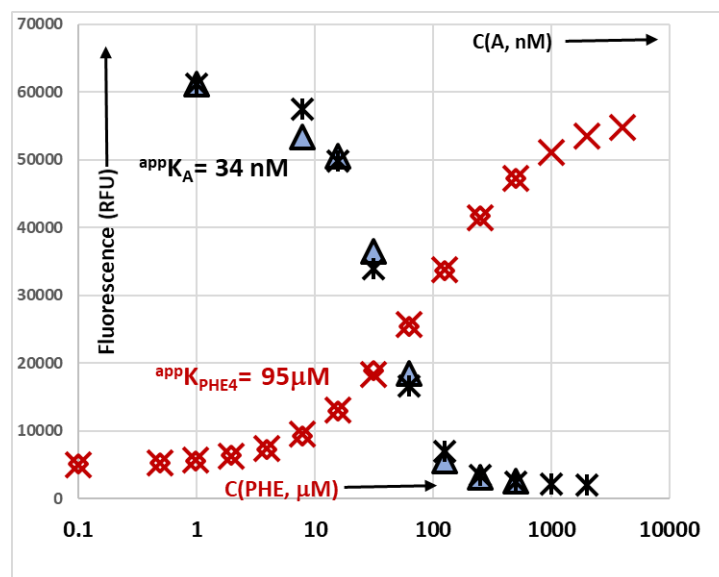| K_A (nM)	HC	K'_X		HC	α	K_X(comp)	K_X(allost)
34	1.84	96 μM		0.93	59	18	20

Figure. (Left) displacement and quenching curves plotted on the same graph; (Right) ThT displacement curve. For methods, see S.1.

NOTE: This aptamer was isolated specifically for this work in PBS-based buffer and is used in further calculations.

Fig. S13.

Apt ID	Apt07 / MBA-apt
Target , X	Methylbutylamine (1-Amino-3-methylbutane hydrochloride), **7**
FAM Sensor, R	/56-FAM/CTC TCG GGA CGA CCA GTA GGG GAT CCG CAG TGT GGG GTT TGT ATG GGT GGT CGT CCC
Quencher Strand , A	GGT CGT CCC GAG AG/3Dab/ (10 times)
Truncated sequence	CGA CCA GTA GGG GAT CCG CAG TGT GGG GTT TGT ATG GGT GGT CG

Fitting parameters:

K_A (nM)	HC	K'_X		HC	α	K_X(comp)	K_X(allost)
184	0.707	0.33 **mM**		0.96	14.8	0.092	0.108

Figure. (Left) displacement and quenching curves plotted on the same graph; (Right) ThT displacement curve. For methods, see S.1.

Fig. S14.

Apt ID	Apt08 / TRPA-apt
Target, X	Tryptamine, **8**
FAM Sensor, R	/56-FAM/CTC TCG GGA CGA CTG GCA GGC TTA GGG TGG CGC TAG GAT AGC GGT TGG GTC GTC CC
Quencher Strand, R	GTC GTC CCG AGA G/3Dab/ (5 times)
Truncated sequence	ACG ACT GGC AGG CTT AGG GTG GCG CTA GGA TAG CGG TTG GGT CGT

Fitting parameters:

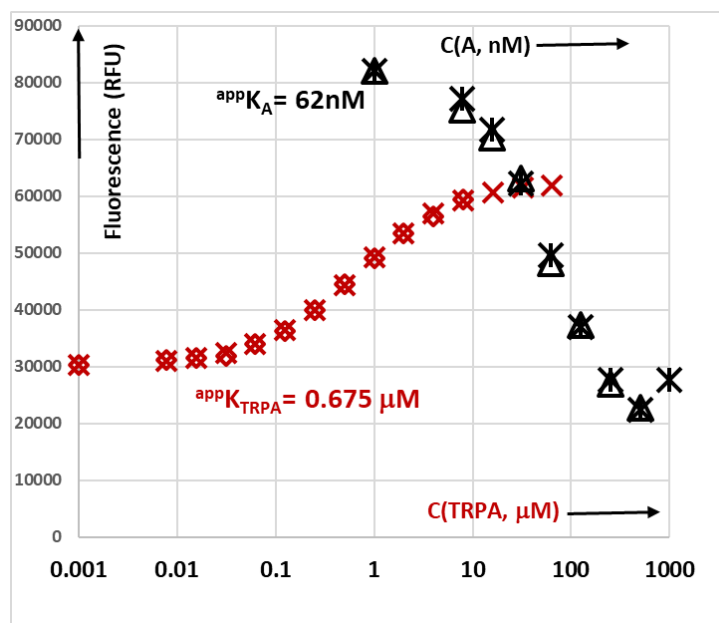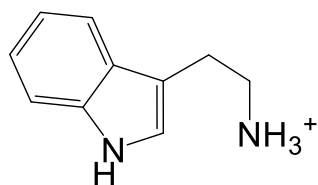| K_A (nM)	HC	K'_X		HC	α	K_X(comp)	K_X(allost)
62	1.2	0.67 μM		0.871	12	0.14	0.19
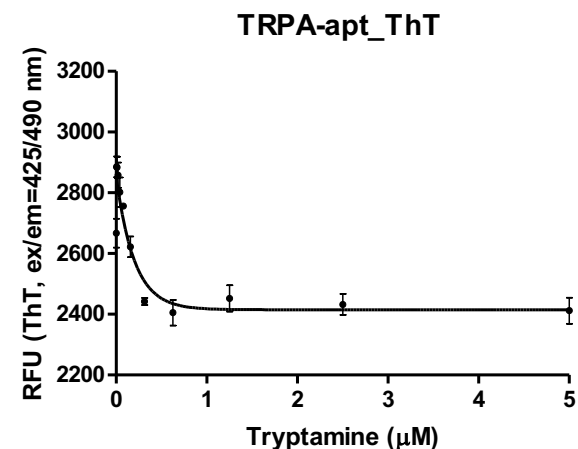
Figure. (Left) displacement and quenching curves plotted on the same graph; (Right) ThT displacement curve. For methods, see S.1.

Fig. S15.

Apt ID	Apt09/ MB-apt
Target, X	Methylene blue, **9**
FAM Sensor, R	/56-FAM/CTC TCG GGA CGA CCA GGA TGC TGT TCC ACC GGG GTA CAG GTA GGT CGC TGT CGT CCC
Quencher Strand, A	GTC GTC CCG AGA G/3Dab/ (3 times)
Truncated sequence	GAC GAC CAG GAT GCT GTT CCA CCG GGG TAC AGG TAG TGC GCT GTC GTC

Fitting parameters:

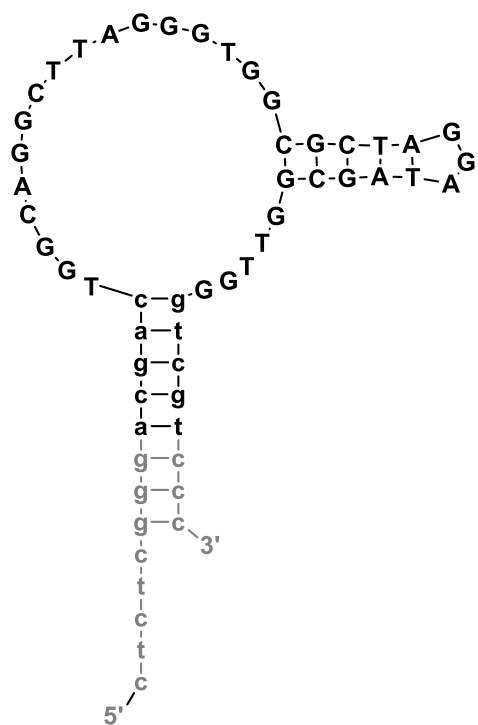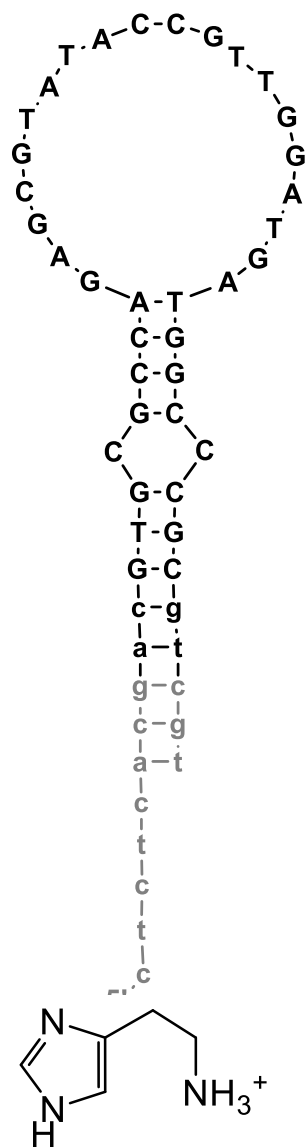| K_A (nM)	HC	K'_X		HC	α	K_X(comp)	K_X(allost)
31	1.33	0.085 μM		1.22	8.5	0.018	0.026

Figure. (Left) displacement and quenching curves plotted on the same graph; (Right) ThT displacement curve. For methods, see S.1.

Fig. S16.

Apt ID	Apt10 / HIS-apt
Target, X	Histamine, **10**
FAM Sensor, R	/56-FAM/CTC TCA CGA CGT GCG CCA GAG CGT ATA CCG TTG GAT GAT GGC CCG CGT CGT
Quencher Strand, A	CAC GTC GTG AGA G/3Dab/ (3 times)
Truncated sequence	ACG TGC GCC AGA GCG TAT ACC GTT GGA TGA TGG CCC GCG T

Fitting parameters:

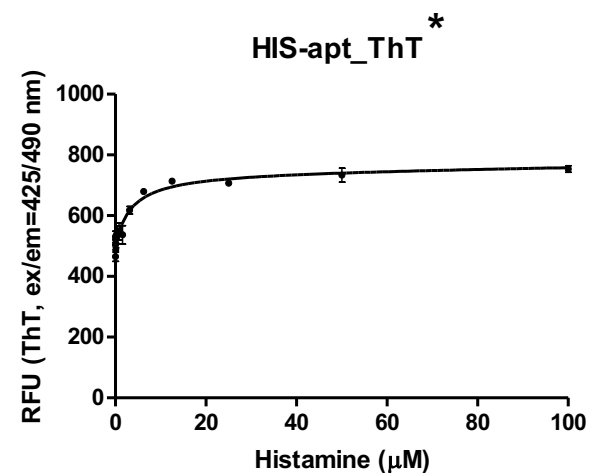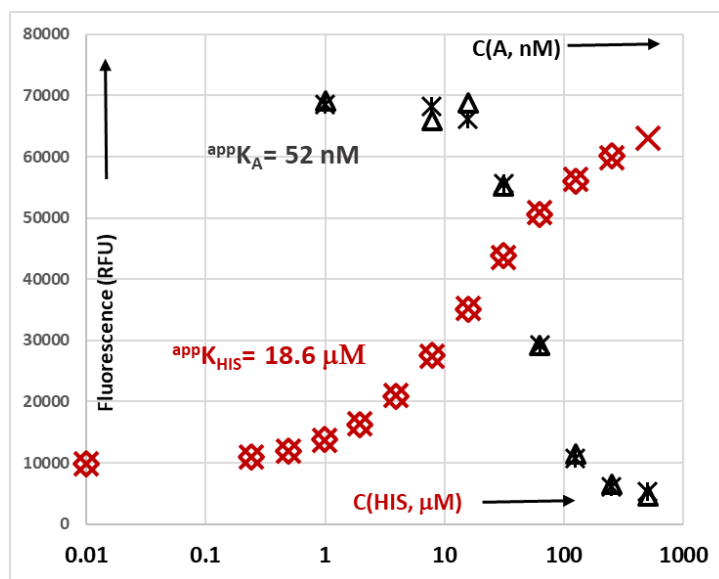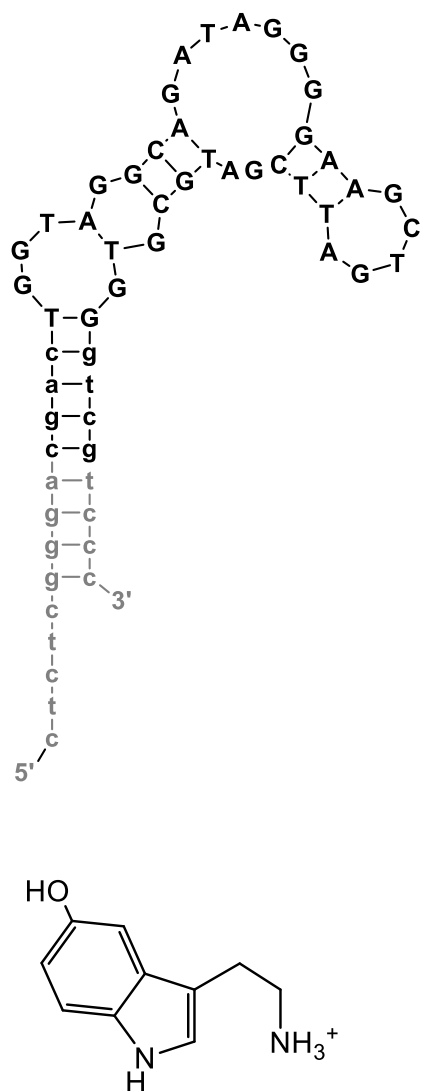| K_A (nM)	HC	K'_X		HC	α	K_X(comp)	K_X(allost)
52	2.66	18.6 μM		0.88	65.6	4.8	5.0

Figure. (Left) displacement and quenching curves plotted on the same graph; (Right) ThT displacement curve. For methods, see S.1.

This aptamer was one of the exceptions. It showed positive cooperativity between the ThT dye and ligand binding.

Fig. S17.

Apt ID	Apt11/ SRTN-apt
Target, X	Serotonin, **11**
FAM Sensor, R	/56-FAM/CTC TCG GGA CGA CTG GTA GGC AGA TAG GGG AAG CTG ATT CGA TGC GTG GGT CGT CCC
Quencher Strand, A	GTC GTC CCG AGA G/3Dab/ (10 times)
Truncated sequence	CGA CTG GTA GGC AGA TAG GGG AAG CTG ATT CGA TGC GTG GGT CG

Fitting parameters:

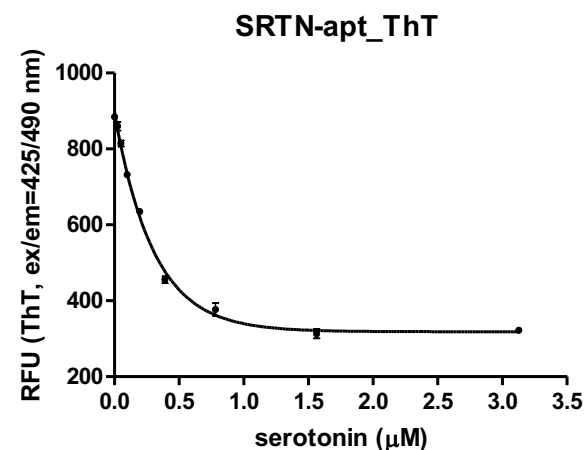| K_A (nM)	HC	K'_X		HC	α	K_X(comp)	K_X(allost)
150	1.3	0.14 μM		1	6.6	0.034	0.050

Figure. (Left) displacement and quenching curves plotted on the same graph; (Right) ThT displacement curve. For methods, see S.1.

Fig. S18.

Apt ID	**Apt12 / TRP-apt**
Target, X	Tryptophan, **12**
FAM Sensor, R	/56-FAM/CTC TCG GGA CGA CGG AAC CGG TGG TGT AGT TCC GGC GTG GGG AAG GTT CGT CGT CCC
Quencher Strand, A	CGT CGT CCC GAG AG/3Dab/ (5 times)
Truncated sequence	CGA CGG AAC CGG TGG TGT AGT TCC GGC GTG GGG AAG GTT CGT CG

Fitting parameters:

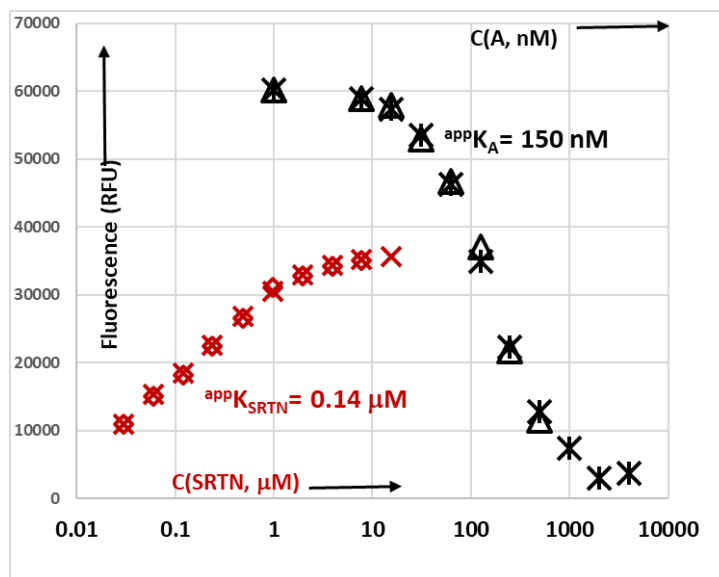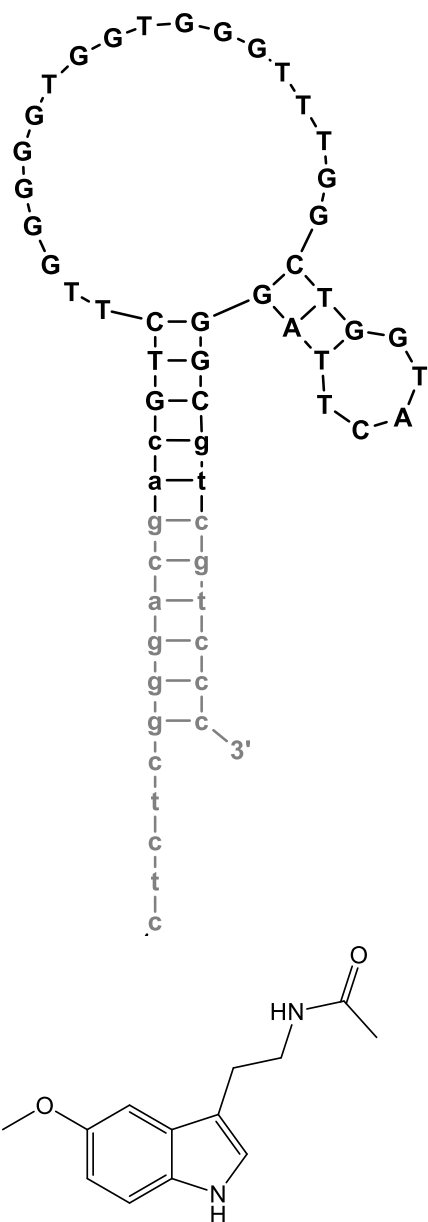| K_A (nM)	HC	K'_X		HC	α	K_X(comp)	K_X(allost)
54	0.774	1.2 μM		1	7.5	0.23	0.35

Figure. (Left) displacement and quenching curves plotted on the same graph; (Right) ThT displacement curve. For methods, see S.1.

Fig. S19.

Apt ID	Apt13/ MLTN-apt
Target , X	Melatonin, **13**
FAM Sensor, R	/56-FAM/CTC TCG GGA CGA CGT CTT GGG GGT GGT GGG TTT GGC TGG TAC TTA GGG CGT CGT CCC
Quencher Strand, A	CGT CGT CCC GAG AG/3Dab/ (10 times)
Truncated sequence	ACG TCT TGG GGG TGG TGG GTT TGG CTG GTA CTT AGG GCG T

Fitting parameters:

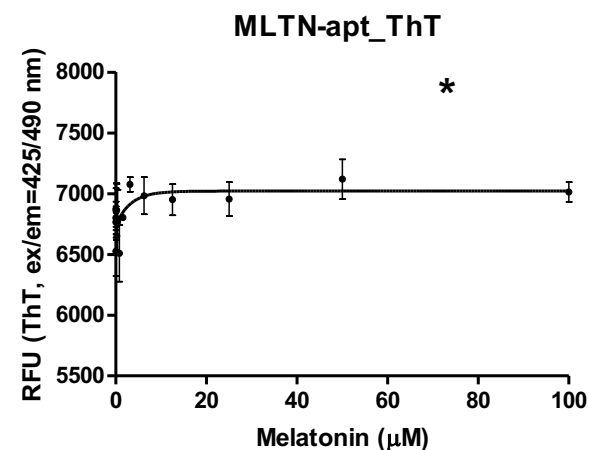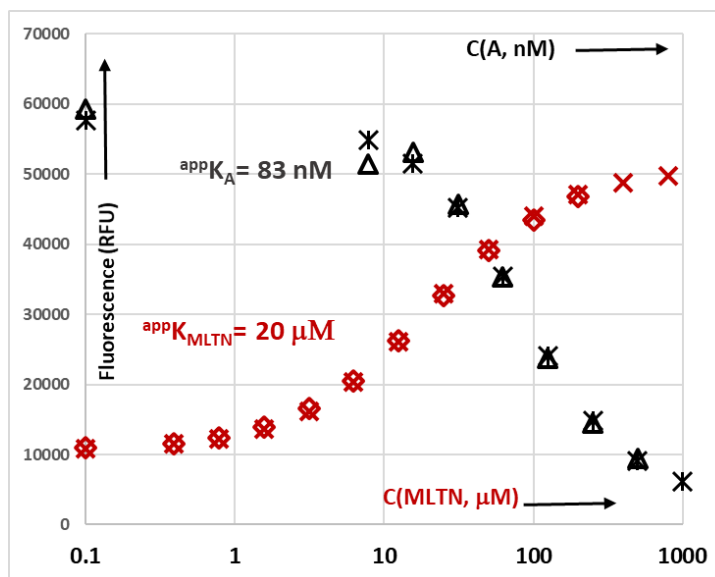| K_A (nM)	HC	K'_X		HC	α	K_X(comp)	K_X(allost)
83	1.23	20 µM		1	48	2.8	3.2

Figure. (Left) displacement and quenching curves plotted on the same graph; (Right) ThT displacement curve. For methods, see S.1.

This aptamer was one of the exceptions. It showed no displacement of the ThT dye but was selected for development because it was the most abundant.

Fig. S20.

Apt ID	Apt14 / DOPA-apt
Target, X	L-DOPA, (3,4-Dihydroxy-L-phenylalanine), **14**
FAM Sensor, R	/56-FAM/CTC TCG GGA CGA CGG CTG AAG TGT GTT CGT TCC GGT GGG AGT TGA TGG CGT CGT CCC
Quencher Strand, A	CCG TCG TCC CGA GAG /3Dab/ (5 times)
Truncated sequence	ACG ACG GCT GAA GTG TGT TCG TTC CGG TGG GAG TTG ATG GCG TCG T

Fitting parameters:

K_A (nM)	HC	K'_X		HC	α	K_X(comp)	K_X(allost)
69	1	16 µM		0.95	17.2	3.6	4.3

Figure. (Left) displacement and quenching curves plotted on the same graph; (Right) ThT displacement curve. For methods, see S.1.

Fig. S21.

Apt ID	Apt15 / NE-apt
Target, X	Norepinephrine, **15**
FAM Sensor, R	/56-FAM/CTC TCG GGA CGA CGG GGC ACA TTG TGC TAT TCA GTT GTT CCG CAG GAG AGT CGT CCC
Quencher Strand, X	GTC GTC CCG AGA G/3Dab/ (5 times)
Truncated sequence	ACG ACG GGG CAC ATT GTG CTA TTC AGT TGT TCC GCA GGA GAG TCG T

Fitting parameters:

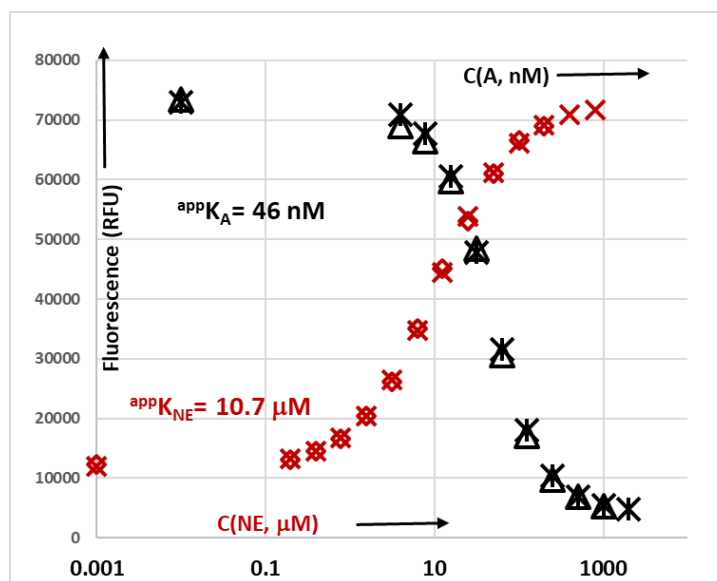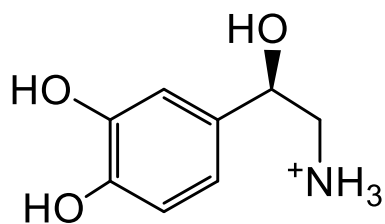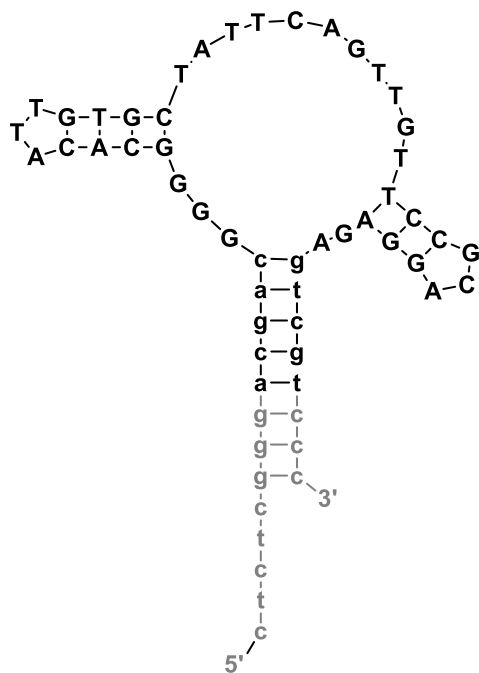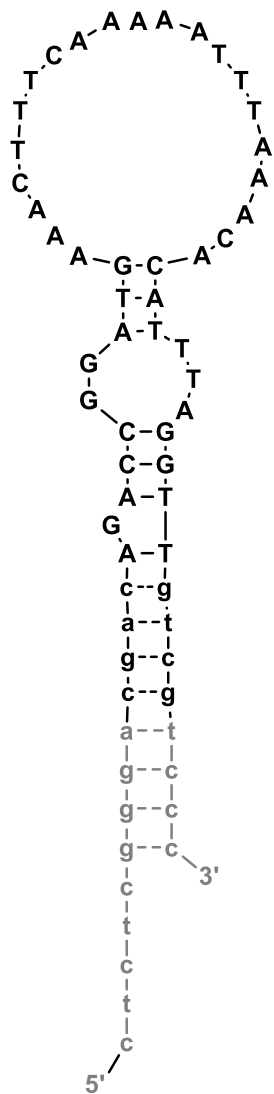| K_A (nM)	HC	K'_X		HC	α	K_X(comp)	K_X(allost)
46	1.4	10.74 μM		0.94	2196	1.67	1.67
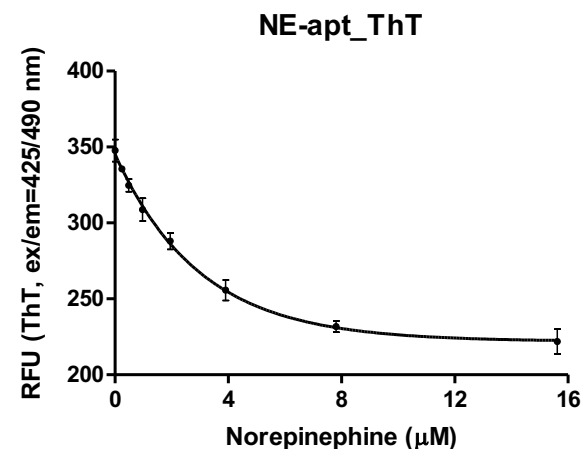
Figure. (Left) displacement and quenching curves plotted on the same graph; (Right) ThT displacement curve. For methods see S.1.

Fig. S22.

Apt ID	Apt16 / EPI-apt
Target , X	Epinephrine, **16**
FAM Sensor, R	/56-FAM/CTC TCG GGA CGA CAG ACC GGA TGA AAC TTT CAA AAA TTT AAA CAC ATT TAG GTT GTC GTC CC
Quencher Strand, A	TGT CGT CCC GAG AG/3Dab/ (10 times)
Truncated sequence	CGA CAG ACC GGA TGA AAC TTT CAA AAA TTT AAA CAC ATT TAG GTT GTC G

Fitting parameters:

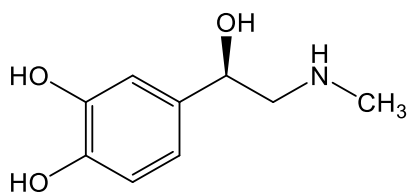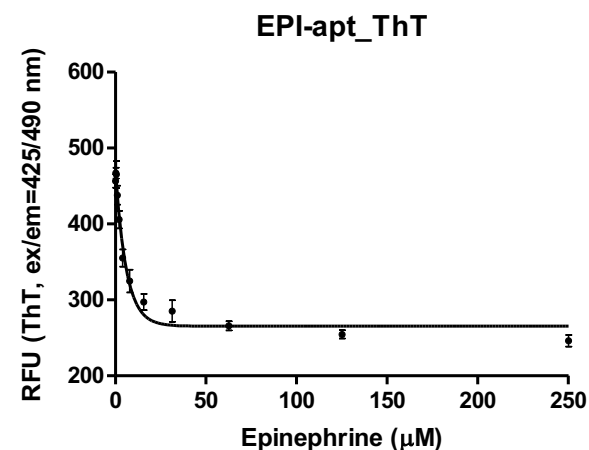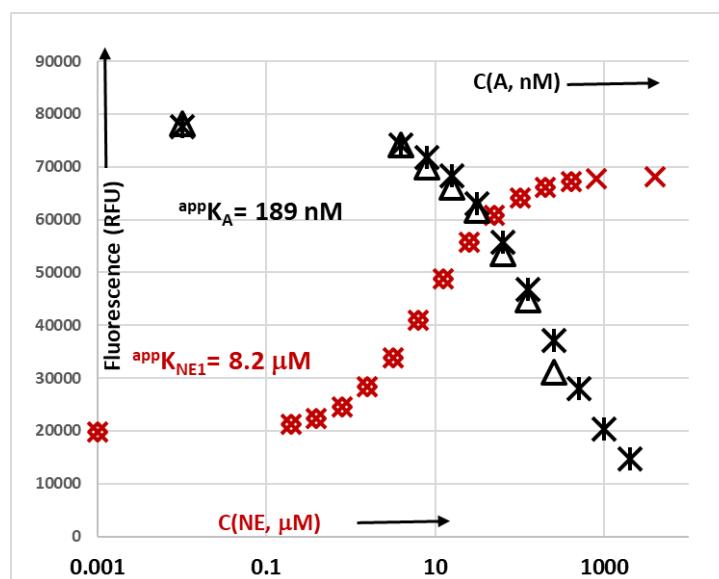| K_A (nM)	HC	K'_X		HC	α	K_X(comp)	K_X(allost)
189	0.77	8.2 μM		0.93	26	2.3	2.5

Figure. (Left) displacement and quenching curves plotted on the same graph; (Right) ThT displacement curve. For methods see S.1.

Fig. S23.

Apt ID	Apt17 / GABA-apt
Target, X	GABA (γ-Aminobutyric acid), **17**
FAM Sensor, R	/56-FAM/CTC TCG GGA CGA CCA CAC TCG CGC CTG TGC GAG CCA TGA GTT ATG GGA GGA TGC TGG GGT CGT CCC
Quencher Strand, A	GGT CGT CCC GAG AG/3Dab/ (3 times)
Truncated sequence	CGA CCA CAC TCG CGC CTG TGC GAG CCA TGA GTT ATG GGA GGA TGC TGG GGT CG

Fitting parameters:

K_A (nM)	HC	K'_X		HC	α	K_X(comp)	K_X(allost)
52	2	36 **mM**		0.91	11	11	13
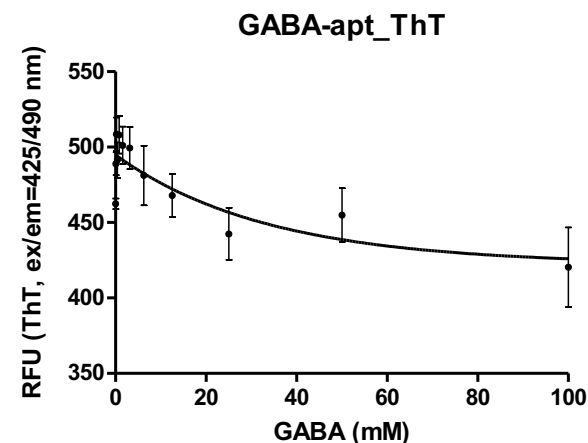
Figure. (Left) displacement and quenching curves plotted on the same graph; (Right) ThT displacement curve. For methods see S.1.

Note: this aptamer was isolated from N44 library, N36 consistently failed.

Fig. S24.

Apt ID	Apt18 / GABM-apt
Target, X	GABA-amid (4-Aminobutyramide hydrochloride), **18**
FAM Sensor, R	/56-FAM/CTC TCG GGA CGA CGT ACG GAT AAA GTG TCT CAG TTT ACC AGC GGT GTG GGT CGT CCC
Quencher Strand, A	CGT CGT CCC GAG AG/3Dab/ (5 times)
Truncated sequence	ACG ACG TAC GGA TAA AGT GTC TCA GTT TAC CAG CGG TGT GGG TCG T

Fitting parameters:

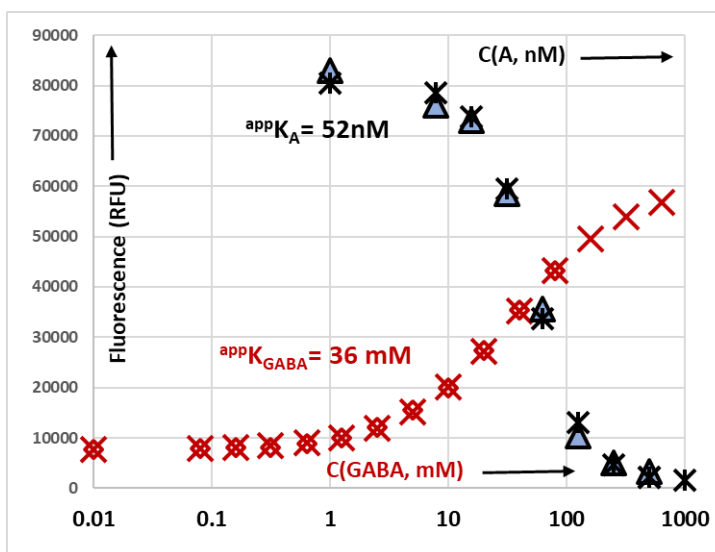| K_A (nM)	HC	K'_X		HC	α	K_X(comp)	K_X(allost)
69	1.2	705	μM	0.9	32	152	170

Figure. (Left) displacement and quenching curves plotted on the same graph; (Right) ThT displacement curve. For methods see S.1.

Fig. S25.

Apt ID	Apt19 / GLN-apt
Target, X	Glutamine, **19**
FAM Sensor, R	/56-FAM/CTC TCG GGA CGA CTA CCG GAT GTT GTC CTG GAG CAG TCG GTC GGA GGT TGT CGT CCC
Quencher Strand, A	GGT CGT CCC GAG AG/3Dab/ (10 times)
Truncated sequence	ACG ACT ACC GGA TGT TGT CCT GGA GCA GTC GGT CGG AGG TTG TCG T

Fitting parameters:

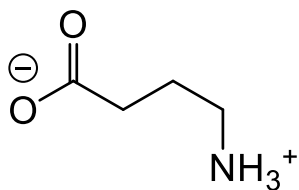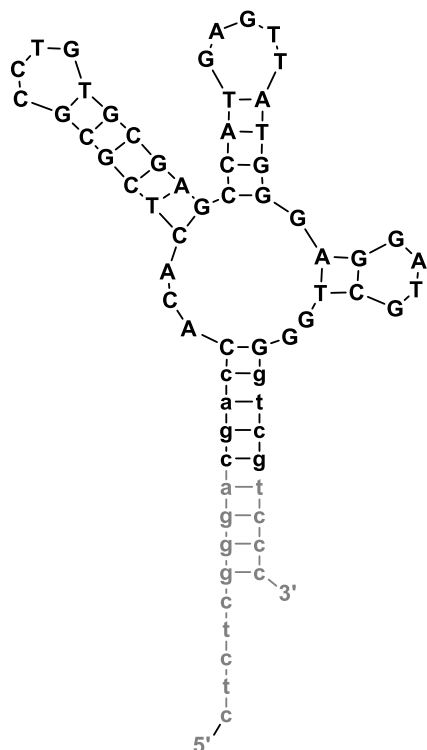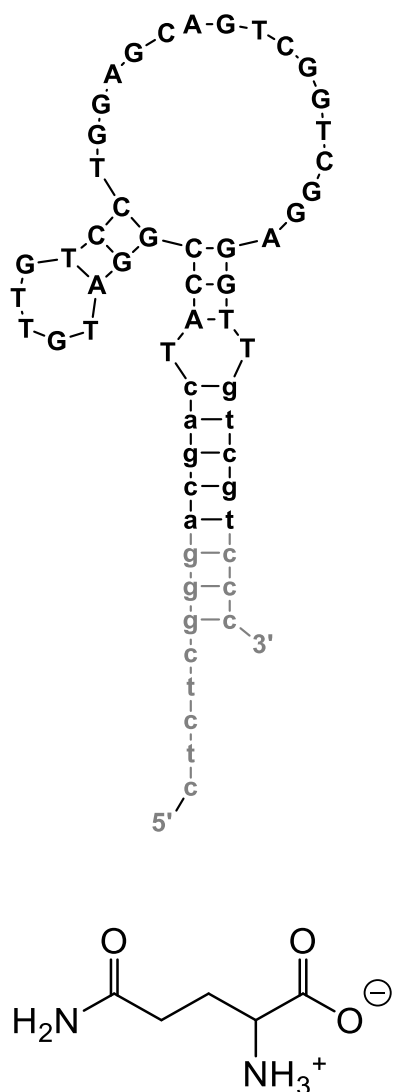| K_A (nM)	HC	K'_X		HC	α	K_X(comp)	K_X(allost)
125	1	0.77	**mM**	1	73	0.15	0.16

Figure. (Left) displacement and quenching curves plotted on the same graph; (Right) ThT displacement curve. For methods see S.1.

Fig. S26.
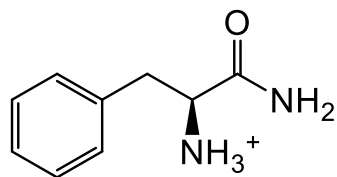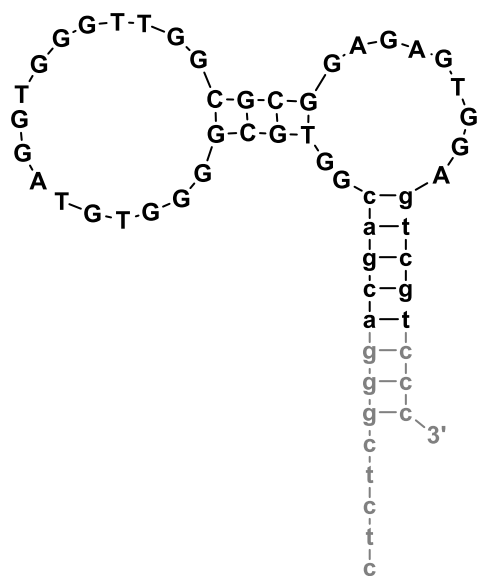
Apt ID	**Apt20 / PHMD-apt**
Target , X	Phenylalaninamide, **20**
FAM Sensor, R	/56-FAM/CTC TCG GGA CGA CGG TGC GGG GTG TAG GTG GGT TGG CGC GGA GAG TGG AGT CGT CCC
Quencher Strand, A	CGT CGT CCC GAG AG/3Dab/ (5 times)
Truncated sequence	ACG ACG GTG CGG GGT GTA GGT GGG TTG GCG CGG AGA GTG GAG TCG T

Fitting parameters:

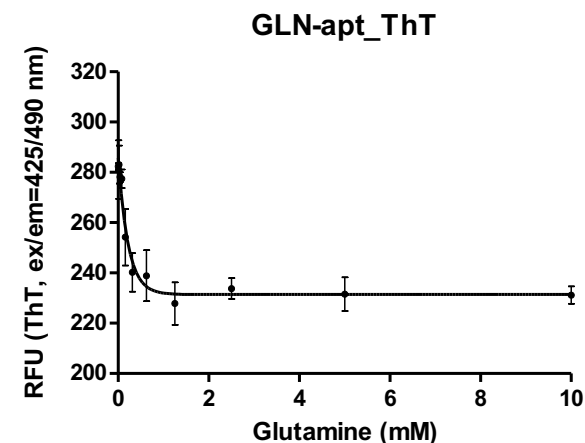| K_A (nM)	HC	K'_X		HC	α	K_X(comp)	K_X(allost)
59	1.8	2	µM	1	1000	0.38	0.39

Figure. (Left) displacement and quenching curves plotted on the same graph; (Right) ThT displacement curve. For methods see S.1.

Fig. S27.

Apt ID	Apt21 / TYRA-apt
Target, X	Tyrosinamide, **21**
FAM Sensor, R	/56-FAM/CTC TCG GGA CGA CCG GTT GGT GGG TGT TTG AGT GCG GTG CCC GGA GAT GGT CGT CCC
Quencher Strand, A	GGT CGT CCC GAG AG/3Dab/ (10 times)
Truncated sequence	GAC CGG TTG GTG GGT GTT TGA GTG CGG TGC CCG GAG ATG GTC

Fitting parameters:

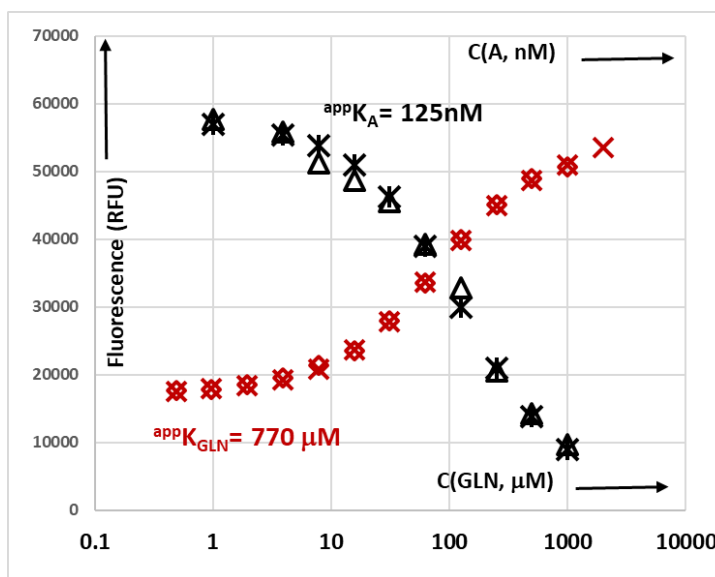| K_A (nM)	HC	K'_X		HC	α	K_X(comp)	K_X(allost)
200.00	1.4	0.756 μM		1	20.46	0.22	0.24

Figure. (Left) displacement and quenching curves plotted on the same graph; (Right) ThT displacement curve. For methods see S.1.

Fig. S28.
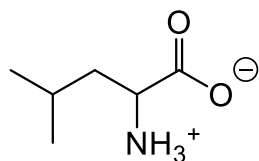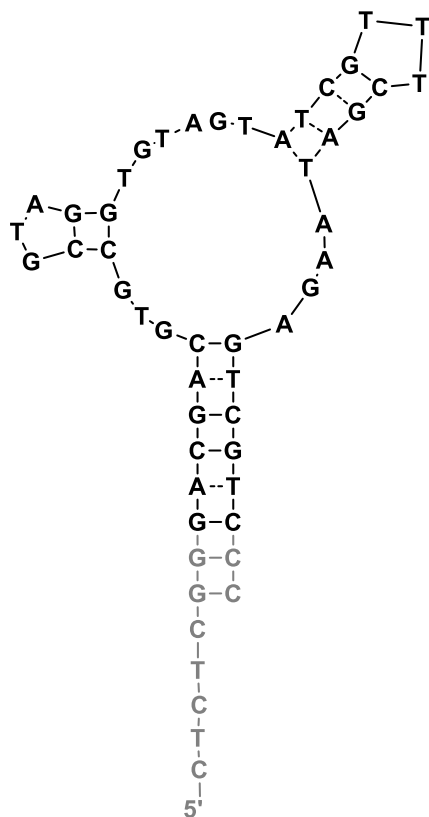
Apt ID	Apt01 / Leu 2.1 apt
Target, X	Leucine, **1**. LEU
FAM Sensor, R	/56-FAM/CTC TCG GGA CGA CGT GCC GTA GGT GTA GTA TCG TTT CGA TAA GAG TCG TCC C
Quencher Strand, A	CGT CGT CCC GAG AG/3Dab/ (10 times)
Truncated sequence	GAC GAC GTG CCG TAG GTG TAG TAT CGT TTC GAT AAG AGT CGT C

Fitting parameters:

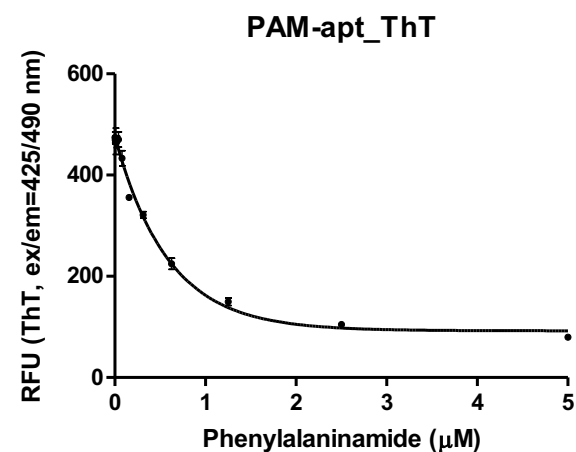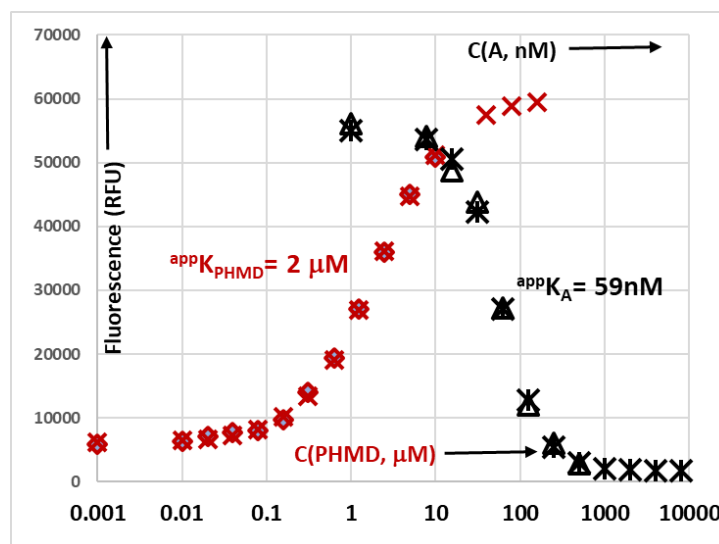| K_A (nM)	HC	K'_X		HC	α	K_X(comp)	K_X(allost)
88	1.1	63 **mM**		0.92	198	9.4	9.7

Figure. (Left) displacement and quenching curves plotted on the same graph; (Right) ThT displacement curve. For methods see S.1.

Fig. S29.

Apt ID	Apt23 / TYR-apt
Target, X	Tyrosine, **23**
FAM Sensor, R	/56-FAM/CTC TCG GGA CGA CGG GGA GGG AGT CCA ATC GAG TGT TAT GGA GGA GCC GTG TCG TCC C
Quencher Strand, A	GTC GTC CCG AGA G/3Dab/ (10 times)
Truncated sequence	ACG ACG GGG AGG GAG TCC AAT CGA GTG TTA TGG AGG AGC CGT GTC GT

Fitting parameters:

| K_A (nM)	HC	K'_X		HC	α	K_X(comp)	K_X(allost)
85	1	9.4 μM		1	19	1.4	1.8

Figure. (Left) displacement and quenching curves plotted on the same graph; (Right) ThT displacement curve. For methods see S.1.

Fig. S30.

Apt ID	Apt24 / TYRA-apt
Target, X	Tyramine, **24**
FAM Sensor, R	/56-FAM/CTC TCG GGA CGA CGG GGA GGA GTT AGT ATG ACG GCA ACT TTA GTA CTT CGT CGT CCC
Quencher Strand, A	GTC GTC CCG AGA G/3Dab/ (5 times)
Truncated sequence	CGA CGG GGA GGA GTT AGT ATG ACG GCA ACT TTA GTA CTT CGT CG

Fitting parameters:

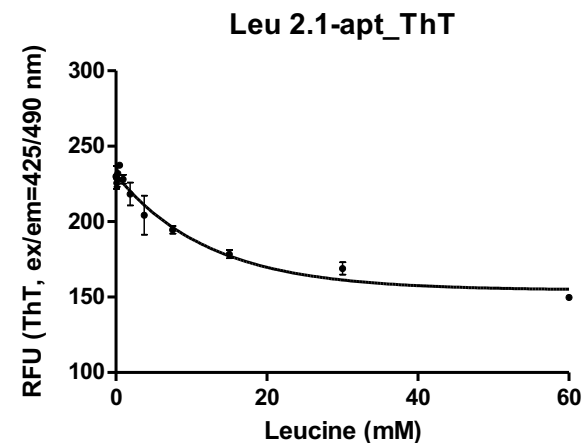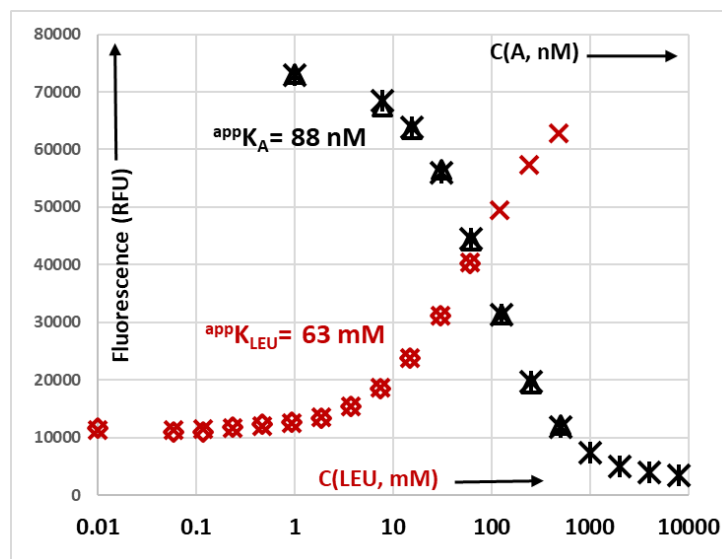| K_A (nM)	HC	K'_X		HC	α	K_X(comp)	K_X(allost)
56	1.51	39.3 μM		0.97	43	7.5	8.2

Figure. (Left) displacement and quenching curves plotted on the same graph; (Right) ThT displacement curve. For methods see S.1.

Fig. S31.

Apt ID	Apt25 / AMT-apt
Target , X	Agmatine, **25**
FAM Sensor, R	/56-FAM/CTC TCG GGA CGA CGG CAG AAG GTC ACG AGT CTT GCG AGC TCA CAC TGG GGT CGT CCC
Quencher Strand, A	CGT CGT CCC GAG AG/3Dab/ (10 times)
Truncated sequence	ACG ACG GCA GAA GGT CAC GAG TCT TGC GAG CTC ACA CTG GGG TCG T

Fitting parameters:

K_A (nM)	HC	K'_X		HC	α	K_X(comp)	K_X(allost)
45	0.88	2.45	**μM**	0.87	9	0.21	0.48

Figure. (Left) displacement and quenching curves plotted on the same graph; (Right) ThT displacement curve. For methods see S.1.

Fig. S32.

Apt ID	**Apt26 / ARG-apt**
Target , X	Arginine, **26**
FAM Sensor, R	/56-FAM/CTC TCG GGA CGA CGG TCG CAC GCG CTG GCG ATG TGT CCT TGG ATA CAT GGT CGT CCC
Quencher Strand , A	GTC GTC CCG AGA G/3Dab/ (5 times)
Truncated sequence	ACG ACG GTC GCA CGC GCT GGC GAT GTG TCC TTG GAT ACA TGG TCG T

Fitting parameters:

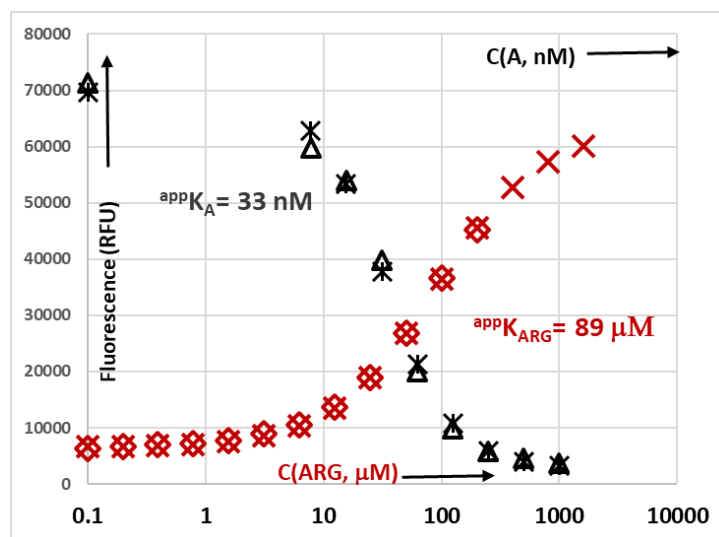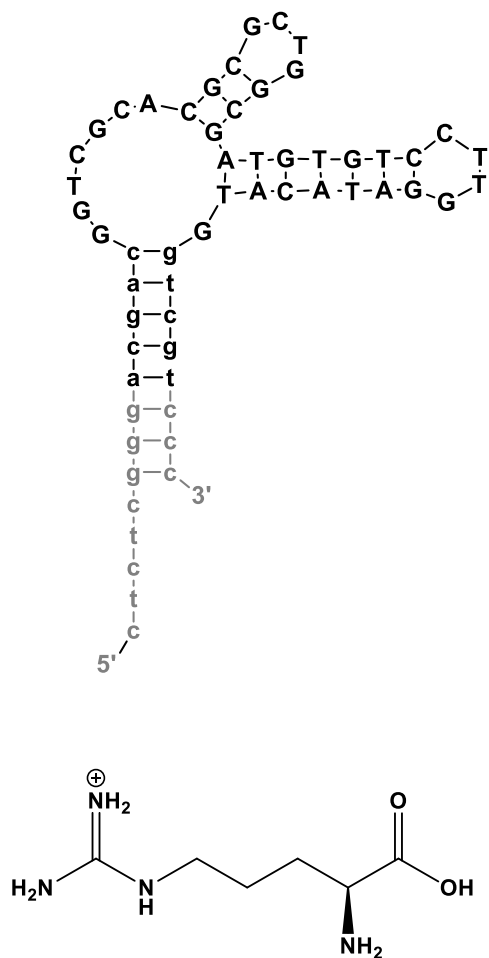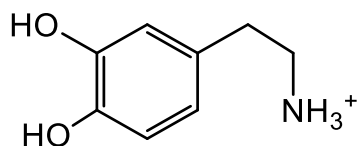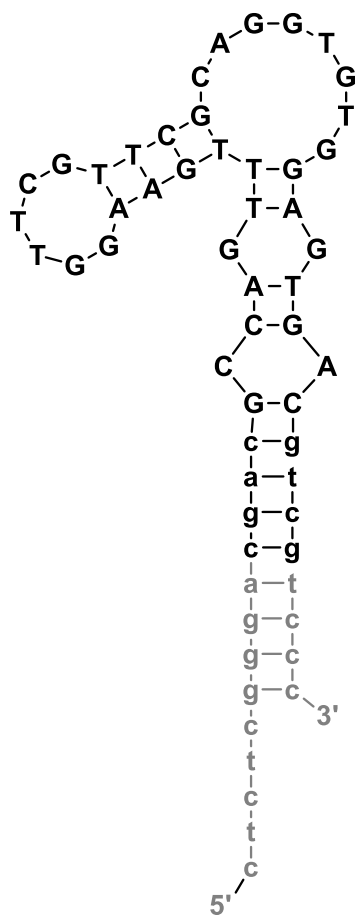| K_A (nM)	HC	K'_X		HC	α	K_X(comp)	K_X(allost)
33	1.5	89 μM		1	77	11	12
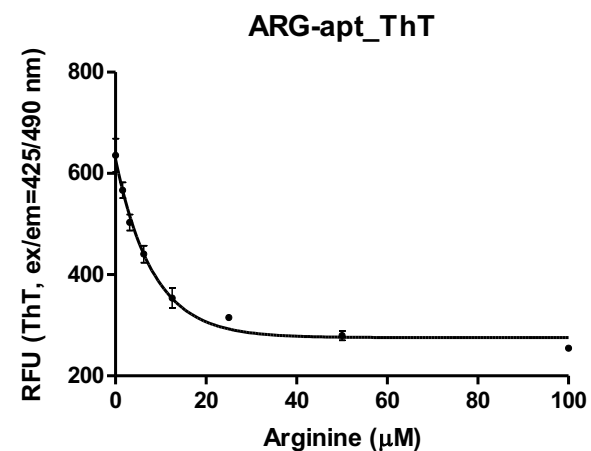
Figure. (Left) displacement and quenching curves plotted on the same graph; (Right) ThT displacement curve. For methods see S.1.

Fig. S33.

Apt ID	Apt27/ DA-apt
Target , X	Dopamine, **27**
FAM Sensor, R	/56-FAM/CTC TCG GGA CGA CGC CAG TTT GAA GGT TCG TTC GCA GGT GTG GAG TGA CGT CGT CCC
Quencher Strand , A	CGT CGT CCC GAG AG/3Dab/ (5 times)
Truncated sequence	CGA CGC CAG TTT GAA GGT TCG TTC GCA GGT GTG GAG TGA CGT CG

Fitting parameters:

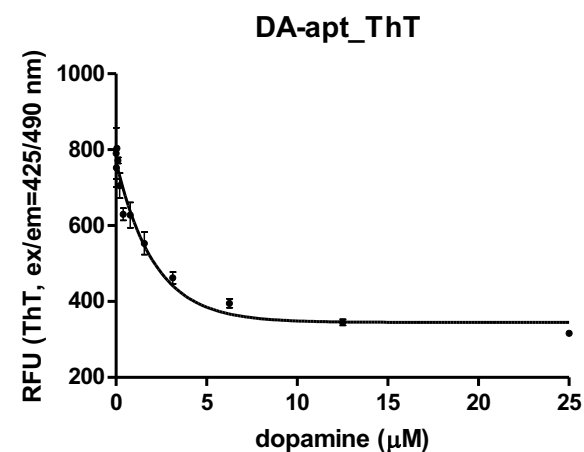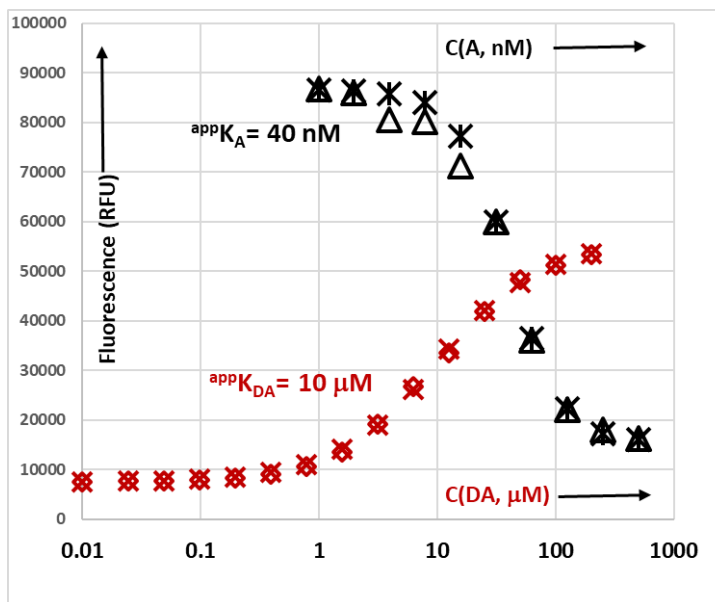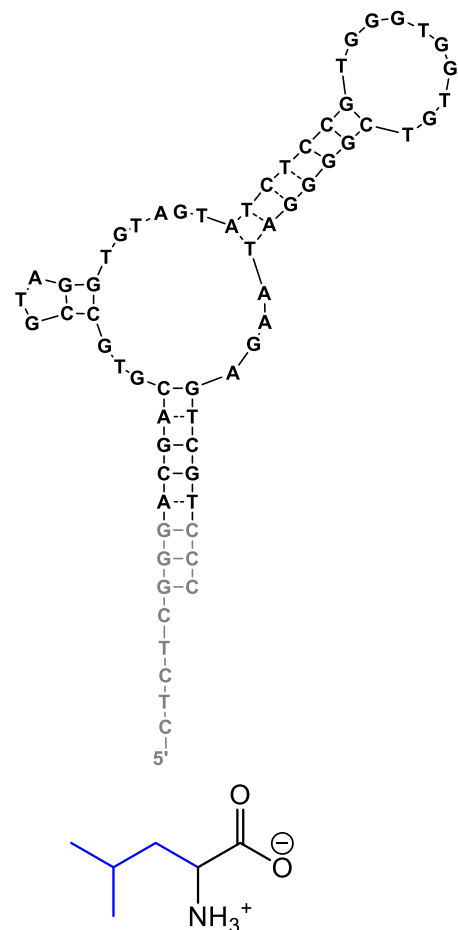| K_A (nM)	HC	K'_X		HC	α	K_X(comp)	K_X(allost)
40	2	10 μM		1	9	1.6	2.6

Figure. (Left) displacement and quenching curves plotted on the same graph; (Right) ThT displacement curve. For methods see S.1.

Fig. S34.

Apt ID	Apt01 / Leu 2.0-apt
Target , X	Leucine, **1**
FAM Sensor, R	/56-FAM/CTC TCG GGA CGA CGT GCC GTA GGT GTA GTA TCT CCG TGG GTG GTG TCG GGG ATA AGA GTC GTC CC
Quencher Strand, A	CGT CGT CCC GAG AG/3Dab/ (10 times)
Truncated sequence	ACG ACG TGC CGT AGG TGT AGT ATC TCC GTG GGT GGT GTC GGG GAT AAG AGT CGT

Fitting parameters:

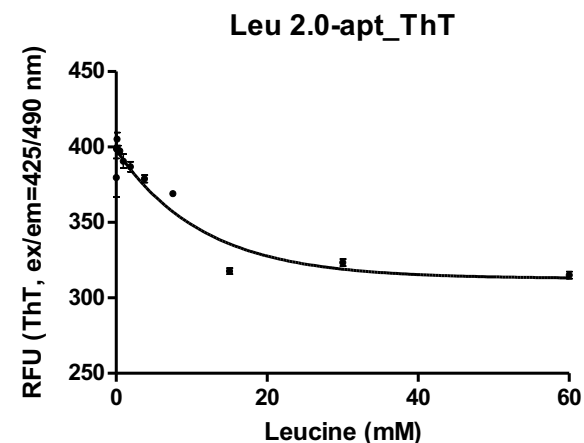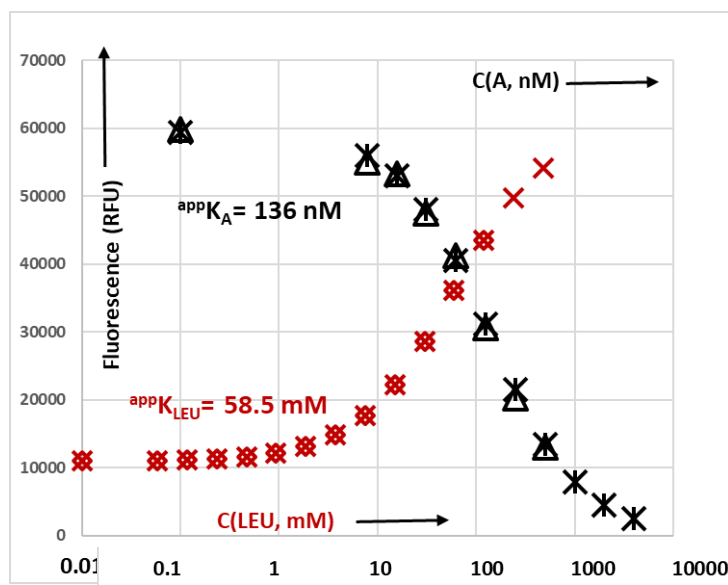| K$_A$ (nM)	HC	K'$_X$		HC	α	K$_X$(comp)	K$_X$(allost)
136.00	0.97	58.5	mM	0.9	1000	12.47127	12.5173

Figure. (Left) displacement and quenching curves plotted on the same graph; (Right) ThT displacement curve. For methods see S.1.

Referenced in the main text as, "(Fig. 3C, this structure had a large stem-loop eliminated, cf. the original aptamer in S-D-28)".

Fig. S35.

Apt ID	Vor 1.0, (Vor-apt)
Target, X	Voriconazole, **2**, **VOR** (cat no. 32483)
FAM Sensor, R	/56-FAM/CTC TCG GGA CGA CGT AGC CGG TCA CGT AGC GAG CTC CCC CAA GGA GGT AGT CGT CCC
Quencher Strand, A	GTC GTC CCG AGA G/3Dab/ (10 times)
Truncated sequence	ACG ACG TAG CCG GTC ACG TAG CGA GCT CCC CCA AGG AGG TAG TCG T

Fitting parameters:

K_A (nM)	HC	K'_X		HC	α	K_X(comp)	K_X(allost)
150	1.1	70 μM		0.97	29	16.5	18.3

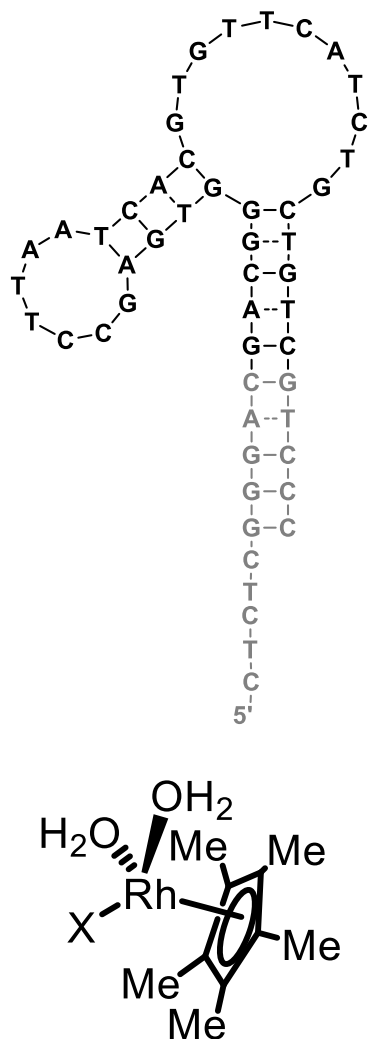**Figure.** (Left) displacement and quenching curves plotted on the same graph; (Right) ThT displacement curve. For methods see S.1.

Fig. S36.

Apt ID	**Vor 1.1,** Tailored from the Vor.1.0
Target, X	Voriconazole, **2**, VOR
FAM Sensor, R	/56-FAM/CTT GAC GTG ACG ACG TAG CCG GTT TCC GGC GAG CTC CCC CAA GGA GGT AGT CGT CAC
Quencher Strand, A	CGT CGT CAC GTC AAG /3Dab/ (5 times)
Truncated sequence	ACG ACG TAG CCG GTT TCC GGC GAG CTC CCC CAA GGA GGT AGT CGT

Fitting parameters:

K_A (nM)	HC	K'_X		HC	α	K_X(comp)	K_X(allost)
77	1.31	89 μM		0.95	58	21	23

Figure. (Left) displacement and quenching curves plotted on the same graph; (Right) ThT displacement curve. For methods see S.1.

Fig. S37.

Apt ID	CpRh 1.0
Target, X	Pentamethylcyclo-pentadienylrhodium(III) chloride, Cp*Rh(III), (cat. no, sigma 338370)
FAM Sensor, R	/56-FAM/CTC TCG GGA CGA CGG GTG AGC CTT AAT CAC GTG TTC ATC TGC TGT CGT CCC
Quencher Strand, A	GTC GTC CCG AGA G/3Dab/ (5 times)
Truncated sequence	GAC GGG TGA GCC TTA ATC ACG TGT TCA TCT GCT GTC

Fitting parameters:

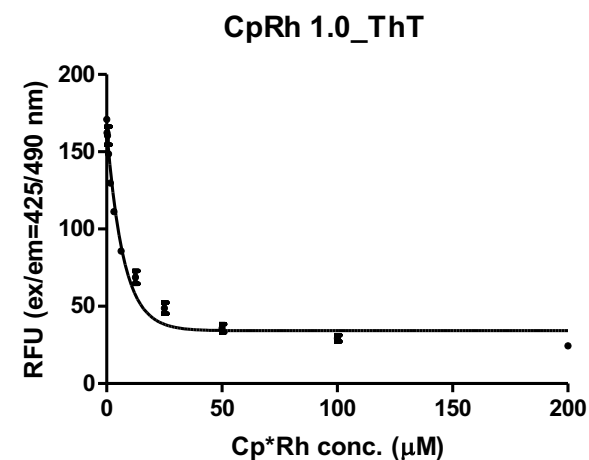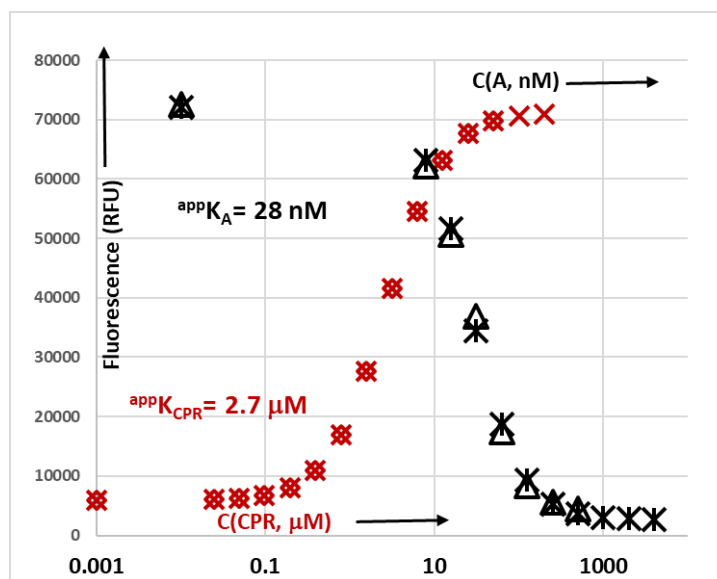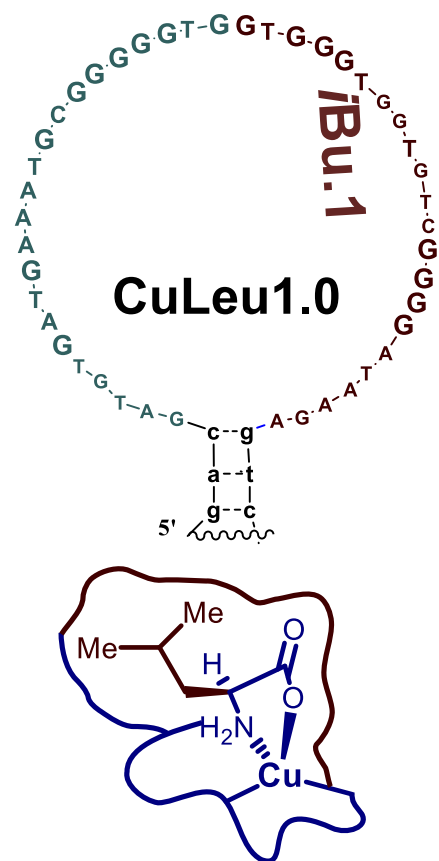| K_A (nM)	HC	K'_X		HC	α	K_X(comp)	K_X(allost)
28	1.5	2.7 μM		1.281	905	0.27	0.28

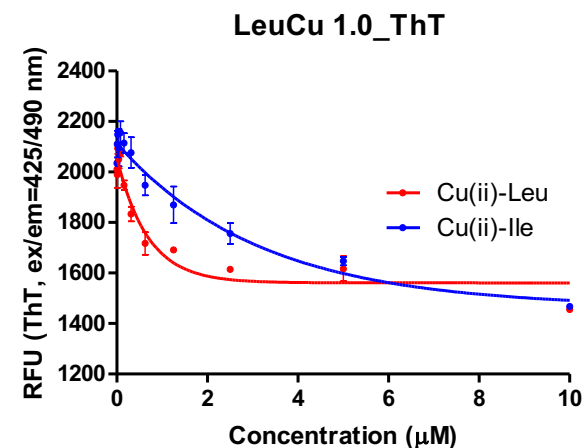**Figure.** (Left) displacement and quenching curves plotted on the same graph; (Right) ThT displacement curve. The monomer concentration of Cp*Rh is shown on the x-axis. For methods see S.1.

Fig. S38. Characterization of CpLeu1.0 Aptamer

Apt ID	CpLeu1.0
Target, X	Leu-Cp*Rh(iii), **14**
FAM Sensor, R	/56-FAM/CTC TCG GGA CGA CGG GTG AGC CTT AAT CGT GGG TGG TGT CGG GGA TAA GAA CGT GTT CAT CTG CTG TCG TCC C
Quencher Strand, A	GTC GTC CCG AGA G/3Dab/ (3 times)
Truncated sequence	GAC GGG TGA GCC TTA ATC GTG GGT GGT GTC GGG GAT AAG AAC GTG TTC ATC TGC TGT C

Oligonucleotide-displacement assay:

with constant amino acid:

with constant Cp*Rh(III):

ThT dye-displacement assay:

The "threshold" effect that is absent in "constant amino acid conditions" is consistent with the removal of bound (Cp*Rh(III) complex without amino acid from the aptamer and subsequent binding of **14**.

14

Fig. S39.

iBu.1

CuLeu1.0

Apt ID	CuLeu1.0
Target, X	Leu-Cu(ii)
FAM Sensor, R	/56-FAM/CTC TCG GGA CGA CGA TGT GAT GAA ATG CGG GGG TGG TGG GTG GTG TCG GGG ATA AGA GTC GTC CC
Quencher Strand, A	CGT CGT CCC GAG AG/3Dab/ (3 times)
Truncated sequence	ACG ACG ATG TGA TGA AAT GCG GGG GTG GTG GGT GGT GTC GGG GAT AAG AGT CGT

Fitting parameters:

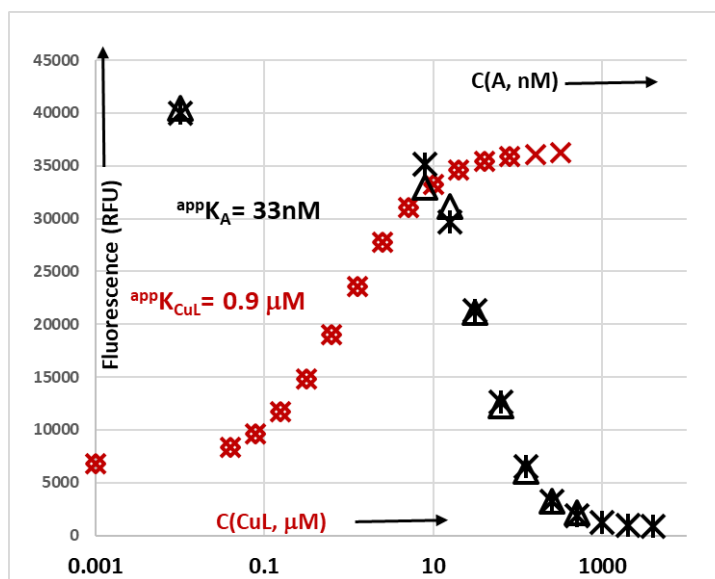| K$_A$ (nM)	HC	K'$_X$		HC	α	K$_X$(comp)	K$_X$(allost)
33.40	1.35	0.92	μM	0.9	52.11026	0.176453	0.190721

Figure. (Left) displacement and quenching curves plotted on the same graph; (Right) ThT displacement curve. For methods see S.1.

Fig. S40. Additional characterization of CuLeu1.0 Aptamer:

Figure. (**Left**) ThT displacement for Cu(II) only in comparison to Cu(II) +Leu. The x-axis is target, either Cu(II) only, or Cu(II), in the presence of constant Leu (100 μM; shows no displacement) or Leu in the presence of constant Cu(II) (40 μM); (**Right**) ThT dye displacement of Leu (only), in the absence of Cu(II). We also show selectivity over Ile. Of note, a high concentration of Leu is necessary to displace ThT.

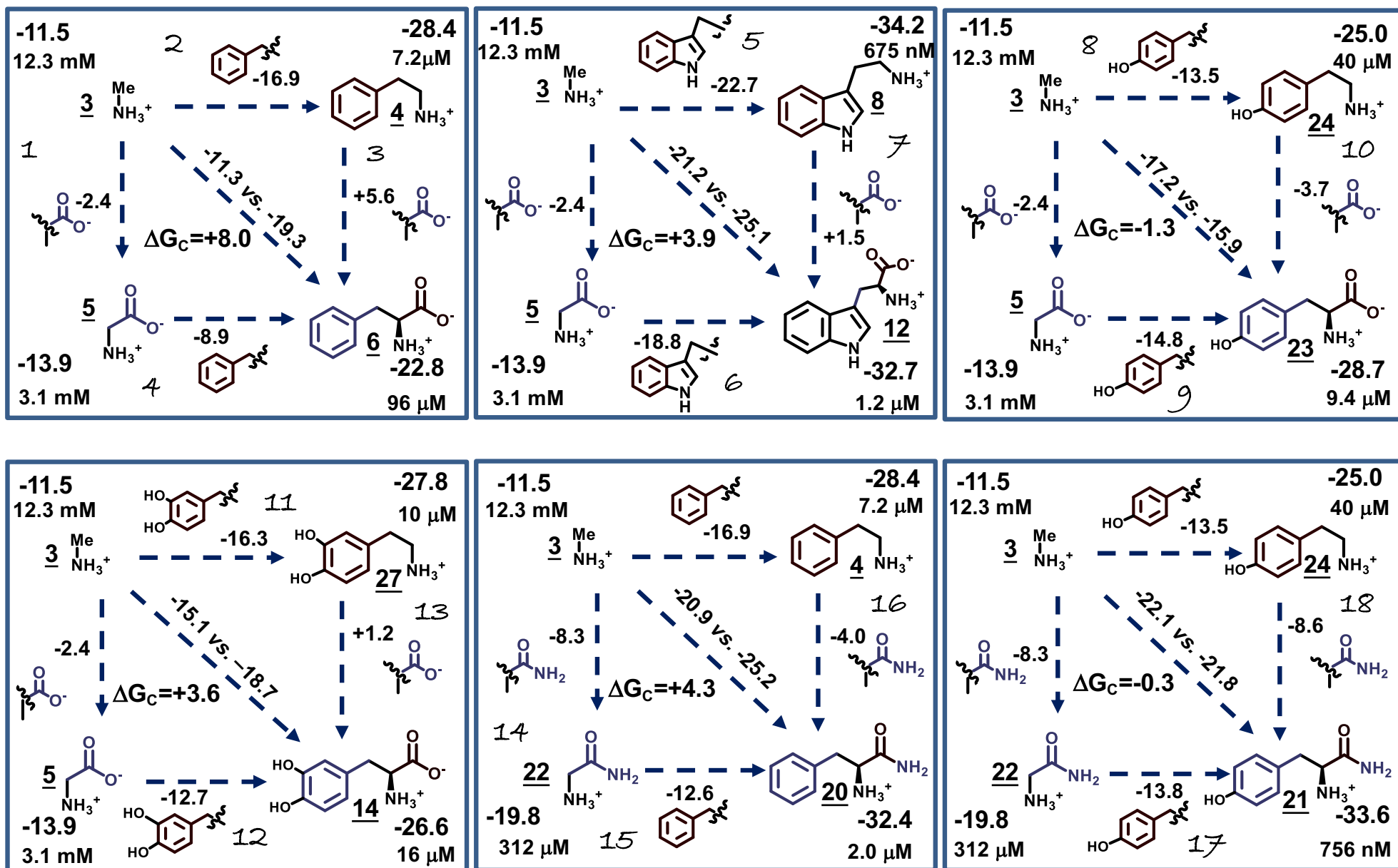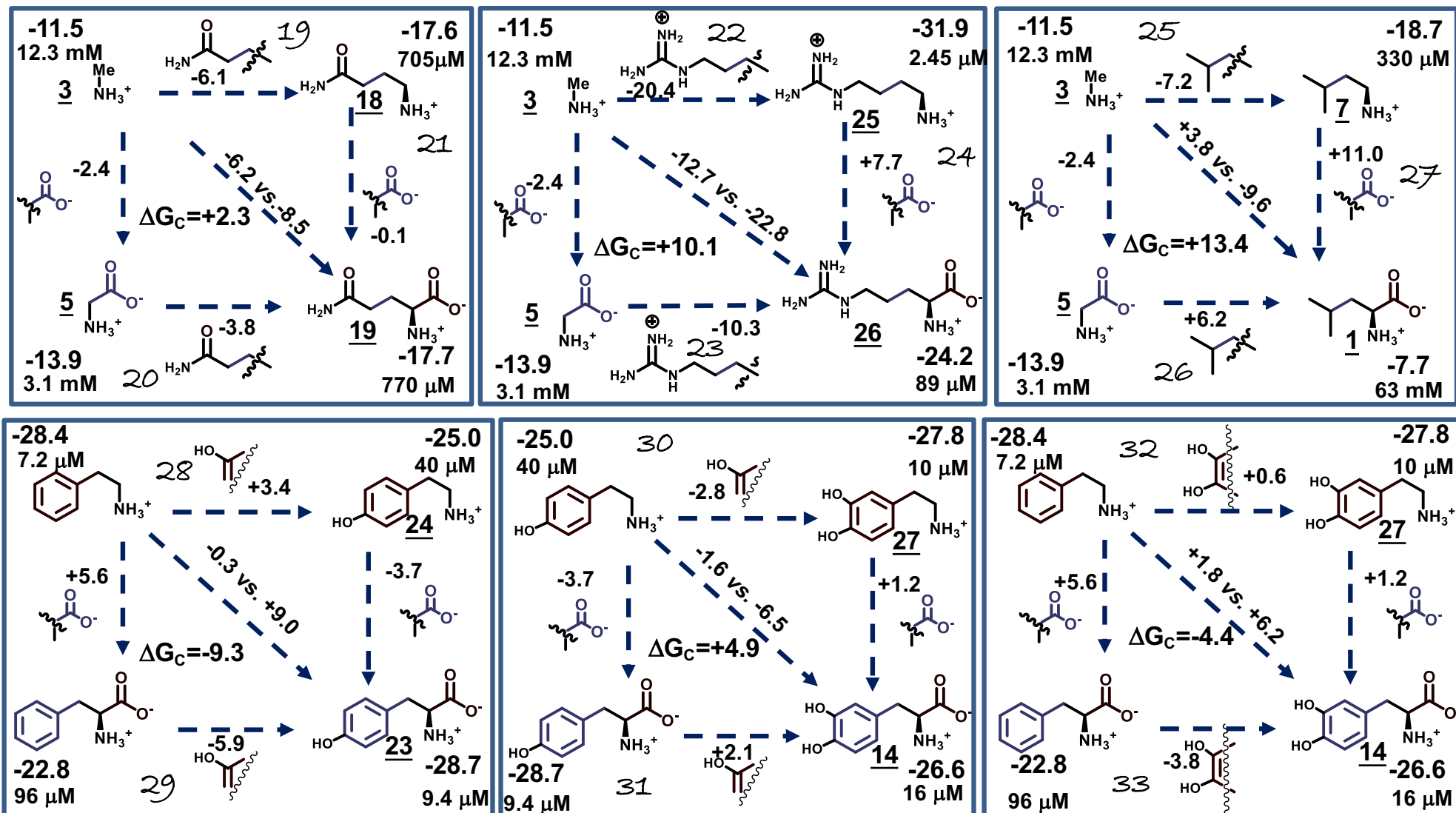**Fig. S41.** **Group binding energies from aptamer*ligand pairs and double functional group replacement cycles**

Key:

ΔG_D (kJ/mol)
(RT ln$^{aap}K_D$)

$^{app}K_D$
($X_{50\%}$)

Functional group added

$\Delta \Delta G_{GBE}$ (kJ/mol)
-13.9-(-11.5)

ΔG_D (actual)
(diagonal)
-22.8-(-11.5)

ΔG_D (calculated)
(adding sides)
-16.9+-2.4

-11.5
12.3 mM

2

-16.9

3   Me
       |
       NH$_3$$^+$

-28.4
7.2µM

4 NH$_3$$^+$

-11.3 vs. -19.3

1

-2.4

ΔG_C=+8.0

3

+5.6

5

-8.9

NH$_3$$^+$

-13.9
3.1 mM

4

6 NH$_3$$^+$

-22.8
96 µM

cooperativity
-19.3-(-11.3)

In this table we use uncorrected ΔG_D values

Fig. S42. Group binding energies from aptamer*ligand pairs and double functional group replacement cycles

In this table we use uncorrected ΔG_D values

Fig. S43.

Panel 1:
-11.5
12.3 mM
2
-16.9
-28.4
7.2 µM
3 Me NH₃⁺
4 NH₃⁺
1
3
-11.3 vs. -19.3
ΔG_C=+8.0
-2.4
+5.6
5 NH₃⁻
-8.9
6 NH₃⁺
4
-13.9
3.1 mM
-22.8
96 µM

Panel 2:
-11.5
12.3 mM
5
-22.7
-34.2
675 nM
3 Me NH₃⁺
8
7
-21.2 vs. -25.1
ΔG_C=+3.9
-2.4
+1.5
5 NH₃⁺
-18.8
12 NH₃⁺
6
-13.9
3.1 mM
-32.7
1.2 µM

Panel 3:
-11.5
12.3 mM
8 HO
-13.5
-25.0
40 µM
3 Me NH₃⁺
24 NH₃⁺
10
-17.2 vs. -15.9
ΔG_C=-1.3
-2.4
-3.7
5 NH₃⁺
-14.8
HO **23** NH₃⁺
9
-13.9
3.1 mM
-28.7
9.4 µM

Panel 4:
-11.5
12.3 mM
HO 11
HO
-16.3
-27.8
10 µM
3 Me NH₃⁺
HO HO **27** NH₃⁺
13
-15.1 vs. -18.7
ΔG_C=+3.6
-2.4
+1.2
5 NH₃⁺
-12.7
HO HO **14** NH₃⁺
12
-13.9
3.1 mM
-26.6
16 µM

Panel 5:
-11.5
12.3 mM
-16.9
-28.4
7.2 µM
3 Me NH₃⁺
4 NH₃⁺
16
-20.9 vs. -25.2
ΔG_C=+4.3
-8.3 NH₂
-4.0 NH₂
14
22 NH₂ NH₃⁺
-12.6
20 NH₃⁺
15
-19.8
312 µM
-32.4
2.0 µM

Panel 6:
-11.5
12.3 mM
HO
-13.5
-25.0
40 µM
3 Me NH₃⁺
HO **24** NH₃⁺
18
-22.1 vs. -21.8
ΔG_C=-0.3
-8.3 NH₂
-8.6 NH₂
22 NH₂ NH₃⁺
HO **21** NH₃⁺
17
-19.8
312 µM
-33.6
756 nM

ΔG_D values were corrected to average competitor
oligonucleotide contribution of 3.5 ± 0.7 kJ/mol.

Fig. S44.

ΔG_D values were corrected to average competitor oligonucleotide contribution of 3.5 ± 0.7 kJ/mol.
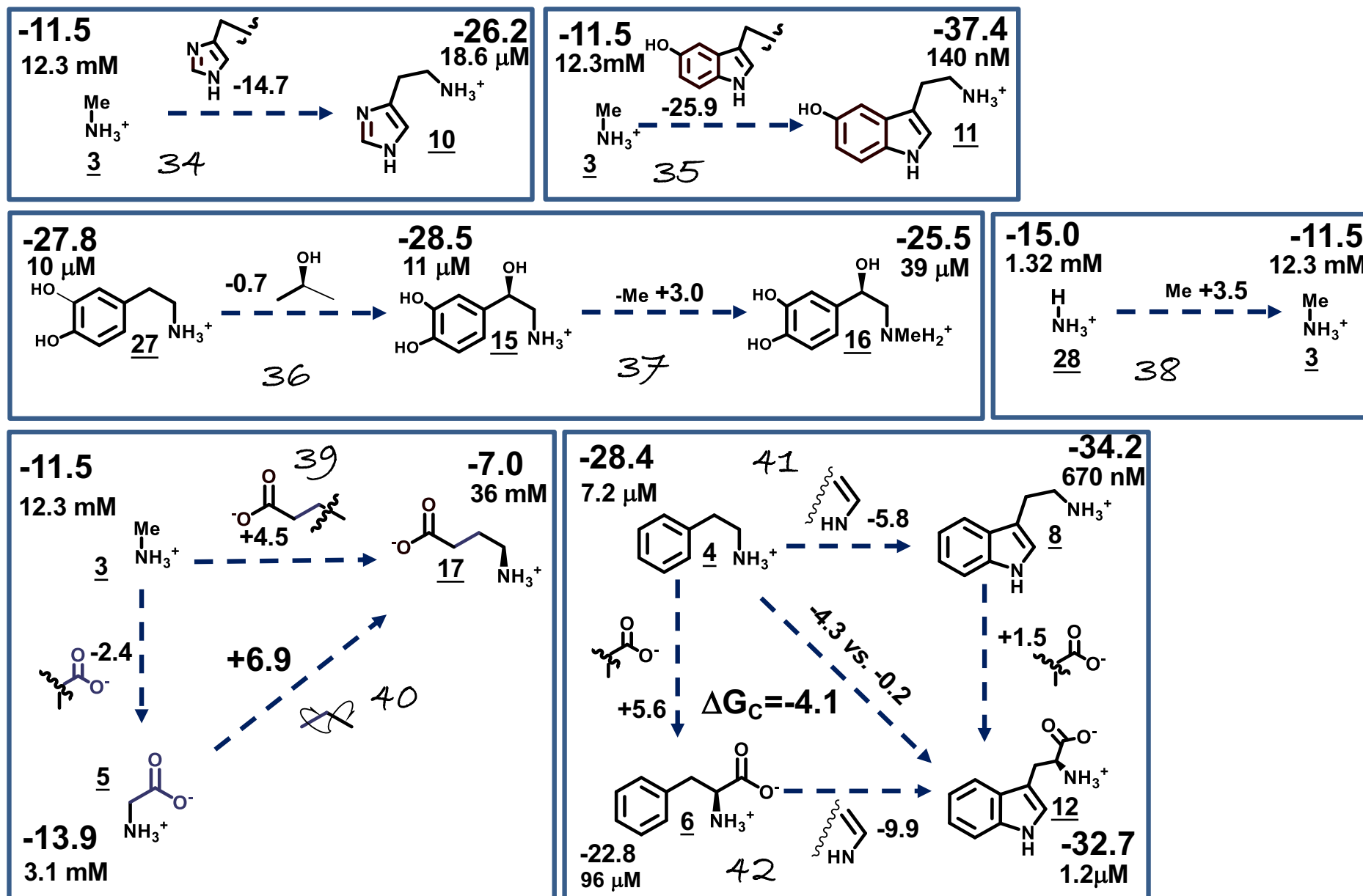
Fig. S45.

ΔG$_D$ values were corrected to average competitor oligonucleotide contribution of 3.5 ± 0.7 kJ/mol.

Fig. S46 (accompanying Fig. 2C)

Calculation of ΔG_B for melatonin based on similar fragments in our set:

Fig. 2C
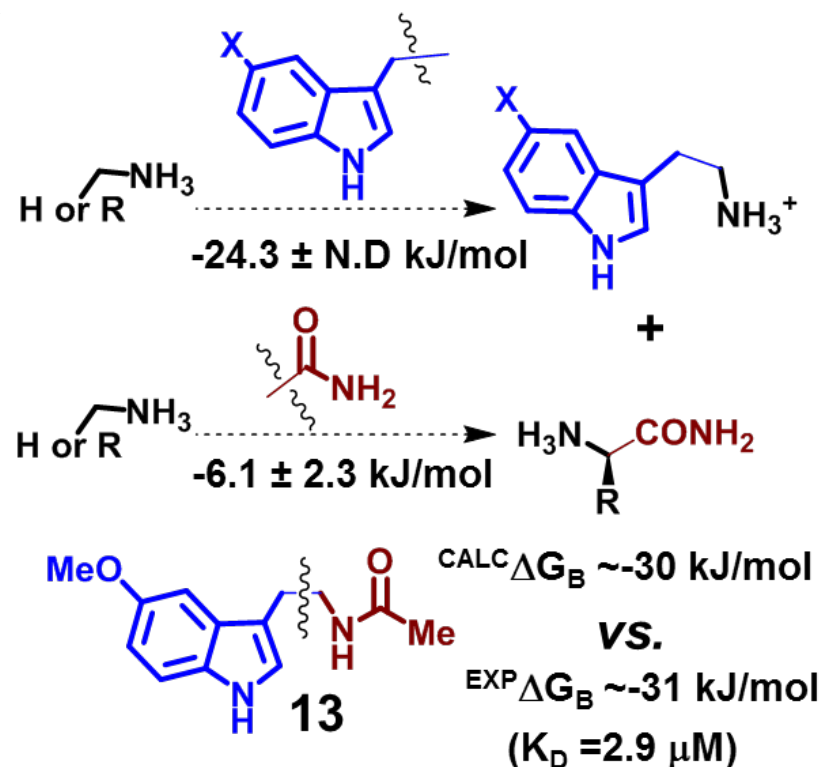
Legend, same as in the main text

Fig. S47. Values used to demonstrate additivity of group binding energies:

Values for amides:

Values for planar indoles:

Avg. $\Delta\Delta G_{GBE}$ =-6.1 +/- 2.3kJ/mol

Avg. $\Delta\Delta G_{GBE}$ = -24.3+/-N.D. kJ/mol

Total = -30.4 kJ/mol
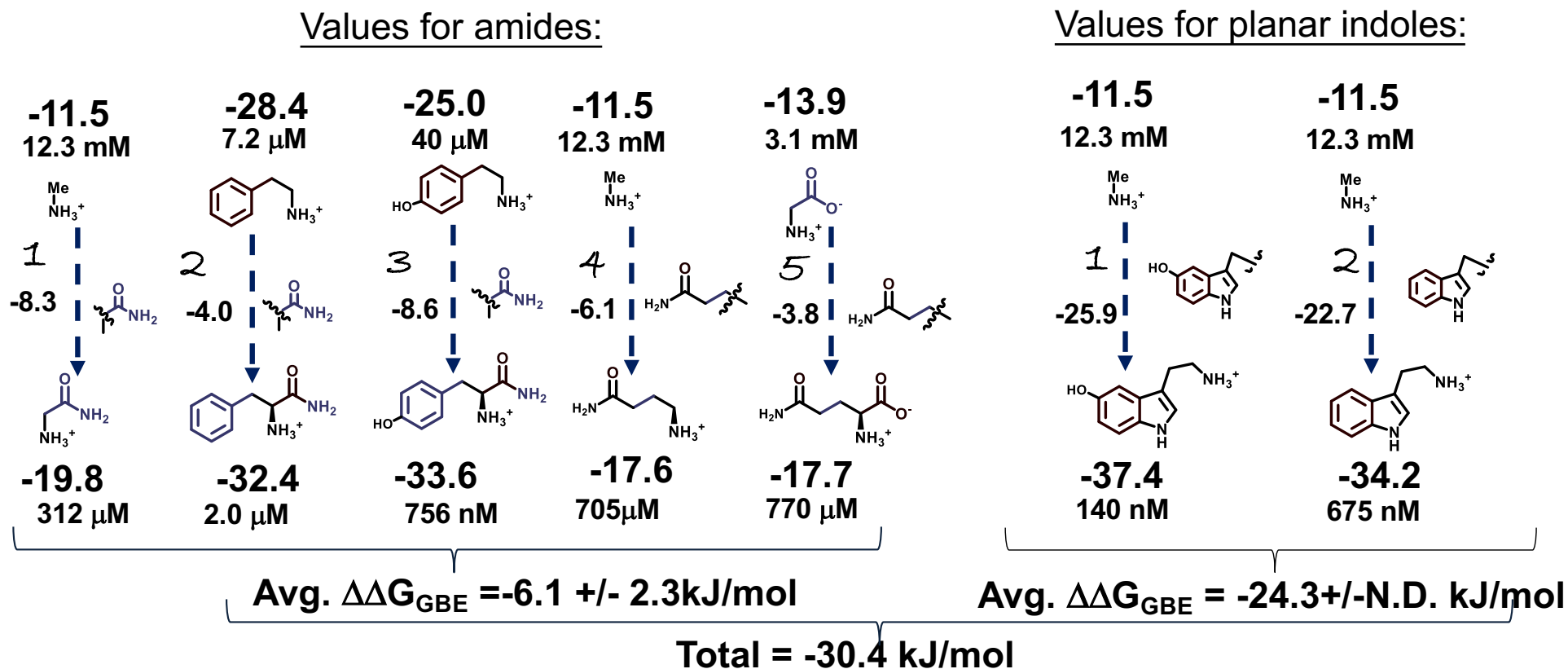
This is compared with experimental values of about -31 kJ/mol.

Note: Primary amides have the potential to form up to four hydrogen bonds, secondary only three. About 4, about 6 and about 8 kJ/mol (uncertainty aside) seem distributed like 2, 3, and 4 hydrogen bonds, with average of 6 kJ/mol being at about 3. This view is supported by larger number being associated with groups that would allow better fit with carboxamide additions (tyrosine and methylamine). Which could be why our average works so well in melatonin. This, of course, while consistent with functional group analysis, is a pure speculation, which would require structural methods to confirm it.

Fig. S48. Relationships:

(i) $\Delta G_D^{K'x}$ (avgAMD) $= \Delta G_D^{K'x}$ (MEA) $+ \Delta\Delta G_{GBE}^{AMD}$

(and) $\Delta G_D^{K'x}$ (avgIND) $= \Delta G_D^{K'x}$ (MEA) $+ \Delta\Delta G_{GBE}^{IND}$

(ii) $\Delta G_D^{K'x}$ (X) $= \Delta G_B^{Kx}$ (X) $+ \Delta G_E$ (COMP)

(iii) $\Delta\Delta G_{GBE}^{AMD} + \Delta\Delta G_{GBE}^{IND} = \Delta G_D^{K'x}$ (AMD) $+ \Delta G_D^{K'x}$ (IND) $- 2*\Delta G_D^{K'x}$ (MEA)

then from (i):

(iv) $\Delta\Delta G_{GBE}^{AMD} + \Delta\Delta G_{GBE}^{IND} = \Delta G_B^{Kx}$ (avgAMD) $+ \Delta G_B^{Kx}$ (avgIND) $- 2\Delta G_B^{Kx}$ (MEA) $= \Delta G_B^{Kx}$ (MLT)

(v) $\Delta G_D^{K'x}$ (MLT) $= \Delta G_B^{Kx}$ (MLT) $+ \Delta G_E$ (COMP) $= \Delta\Delta G_{GBE}^{AMD} + \Delta\Delta G_{GBE}^{IND} + \Delta G_E$ (COMP)

LEGEND:

$\Delta G_D^{K'x}$ (MEA)   For methylamine

$\Delta G_D^{K'x}$ (avgAMD)   For average amide, based on the set of five

$\Delta G_D^{K'x}$ (avgIND)   For average indole, based on the set of two

$\Delta G_D^{K'x}$ (MLT)   For melatonin

$\Delta\Delta G_{GBE}^{AMD}$

$\Delta\Delta G_{GBE}^{IND}$ Group binding energy contributions to displacement

ΔG_E (COMP)   Impact of complementary oligo on equilibrium, also:

ΔG_E (COMP) $= \Delta G_D^{K'x}$ (X) $- \Delta G_B^{Kx}$ (X)

$\Delta G_D^{K'x}$ (X)   Impact on equilibrium of target

ΔG_B^{Kx} (X)   Free energy of binding

Fig. S49.   Selectivity of Leu2.1:

Referenced in the main text as:

The Leu2.1 aptamer had a K_D of ~10 mM and an ~4:1 preference for Leu over Ile (S49).   and   Further, Leu2.1 had a higher affinity for phenylalanine than leucine (Fig. S49).
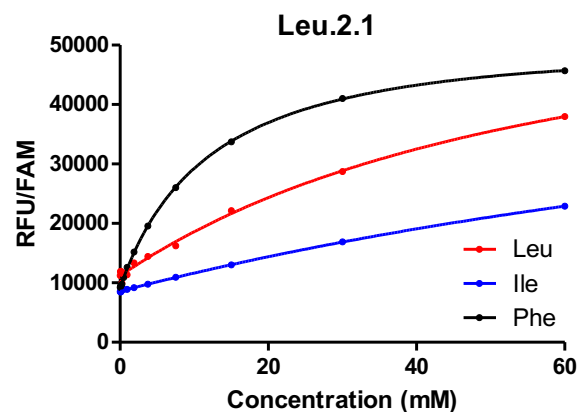

Target concentration-response curve in the displacement assay using Leu2.1, showing higher affinity for Phe.
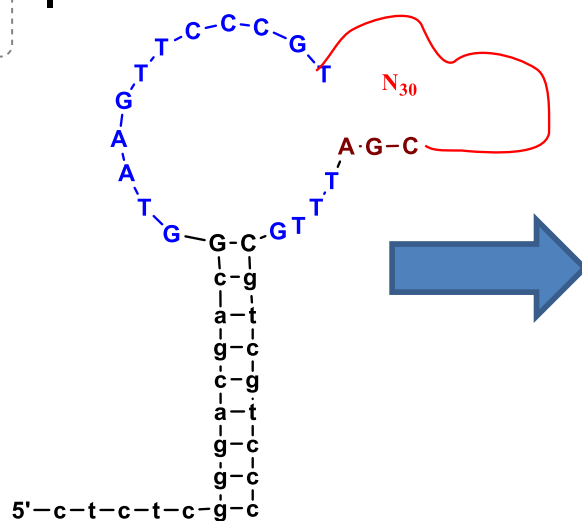
The Phe preference surprised us, because we were initially guided by a displacement assay per S38.

Fig. S50. Support for AAGA as "compatible" sequence, rather than absolutely necessary

Insertion reselection to eliminate Cu(II) binding site, S50, also generates aptamers related to Leu2.1:
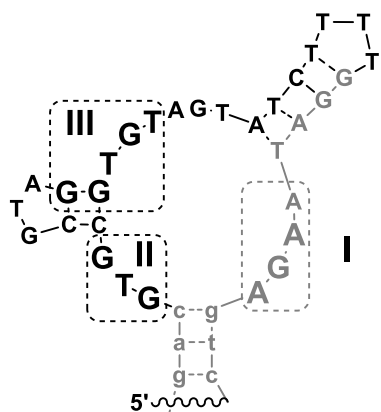
Leu2.1

See **SI-M-1**

Derived from: **Cu(II)-Leu (direct)- 2**.

Insert-Cu-Leu-1

K_A (nM)	HC	K'_X		HC	α	K_X(comp)	K_X(allost)
364.00	1.02	17.26	mM	0.88	65.8519	7.301295	7.452523
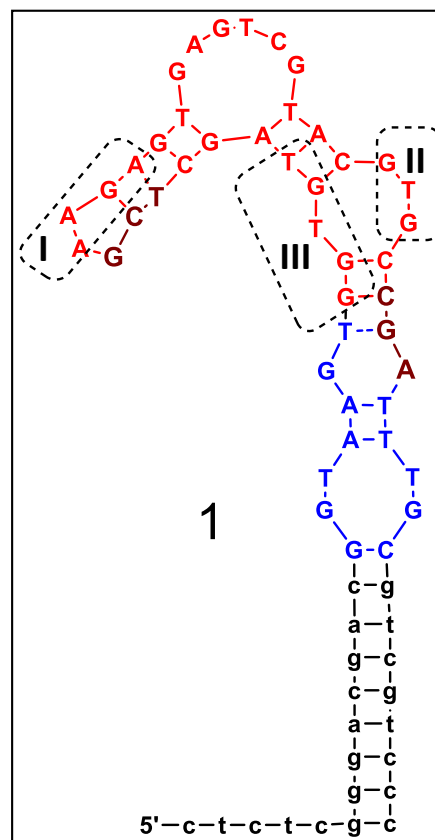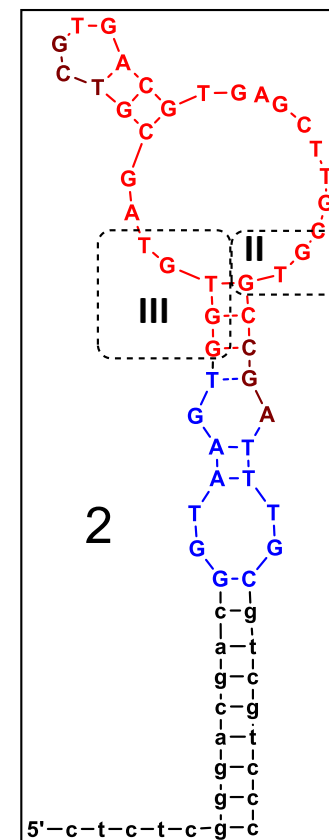
Insert-Cu-Leu-2

K_A (nM)	HC	K'_X		HC	α	K_X(comp)	K_X(allost)
467.00	0.74	10.64	mM	0.7694	14.98367	5.207102	5.56969

Comment: We hypothesize that the blue/brown-colored domain increases chances of capture of aptamers on column, while brown sequences provides a switching mechanism.

# Fig. S51. Direct selection for Leu aptamers using Cp*Rh(III) cofactor:

Results of earlier attempts to perform direct selections using only Cp*Rh(III) complex as a cofactor. On the left we have three related sequences that were identified as responsive to Leu, but preferred Phe. We tested all three, because hydrophobic pocket binding to side chain might be slightly adjusted. On the far right, we have a sequence isolated after counter-selecting with Phe; nevertheless, cross-reactivity persisted.
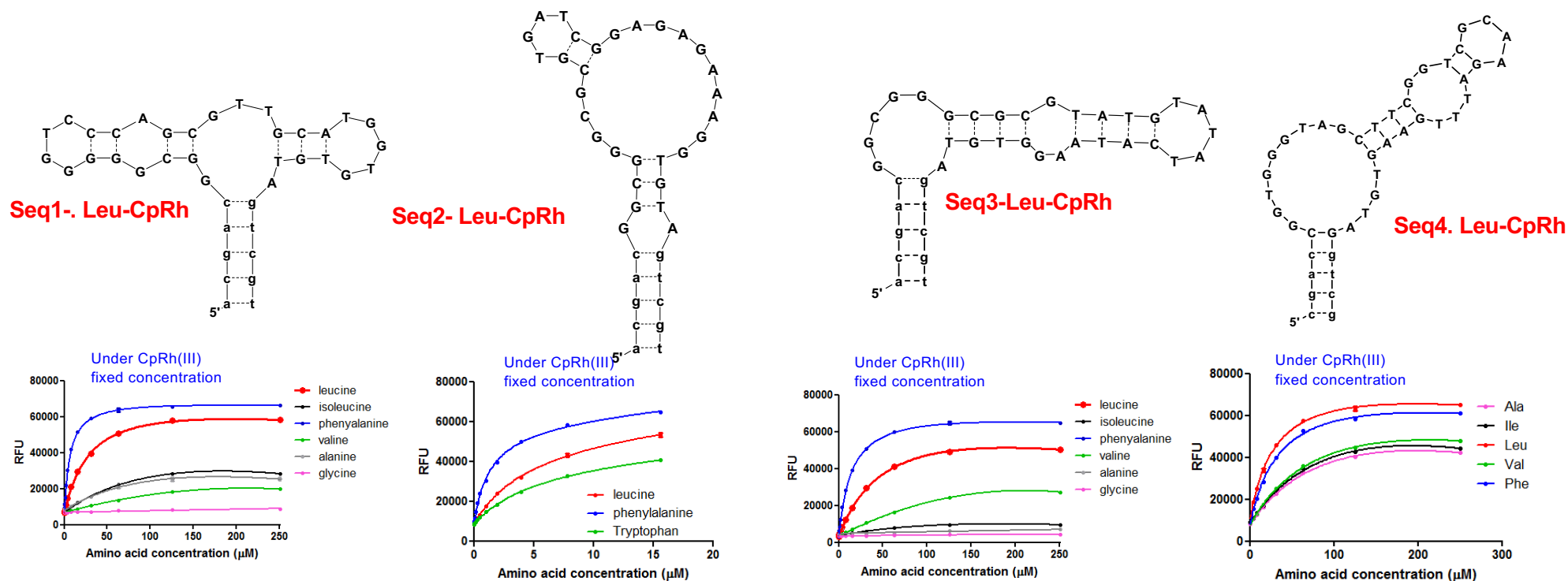
No. ID	Leu-CpRh, Sequence composition (5'-3')
N30 lib.	*GGA GGC TCT CGG G**AC GAC N(30)GTC GT**C CCG ATG CTG CAA TCG TAA*
1	ACG ACG GCG GGG GTC CCA GCG TTG CAT GGT GTG TAG TCG T
2	ACG ACG GCG GGC GCG TGA TCG GAG AGA AAG GTG TAG TCG T
3	ACG ACG GCG GGC GCG TAT GTA TAT CAT AAG GTG TAG TCG T
N36 lib	Same library used for other GBE aptamer isolation, with Phe/Ile counter-selection
4	-CG ACC GGT GGG TAG CTT CGG TCG CAA GAT TTG AAG TGT AGG TCG

Fig. S52. Newman projection explain specificity through a binding pocket model

Referenced in the main text as, "While **CuLeu1.0** had selectivity for leucine over isoleucine, valine, and phenylalanine, we noted strong cross-reactivity with *allo*-isoleucine (**Fig. 3E**, Newman projections in **S52**)."
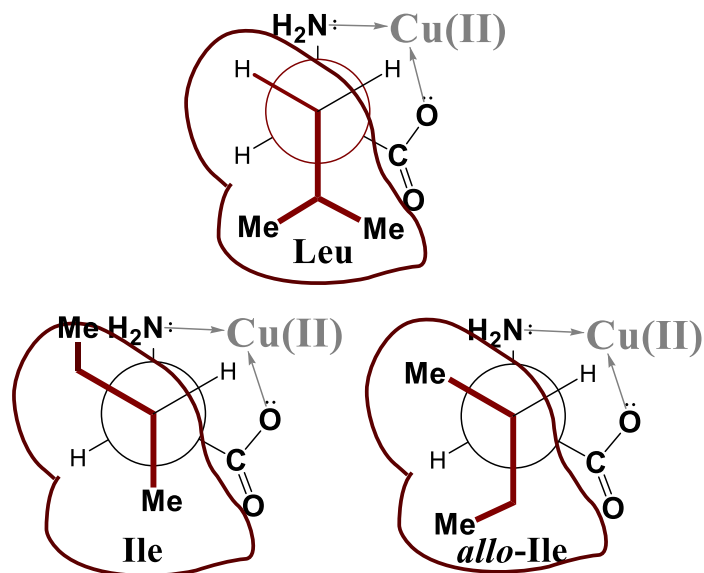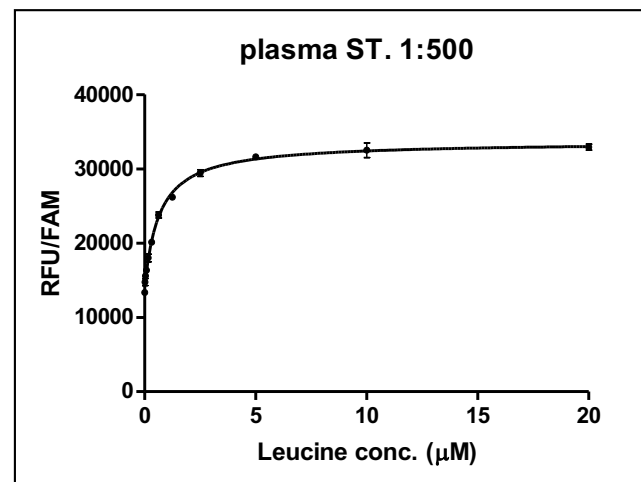

The upper section shows the fit between a hypothetical binding pocket and the Leu side chain, while the lower section show other amino acids. Ile shows steric hindrance, which prevents binding, while *allo*-Ile fits, although with a smaller contact area.

Table S5. Mock sample formulations for X'Le Studies

#	Leu	Ile	Allo-ile	Val	X'Le
1	203	127	0	342	203
2	260	313	158	806	350
3	50	516	240	692	187
4	98	53	0	205	98
5	135	139	97	384	190
6	247	160	121	571	316
7	546	432	496	1286	829
8	981	749	590	1096	1317
9	527	587	510	652	818
10	39	564	538	586	346
11	275	568	557	831	592
12	50	500	500	500	335
13	40	450	260	700	188
14	100	50	0	200	100
15	150	150	100	300	207
16	220	150	0	350	220
17	250	150	120	600	318
18	250	300	150	700	336
19	500	500	500	700	785
20	550	400	500	1300	835
21	1000	750	590	1100	1336

All values are micromolar.

plasma ST. 1:500

These evaluations are done strictly as preliminary screening, with sensors coming *as they are* from selections, with no further optimizations. Here we show a typical calibration curve at dilutions of 1:500, which is optimal for 75-600 μM range. The midpoint of the "pseudo-linear" range could be adjusted by either dilution or mutagenesis to reduce affinity of the aptamer. For cross-reactive arrays, for example, both quenching and release would be improved by systematic studies of aptamer and capture oligonucleotide to increase signal.
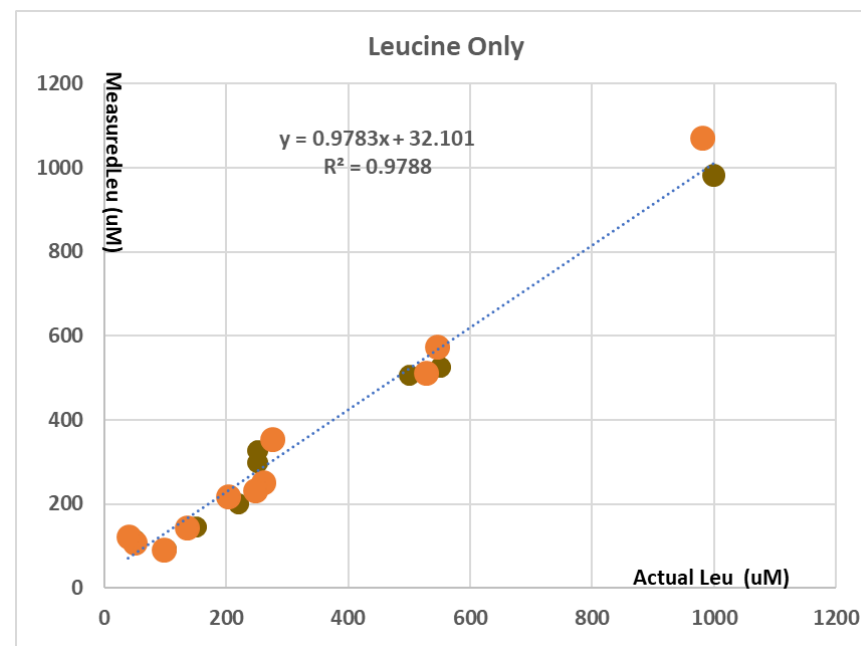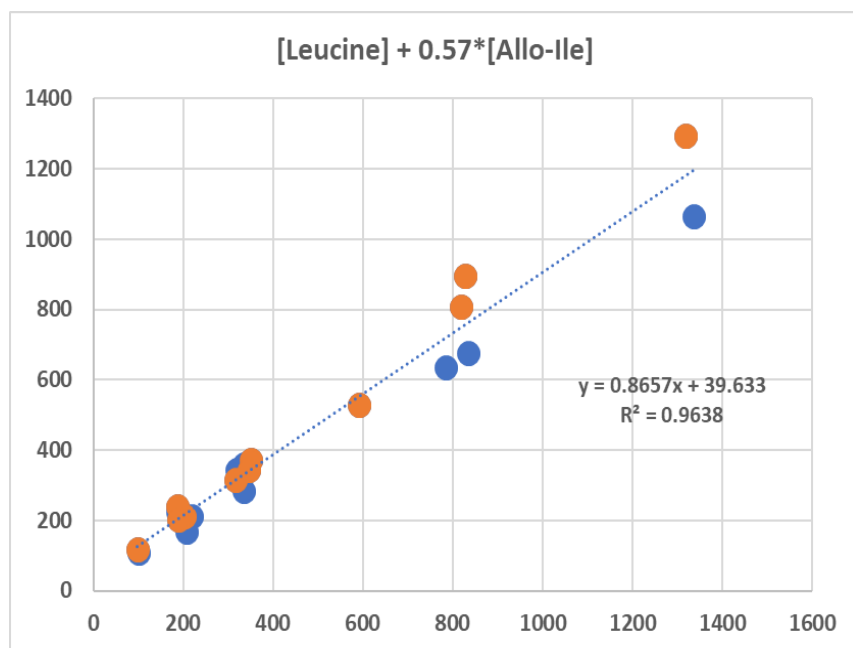
All samples were made in stripped plasma. Numbers for real patient samples were provided by Karlla Brigatti and Kevin Strauss, Clinic for Special Children, Strasburg, PA, through mediation of the MSUD Family Group, to which we added also a second set with similar numbers. Then, identical samples were also made, but without *allo*-Ile.

Fig. S53. Expanded measurements on mock samples

[Leucine] + 0.57*[Allo-Ile]

y = 0.8657x + 39.633
R² = 0.9638

Leucine Only

y = 0.9783x + 32.101
R² = 0.9788

Measured Leu (uM)

Actual Leu (uM)

Here, we show the follow up studies, now over two different days, of ability of CuLeu1.0 to measure X'Le and Leu concentrations, using mock samples with (left) and without (right) *allo*-Ile. We see that it would be beneficial to increase dilution to improve measurements at higher X'Le values. As is logical, the parallel Leu measurements are better fit with higher precision sensor range. Interestingly, even higher concentrations of Ile and Val do not have much of an impact. All measurements are in triplicates.

Fig. S54. Multistep selection leading to Ile aptamer

Referenced in the main text as, "The multi-step approach with Cu(II) can be generalized to amino acids that display a side chain away from the Cp*Rh(III) complex, such as Ile (*cf.* **CuIle1.1**, **Fig. S54-56**).".
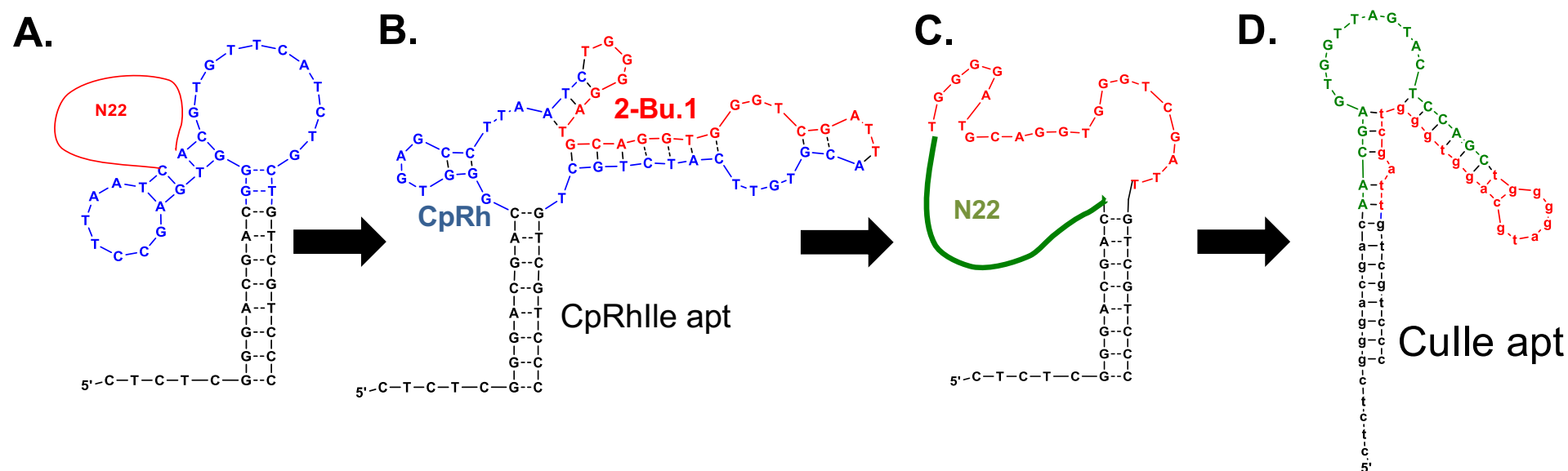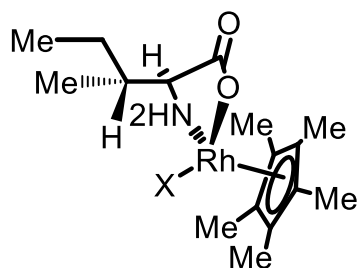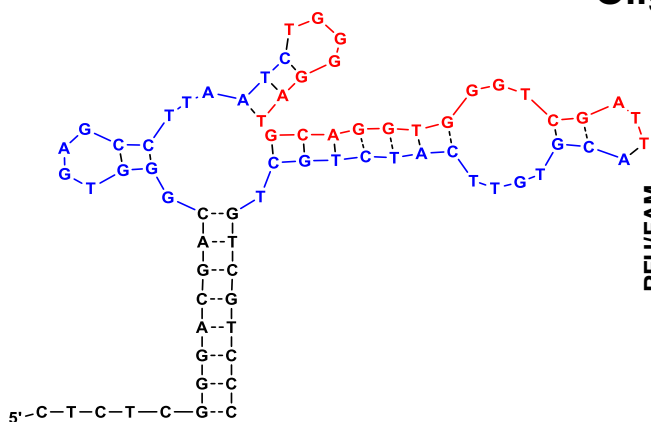

Figure SI-K. A multi-step selection for isoleucine was performed as a control. (A) The insertion library based on the CpRh 1.0 aptamer backbone uses the complex as a placeholder for 2-aminoetanoate. **(B)** The isolated Ile-Cp*Rh(iii) aptamer (CpRhIle-apt) using *insertion-reselection*, **(C)** Re-randomized library while using Ile-binding sequence to anchor our search. **(D)** The isolated aptamer (CuIle1.1_apt) recognizing Ile-Cu(ii) complex from the library *per* **(C)**. *

Fig. S55.

Apt ID	CpRhIle-apt
Target, X	CpRh(III)*Ile
FAM Sensor, A	/56-FAM/CTC TCG GGA CGA CGG GTG AGC CTT AAT CTG GGG ATG CAG GTG GGT CGA TTA CGT GTT CAT CTG CTG TCG TCC C
Quencher Strand, A	GTC GTC CCG AGA G/3Dab/ (3 times)
Truncated sequence	ACG ACG GGT GAG CCT TAA TCT GGG GAT GCA GGT GGG TCG ATT ACG TGT TCA TCT GCT GTC GT

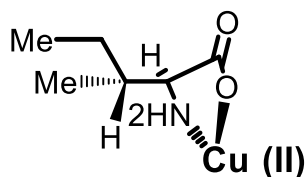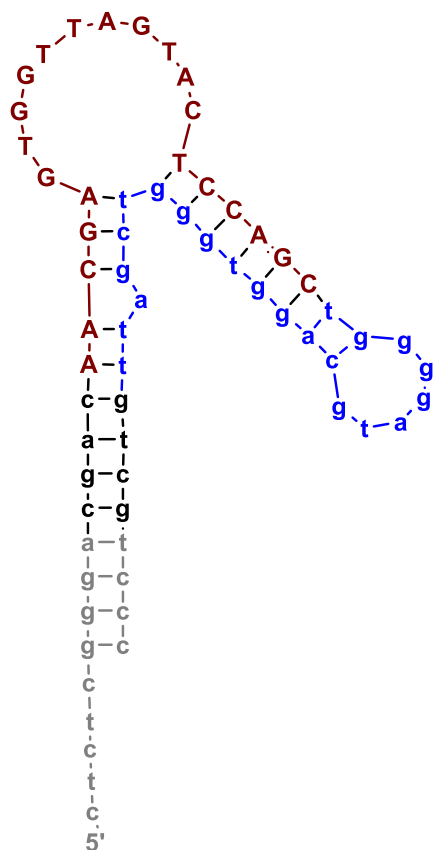## Oligonucleotide-displacement assay:

with constant amino acid:

ThT dye-displacement assay:

with constant Cp*Rh(III):
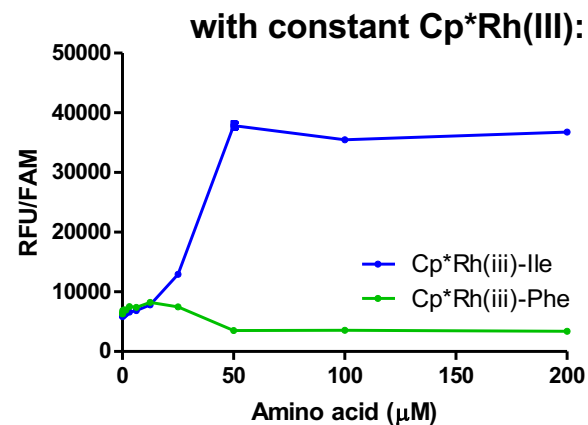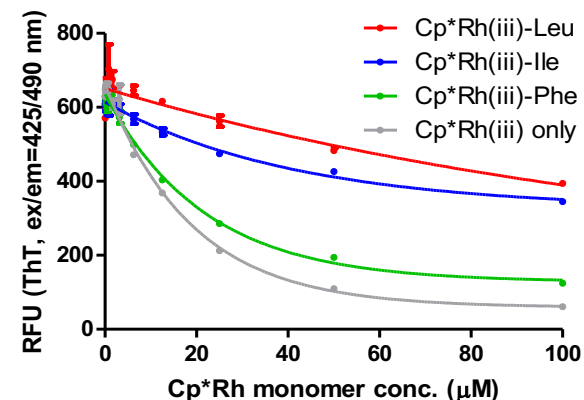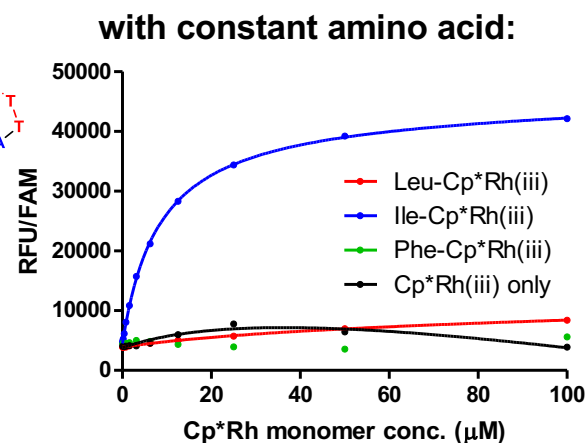
The threshold effect renders this sensor unsuitable for analytical purposes. Further, we see preference for Phe.

Fig. S56.

Apt ID	Culle-apt
Target, X	Ile-Cu(ii)
FAM Sensor, R	/56-FAM/CTC TCG GGA CGA CAA CGA GTG GTT AGT ACT CCA GCT GGG GAT GCA GGT GGG TCG ATT GTC GTC CC
Quencher Strand, A	TGT CGT CCC GAG AG/3Dab/ (10 times)
Truncated sequence	CGA CAA CGA GTG GTT AGT ACT CCA GCT GGG GAT GCA GGT GGG TCG ATT GTC G

Fitting parameters:

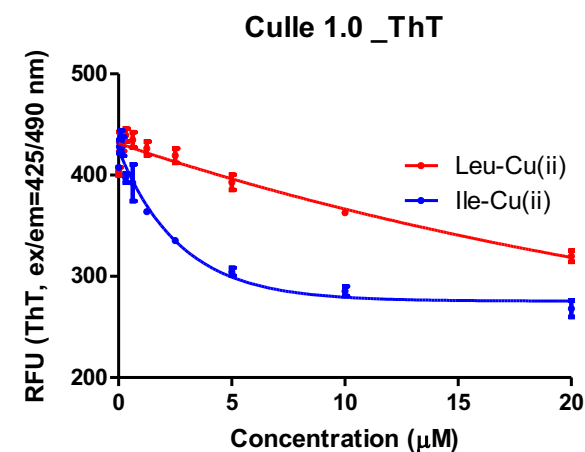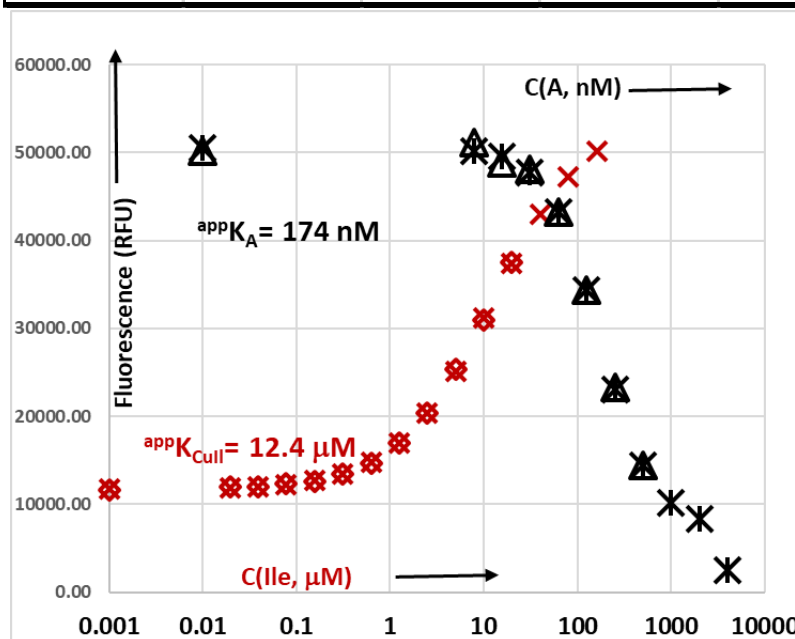| K$_A$ (nM)	HC	K'$_X$		HC	α		K$_X$(comp)	K$_X$(allost)
174	1.55	12.4	μM	0.86	1000		3.1	3.2

Figure. (Left) displacement and quenching curves plotted on the same graph; (Right): ThT displacement curve. For methods, see S.1.

Fig. S57. Direct & two step selections of Glu aptamers with Cp*Rh(III) cofactor

Referenced in the main text as, "The multi-step approach with Cu(II) can be generalized to amino acids that display a side chain away from the Cp*Rh(III) complex, such as Ile (*cf.* **CuIle1.1**, **Fig. S54-56**). This approach would not work for amino acids that carry a chelating group beyond 2-aminoethanoate, *e.g.*, glutamate (**Fig. S57**). "
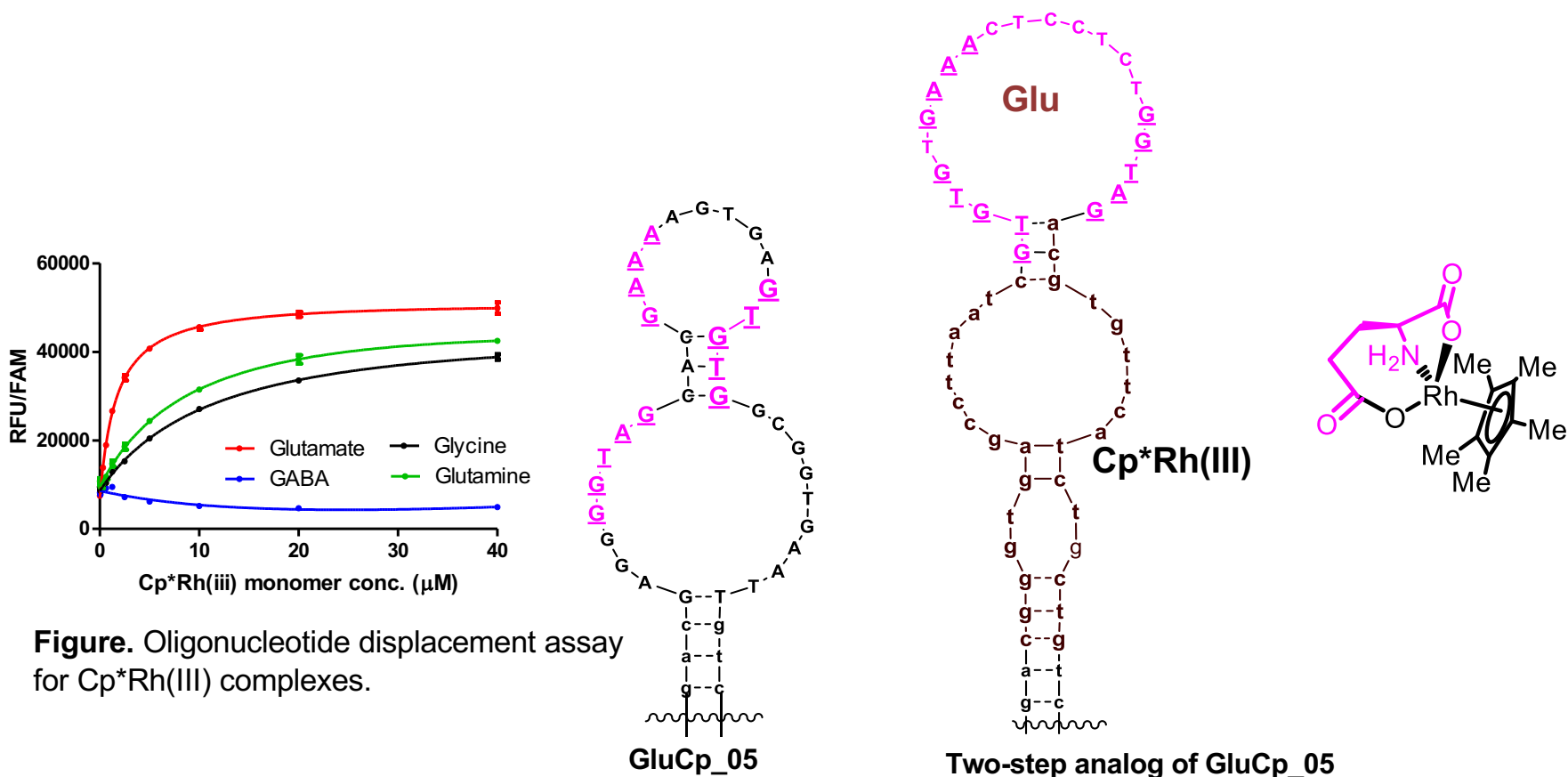
Figure. Oligonucleotide displacement assay for Cp*Rh(III) complexes.

GluCp_05

Two-step analog of GluCp_05

On the left, we have an example of an aptamer isolated directly from a Cp*Rh(III)*Glu selection, chosen for this demonstration. On the right is its analog from the two-step selection, *cf.* main text. These aptamers have substantial sequence overlap in sections that recognize Glu-but only in coordination with Cp*Rh(III). Subsequent attempts to generate a Glu aptamer did not result in any sequences that could be firmly identified as responding to Glu with sufficient confidence because we could not exclude coordination with sodium cations. Attempts to use Cu(II) lead only to Cu(II)-sensitive receptors (removal of Cu^{2+}).

Fig. S58. Cu(II)-Leu (direct selection)-Aptamer 2

Referenced in text as, "For comparison, we performed a single-step Leu selection with Cu(II) as the cofactor. We isolated receptors with fivefold lower affinities compared to **CuLeu1.0**. The two most abundant sequences preferred isoleucine or methionine (**Fig. S58-60**)."

Highly selective over BCAAs but prefers methionine:
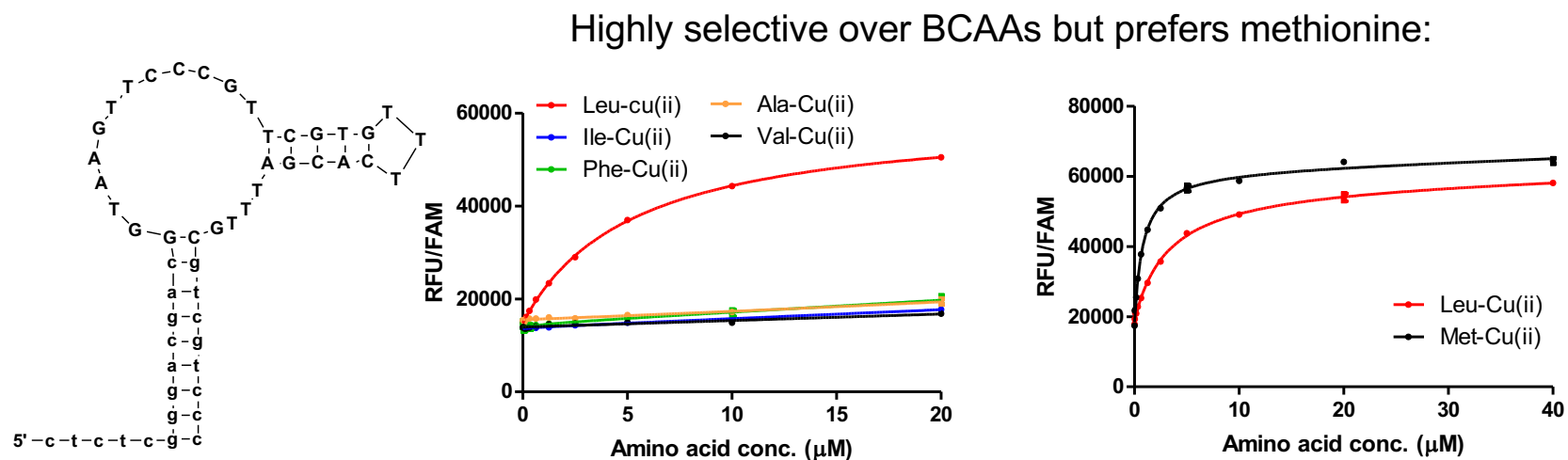
Cu(II)-Leu (direct)-2

Figure. (Left) displacement showing selectivity of standard set of amino acid; (Right) Displacement assay showing preferred, unexpected, binding to methionine.

Table: parameters for binding to leucine

K_A (nM)	HC	K'_X		HC	α	K_X(comp)	K_X(allost)
132.0	1.7	5.3	μM	1.0	-35.3	1.1	1.0

Fig. S59. Cu(II)-Leu (direct selection)-Aptamer 2

Cu(II)-Leu(direct)-2 is a minimized aptamer initially identified as a promising hit. (sequence 02 below). Thinking was like this: We focus on sequences that were above 1% of a pool (nine fulfilled this initial criteria, see below), ThT displacement midpoint <20 μM, and selectivity over Ile and Phe (identified as important based on Leu2.0 crossreactivity). From those that bound, 01 was eliminated based on its preference for Ile, 03 because it did not respond to Leu very well, 04 because of cross-reactivity with Phe, with 02 selected as a candidate for testing on clinical samples.

<u>This pool, will be further mined in future, *e.g.*, for an array with CuLeu1.0, *cf.* text.</u> The panels below were generated in the follow-up testing, ThT displacement, after we hypothesized that methionine is the potential interferent that led to failure of sensors in blind tests. This discovery needs to be taken into account when final sensors are chosen.

Lib	ctctcgggacgac_	_nnnnnnnnnnnnnnnnnnnnnnnnnnnnnnnnnnnn_	_gtcgtccc	% in total
N36_LeuCu(ii)_01	ctctcgggacgac_	_CGTTTGAACTCAATTAGGTTGCATCGGTCCCACGAG_	_gtcgtccc	29.50
N36_LeuCu(ii)_02	ctctcgggacgac_	_GGTAAGTTCCCGTTCATGTTGTCCATCATGATTTGC_	_gtcgtccc	29.47
N36_LeuCu(ii)_03	ctctcgggacgac_	_CAGTTTGGCGTTTTGTACGCGCATCGGTCCCACGTG_	_gtcgtccc	10.93
N36_LeuCu(ii)_04	ctctcgggacgac_	_GGCCCCGGGGCAAACAACAGCATAGGTTGTTTACGA_	_gtcgtccc	9.77
N36_LeuCu(ii)_05	ctctcgggacgac_	_GGGCAATTTGTAGCCTGATAGTAAGTTCCCGTTGAAC_	_gtcgtccc	3.25
N36_LeuCu(ii)_06	ctctcgggacgac_	_GGGTAAGTTCCCGTACGCTATACATAACGTTTTGTC_	_gtcgtccc	3.04
N36_LeuCu(ii)_07	ctctcgggacgac_	_GAGAAAAGGGTTGATCAATACTATTGGAATGTCGCA_	_gtcgtccc	1.45
N36_LeuCu(ii)_08	ctctcgggacgac_	_GGCCAATGGGAGAAATTAGGGGTAGCCGCCTGGGTT_	_gtcgtccc	1.05
N36_LeuCu(ii)_09	ctctcgggacgac_	_CGCCTGACTACAAGTGGTAGACATGGGAGCAATTAG_	_gtcgtccc	1.05
N36_LeuCu(ii)_10	ctctcgggacgac_	_GGTTCCAGGGCACCAAGATGATTAATCGTGGTACGA_	_gtcgtccc	0.80
N36_LeuCu(ii)_11	ctctcgggacgac_	_CAGTAAGTTCCCGTACGCATTTGGTTAGTACTTGTG_	_gtcgtccc	0.50
N36_LeuCu(ii)_12	ctctcgggacgac_	_GGAGTGTGGGAGAAATTAGCATACAGCGCCCAGGAT_	_gtcgtccc	0.34
N36_LeuCu(ii)_13	ctctcgggacgac_	_CATTTGTCCTGTGAACATAGGAGTAAGTGCCCGTTG_	_gtcgtccc	0.15

Initial cut-off for follow-up studies.

Fig. S60. Cu(II)-Leu (direct selection)-Aptamer 2

This same structure re-appears in other Cu(II) directed selections, with larger libraries, when counter-selection with Ile is introduced. Here we show it from a selection using N44 randomized regions (capital font in the aptamer on the right), in which we attempted to introduce additional structure switching mechanisms:

Cu(II)-Leu (direct)-2

Direct Leu aptamer from N44

Fig. S61. Referenced in the main text as, "This specific family of voriconazole-binding three-way junctions, despite being common, are eliminated from direct selections by exceptionally poor interactions with capture oligonucleotides, which was prevented in **Vor1.0** by structure switching (**Fig. 4B, S61**).".
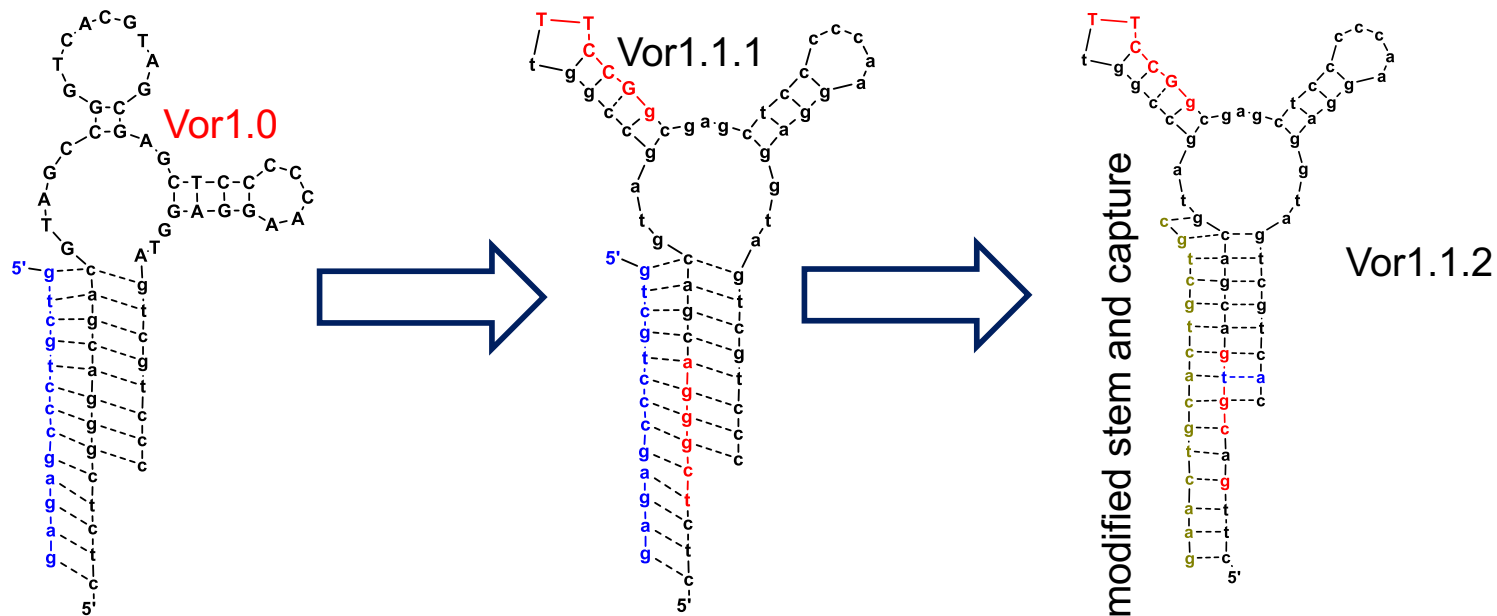
Testing sensors with the original quencher:
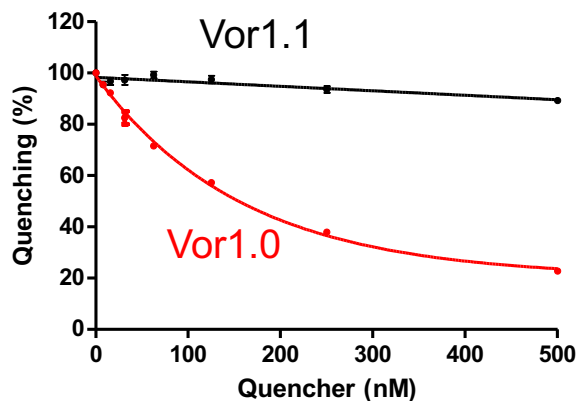
conclusion: no capture of Vor1.1 by complementary oligonucleotide on column!

Improved quenching and then displacement:
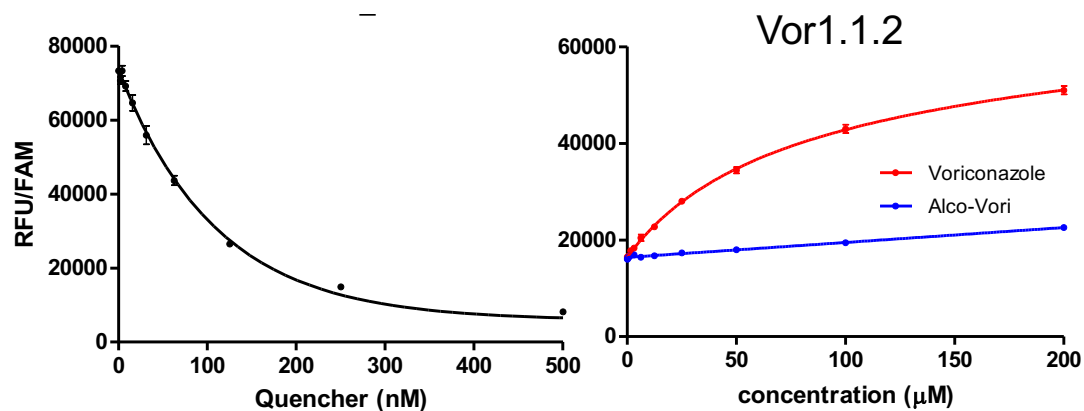
conclusion: choice of capture impacts selection!

Fig.S62. Other voriconazole data:

Binding of V1.0 and V1.1.2 to 2 and its analog, 2a, standard fluorescence displacement assay:
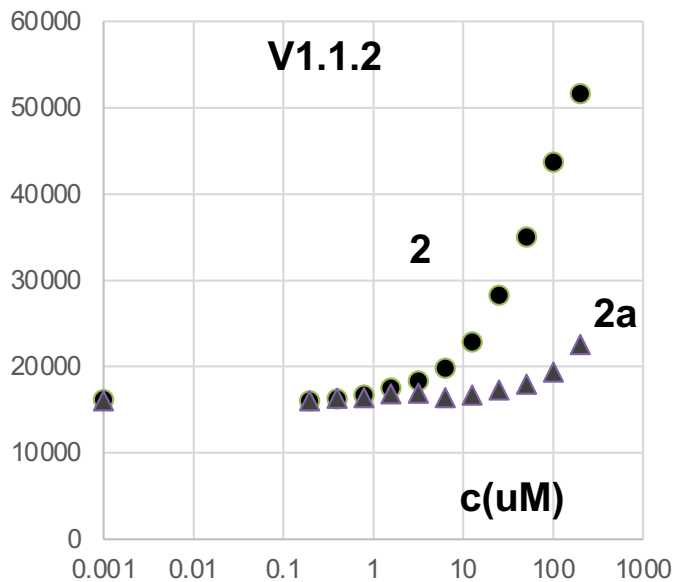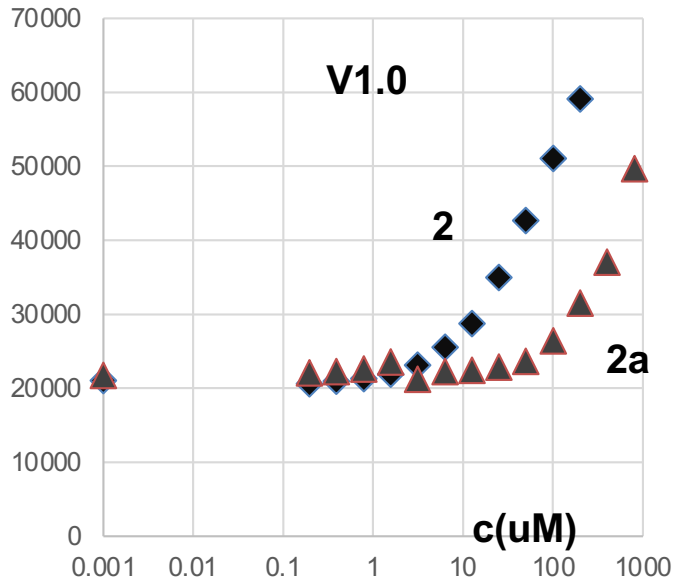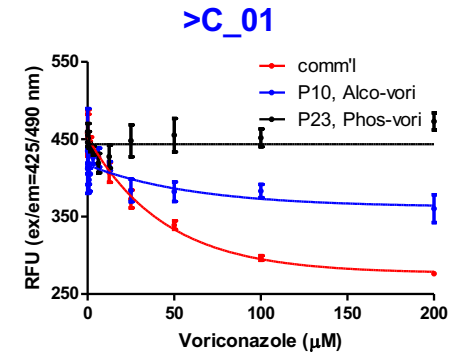

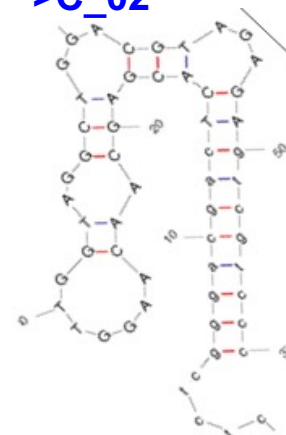Sequences identified in initial ThT screen to be the most promising:
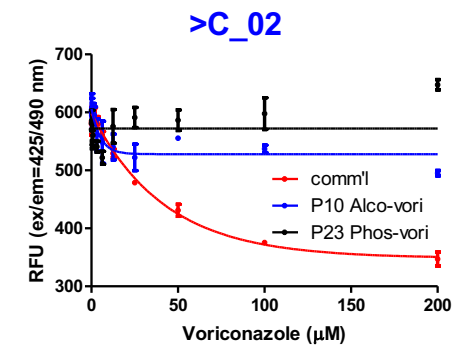
>C_01

Subsequently: V1.0

Not followed up.

>C_02
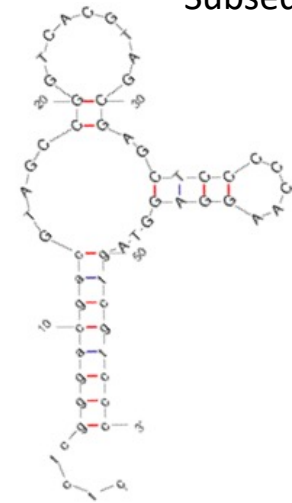
References and Notes

1. A. D. Ellington, J. W. Szostak, In vitro selection of RNA molecules that bind specific ligands. *Nature* **346**, 818–822 (1990).

2. C. Tuerk, L. Gold, Systematic evolution of ligands by exponential enrichment: RNA ligands to bacteriophage T4 DNA polymerase. *Science* **249**, 505–510 (1990).

3. A. Ruscito, M. C. DeRosa, Small-molecule binding aptamers: Selection strategies, characterization, and applications. *Front Chem.* **4**, 14 (2016).

4. H. Yu, O. Alkhamis, J. Canoura, Y. Liu, Y. Xiao, Advances and challenges in small-molecule DNA aptamer isolation, characterization, and sensor development. *Angew. Chem. Int. Ed.* **60**, 16800–16823 (2021).

5. N. Nakatsuka, K. A. Yang, J. M. Abendroth, K. M. Cheung, X. Xu, H. Yang, C. Zhao, B. Zhu, Y. S. Rim, Y. Yang, P. S. Weiss, M. N. Stojanović, A. M. Andrews, Aptamer-field-effect transistors overcome Debye length limitations for small-molecule sensing. *Science* **362**, 319–324 (2018).

6. K. A. Yang, M. Barbu, M. Halim, P. Pallavi, B. Kim, D. M. Kolpashchikov, S. Pecic, S. Taylor, T. S. Worgall, M. N. Stojanovic, Recognition and sensing of low-epitope targets via ternary complexes with oligonucleotides and synthetic receptors. *Nat. Chem.* **6**, 1003–1008 (2014).

7. K. M. Cheung, K.-A. Yang, N. Nakatsuka, C. Zhao, M. Ye, M. E. Jung, H. Yang, P. S. Weiss, M. N. Stojanović, A. M. Andrews, Phenylalanine monitoring via aptamer-field-effect transistor sensors. *ACS Sens.* **4**, 3308–3317 (2019).

8. N. Tejavibulya, D. A. M. Colburn, F. A. Marcogliese, K.-A. Yang, V. Guo, S. Chowdhury, M. N. Stojanovic, S. K. Sia, Hydrogel microfilaments toward intradermal health monitoring. *iScience* **21**, 328–340 (2019).

9. B. S. Ferguson, D. A. Hoggarth, D. Maliniak, K. Ploense, R. J. White, N. Woodward, K. Hsieh, A. J. Bonham, M. Eisenstein, T. E. Kippin, K. W. Plaxco, H. T. Soh, Real-time, aptamer-based tracking of circulating therapeutic agents in living animals. *Sci. Transl. Med.* **5**, 213ra165 (2013).

10. C. Zhao, K. M. Cheung, I.-W. Huang, H. Yang, N. Nakatsuka, W. Liu, Y. Cao, T. Man, P. S. Weiss, H. G. Monbouquette, A. M. Andrews, Implantable aptamer-field-effect transistor neuroprobes for in vivo neurotransmitter monitoring. *Sci. Adv.* **7**, eabj7422 (2021).

11. K. Stroek, A. Boelen, M. J. Bouva, M. De Sain-van der Velden, P. C. J. I. Schielen, R. Maase, H. Engel, B. Jakobs, L. A. J. Kluijtmans, M. F. Mulder, M. E. Rubio-Gozalbo, F. J. van Spronsen, G. Visser, M. C. de Vries, M. Williams, A. C. Heijboer, E. A. Kemper, A. M. Bosch, Evaluation of 11 years of newborn screening for maple syrup urine disease in the Netherlands and a systematic review of the literature: Strategies for optimization. *JIMD Rep.* **54**, 68–78 (2020).

12. P. Dauphin-Ducharme, K. Yang, N. Arroyo-Currás, K. L. Ploense, Y. Zhang, J. Gerson, M. Kurnik, T. E. Kippin, M. N. Stojanovic, K. W. Plaxco, Electrochemical aptamer-based sensors for improved therapeutic drug monitoring and high-precision, feedback-controlled drug delivery. *ACS Sens.* **4**, 2832–2837 (2019).

13. H. Elewa, E. El-Mekaty, A. El-Bardissy, M. H. H. Ensom, K. J. Wilby, Therapeutic drug monitoring of voriconazole in the management of invasive fungal infections: A critical review. *Clin. Pharmacokinet.* **54**, 1223–1235 (2015).

14. R. Nutiu, Y. Li, In vitro selection of structure-switching signaling aptamers. *Angew. Chem. Int. Ed.* **44**, 1061–1065 (2005).

15. M. Rajendran, A. D. Ellington, Selection of fluorescent aptamer beacons that light up in the presence of zinc. *Anal. Bioanal. Chem.* **390**, 1067–1075 (2008).

16. M. Yarus, Amino acids as RNA ligands: A direct-RNA-template theory for the code's origin. *J. Mol. Evol.* **47**, 109–117 (1998).

17. G. R. Wiedman, Y. Zhao, D. S. Perlin, A novel, rapid, and low-volume assay for therapeutic drug monitoring of posaconazole and other long-chain azole-class antifungal drugs. *MSphere* **3**, ee00623–18 (2018).

18. F. J. Ehlert, Estimation of the affinities of allosteric ligands using radioligand binding and pharmacological null methods. *Mol. Pharmacol.* **33**, 187–194 (1988).

19. S. M. Free Jr., J. W. Wilson, A mathematical contribution to structure-activity studies. *J. Med. Chem.* **7**, 395–399 (1964).

20. C. Bissantz, B. Kuhn, M. Stahl, A medicinal chemist's guide to molecular interactions. *J. Med. Chem.* **53**, 5061–5084 (2010).

21. J. R. Lorsch, J. W. Szostak, Chance and necessity in the selection of nucleic acid catalysts. *Acc. Chem. Res.* **29**, 103–110 (1996).

22. S. E. Osborne, A. D. Ellington, Nucleic acid selection and the challenge of combinatorial chemistry. *Chem. Rev.* **97**, 349–370 (1997).

23. H. Gohlke, G. Klebe, Approaches to the description and prediction of the binding affinity of small-molecule ligands to macromolecular receptors. *Angew. Chem. Int. Ed.* **41**, 2644–2676 (2002).

24. B. Baum, L. Muley, M. Smolinski, A. Heine, D. Hangauer, G. Klebe, Non-additivity of functional group contributions in protein-ligand binding: A comprehensive study by crystallography and isothermal titration calorimetry. *J. Mol. Biol.* **397**, 1042–1054 (2010).

25. J. M. Carothers, S. C. Oestreich, J. H. Davis, J. W. Szostak, Informational complexity and functional activity of RNA structures. *J. Am. Chem. Soc.* **126**, 5130–5137 (2004).

26. A. Buryak, K. Severin, A chemosensor array for the colorimetric identification of 20 natural amino acids. *J. Am. Chem. Soc.* **127**, 3700–3701 (2005).

27. Z. Liu, A. Mariani, L. Wu, D. Ritson, A. Folli, D. Murphy, J. Sutherland, Tuning the reactivity of nitriles using Cu(ii) catalysis - potentially prebiotic activation of nucleotides. *Chem. Sci.* **9**, 7053–7057 (2018).

28. K.-A. Yang, R. Pei, D. Stefanovic, M. N. Stojanović, Optimizing cross-reactivity with evolutionary search for sensors. *J. Am. Chem. Soc.* **134**, 1642–1647 (2012).

29. W. Yang, H. Yu, O. Alkhamis, Y. Liu, J. Canoura, F. Fu, Y. Xiao, *In vitro* isolation of class-specific oligonucleotide-based small-molecule receptors. *Nucleic Acids Res.* **47**, e71 (2019).

30. K. Ravikumar, B. Sridhar, K. D. Prasad, A. K. S. Bhujanga Rao, Voriconazole, an antifungal drug. *Acta Crystallogr. Sect. E Struct. Rep. Online* **63**, o565–o567 (2007).

31. E. J. Corey, *The Logic of Chemical Synthesis* (Wiley, 1989).

32. D. Angeletti, I. Kosik, J. J. S. Santos, W. T. Yewdell, C. M. Boudreau, V. V. A. Mallajosyula, M. C. Mankowski, M. Chambers, M. Prabhakaran, H. D. Hickman, A. B. McDermott, G. Alter, J. Chaudhuri, J. W. Yewdell, Outflanking immunodominance to target subdominant broadly neutralizing epitopes. *Proc. Natl. Acad. Sci. U.S.A.* **116**, 13474–13479 (2019).

33. H. Ochiai, The logical structure of organic chemistry and the empirical adequacy of the classical concept of the molecule. *HYLE-Int. J. Phil.Chem.* **19**, 139–160 (2013).

34. J. C. Manimala, S. L. Wiskur, A. D. Ellington, E. V. Anslyn, Tuning the specificity of a synthetic receptor using a selected nucleic acid receptor. *J. Am. Chem. Soc.* **126**, 16515–16519 (2004).

35. F. Pfeiffer, F. Tolle, M. Rosenthal, G. M. Brändle, J. Ewers, G. Mayer, Identification and characterization of nucleobase-modified aptamers by click-SELEX. *Nat. Protoc.* **13**, 1153–1180 (2018).

36. H. Saito, The RNA world 'hypothesis'. *Nat. Rev. Mol. Cell Biol.* **23**, 582 (2022).

37. F. Jacob, Evolution and tinkering. *Science* **196**, 1161–1166 (1977).

38. J. R. Lorsch, J. W. Szostak, In vitro evolution of new ribozymes with polynucleotide kinase activity. *Nature* **371**, 31–36 (1994).

39. K. D. Warner, C. E. Hajdin, K. M. Weeks, Principles for targeting RNA with drug-like small molecules. *Nat. Rev. Drug Discov.* **17**, 547–558 (2018).

40. W. M. Billings, B. Hedelius, T. Millecam, D. Wingate, D. D. Corte, ProSPr: Democratized implementation of Alphafold protein distance prediction network. bioRxiv 830273 [Preprint] (2019). https://doi.org/10.1101/830273.

41. K.-A. Yang, R. Pei, M. N. Stojanović, In vitro selection and amplification protocols for isolation of aptameric sensors for small molecules. *Methods* **106**, 58–65 (2016).

42. M. Zuker, Mfold web server for nucleic acid folding and hybridization prediction. *Nucleic Acids Res.* **31**, 3406–3415 (2003).

43. N. Nakatsuka, J. M. Abendroth, K.-A. Yang, A. M. Andrews, Divalent cation dependence enhances dopamine aptamer biosensing. *ACS Appl. Mater. Interfaces* **13**, 9425–9435 (2021).

44. T. S. Najdi, C.-R. Yang, B. E. Shapiro, G. W. Hatfield, E. D. Mjolsness, Application of a generalized MWC model for the mathematical simulation of metabolic pathways regulated by allosteric enzymes. *J. Bioinform. Comput. Biol.* **4**, 335–355 (2006).

45. E. F. Douglass Jr., C. J. Miller, G. Sparer, H. Shapiro, D. A. Spiegel, A comprehensive mathematical model for three-body binding equilibria. *J. Am. Chem. Soc.* **135**, 6092–6099 (2013).

46. A. Brown, Analysis of cooperativity by isothermal titration calorimetry. *Int. J. Mol. Sci.* **10**, 3457–3477 (2009).